Calhoun: The NPS Institutional Archive

DSpace Repository

Theses and Dissertations | 1. Thesis and Dissertation Collection, all items

2009-03

Impact of aerosols on scene collection and scene correction

Quinn, Kevin M.

Monterey, California: Naval Postgraduate School

http://hdl.handle.net/10945/4794

Downloaded from NPS Archive: Calhoun

http://www.nps.edu/library

Calhoun is the Naval Postgraduate School's public access digital repository for research materials and institutional publications created by the NPS community. Calhoun is named for Professor of Mathematics Guy K. Calhoun, NPS's first appointed -- and published -- scholarly author.

Dudley Knox Library / Naval Postgraduate School
411 Dyer Road / 1 University Circle
Monterey, California USA 93943

NAVAL POSTGRADUATE SCHOOL

MONTEREY, CALIFORNIA

THESIS

IMPACT OF AEROSOLS ON SCENE COLLECTION AND SCENE CORRECTION

by

Kevin M. Quinn

March 2009

Thesis Advisor:	Philip A. Durkee
Second Reader:	Mary S. Jordan

Approved for public release; distribution is unlimited

THIS PAGE INTENTIONALLY LEFT BLANK

REPORT DOCUMENTATION PAGE			Form Approved OMB No. 0704-0188
Public reporting burden for this collection of information is estimated to average 1 hour per response, including the time for reviewing instruction, searching existing data sources, gathering and maintaining the data needed, and completing and reviewing the collection of information. Send comments regarding this burden estimate or any other aspect of this collection of information, including suggestions for reducing this burden, to Washington headquarters Services, Directorate for Information Operations and Reports, 1215 Jefferson Davis Highway, Suite 1204, Arlington, VA 22202-4302, and to the Office of Management and Budget, Paperwork Reduction Project (0704-0188) Washington DC 20503.			
1. AGENCY USE ONLY *(Leave blank)*	**2. REPORT DATE** March 2009	**3. REPORT TYPE AND DATES COVERED** Master's Thesis	
4. TITLE AND SUBTITLE Impact of Aerosols on Scene Collection and Scene Correction		**5. FUNDING NUMBERS**	
6. AUTHOR(S) Kevin M. Quinn			
7. PERFORMING ORGANIZATION NAME(S) AND ADDRESS(ES) Naval Postgraduate School Monterey, CA 93943-5000		**8. PERFORMING ORGANIZATION REPORT NUMBER**	
9. SPONSORING /MONITORING AGENCY NAME(S) AND ADDRESS(ES) N/A		**10. SPONSORING/MONITORING AGENCY REPORT NUMBER**	
11. SUPPLEMENTARY NOTES The views expressed in this thesis are those of the author and do not reflect the official policy or position of the Department of Defense or the U.S. Government.			
12a. DISTRIBUTION / AVAILABILITY STATEMENT Approved for public release; distribution is unlimited		**12b. DISTRIBUTION CODE** A	

13. ABSTRACT (maximum 200 words)

Airborne aerosols contaminate satellite imagery, making it difficult for analysts to characterize surface targets. The amount of contamination is due to aerosol loading, best quantified by aerosol optical depth (AOD). Level 2 AERONET data provides "ground truth" AOD measurements. Unfortunately, targets are not likely to be near an AERONET station. This thesis examines two methods of quantifying AOD in lieu of AERONET data: Moderate Resolution Imaging Spectroradiometer (MODIS) AOD retrievals and Navy Aerosol Analysis and Prediction System (NAAPS) AOD forecasts (with MODIS data assimilation). Over the Persian Gulf and Japan, MODIS accurately retrieved AOD at 0.55μm wavelength. MODIS may have accurately retrieved AOD over Korea, but uncertainty in the retrieval was high due to a small sample size. Over West Africa, MODIS underestimated AOD. Over the Persian Gulf and Japan, NAAPS accurately estimated AOD at 0.55μm. Over Korea, the model displayed mixed results. Finally, over West Africa, NAAPS tended to underestimate AOD.

14. SUBJECT TERMS Aerosol Optical Depth, AERONET, MODIS, NAAPS, Radiance, Surface Reflectance			**15. NUMBER OF PAGES** 135
			16. PRICE CODE
17. SECURITY CLASSIFICATION OF REPORT Unclassified	**18. SECURITY CLASSIFICATION OF THIS PAGE** Unclassified	**19. SECURITY CLASSIFICATION OF ABSTRACT** Unclassified	**20. LIMITATION OF ABSTRACT** UU

NSN 7540-01-280-5500 Standard Form 298 (Rev. 2-89)
Prescribed by ANSI Std. 239-18

THIS PAGE INTENTIONALLY LEFT BLANK

Approved for public release; distribution is unlimited

IMPACT OF AEROSOLS ON SCENE COLLECTION AND SCENE CORRECTION

Kevin M. Quinn
Captain, United States Air Force
B.S., Cornell University, 2003

Submitted in partial fulfillment of the
requirements for the degree of

MASTER OF SCIENCE IN METEOROLOGY

from the

NAVAL POSTGRADUATE SCHOOL
March 2009

Author: Kevin M. Quinn

Approved by: Philip A. Durkee
Thesis Advisor

Mary S. Jordan
Second Reader

Philip A. Durkee
Chairman, Department of Meteorology

THIS PAGE INTENTIONALLY LEFT BLANK

ABSTRACT

Airborne aerosols contaminate satellite imagery, making it difficult for analysts to characterize surface targets. The amount of contamination is due to aerosol loading, best quantified by aerosol optical depth (AOD). Level 2 AERONET data provides "ground truth" AOD measurements. Unfortunately, targets are not likely to be near an AERONET station. This thesis examines two methods of quantifying AOD in lieu of AERONET data: Moderate Resolution Imaging Spectroradiometer (MODIS) AOD retrievals and Navy Aerosol Analysis and Prediction System (NAAPS) AOD forecasts (with MODIS data assimilation). Over the Persian Gulf and Japan, MODIS accurately retrieved AOD at 0.55μm wavelength. MODIS may have accurately retrieved AOD over Korea, but uncertainty in the retrieval was high due to a small sample size. Over West Africa, MODIS underestimated AOD. Over the Persian Gulf and Japan, NAAPS accurately estimated AOD at 0.55μm. Over Korea, the model displayed mixed results. Finally, over West Africa, NAAPS tended to underestimate AOD.

THIS PAGE INTENTIONALLY LEFT BLANK

TABLE OF CONTENTS

I. INTRODUCTION....1

II. BACKGROUND....3
- **A. AEROSOLS, SCATTERING, AND THE VISIBLE SPECTRUM....3**
- **B. TROPOSPHERIC DUST AND SMOKE CLIMATOLOGY....5**
  - **1. Persian Gulf....5**
  - **2. East Asia....6**
  - **3. West Africa....7**

III. DATA AND METHODOLOGY....9
- **A. AEROSOL ROBOTIC NETWORK (AERONET)....9**
  - **1. Network Description....9**
  - **2. Site Selection....9**
  - **3. AERONET Wavelength Variability....12**
- **B. MODERATE RESOLUTION IMAGING SPECTRORADIOMETER (MODIS)....12**
  - **1. MODIS Data Description....12**
  - **2. MODIS Climatology....13**
  - **3. MODIS/AERONET Comparison Methodology....13**
  - **4. MODIS Grid Locations....14**
- **C. NAVY AEROSOL ANALYSIS AND PREDICTION SYSTEM (NAAPS)....16**
  - **1. NAAPS AOD Description....16**
  - **2. NAAPS/AERONET Comparison Methodology....17**
- **D. RADIANCE-BASED TARGET DETECTION....18**
  - **1. MODTRAN ™ Model Runs....18**
  - **2. MODTRAN™ Radiance Comparison with MODIS Imagery....18**

IV. RESULTS....19
- **A. AERONET CLIMATOLOGY....19**
  - **1. Basin Composite....19**
  - **2. Persian Gulf....23**
  - **3. East Asia....26**
  - **4. West Africa....32**
- **B. MODIS/AERONET COMPARISON....37**
  - **1. Persian Gulf....37**
  - **2. East Asia....41**
    - ***a. Korea....41***
    - ***b. Japan....45***
  - **3. West Africa....49**
  - **4. Summary....53**
- **C. NAAPS/AERONET COMPARISON....53**
  - **1. Persian Gulf....53**

2. East Asia 56
a. Korea..... 56
b. Japan 59
3. West Africa 62
4. Summary..... 65
D. RADIANCE-BASED TARGET DETECTION 66
V. CONCLUSIONS AND RECOMMENDATIONS FOR FUTURE RESEARCH 71
A. CONCLUSIONS 71
B. RECOMMENDATIONS FOR FUTURE RESEARCH..... 72
APPENDIX A: AOD VARIATION BY WAVELENGTH 73
APPENDIX B: AERONET CLIMATOLOGY 77
A. PERSIAN GULF 77
B. EAST ASIA..... 81
C. WEST AFRICA 87
APPENDIX C: MODIS/AERONET COMPARISON 93
A. PERSIAN GULF 93
B. EAST ASIA..... 95
1. Korea 95
2. Japan 97
C. WEST AFRICA 99
APPENDIX D: NAAPS/AERONET COMPARISON..... 101
A. PERSIAN GULF 101
B. EAST ASIA..... 103
1. Korea 103
2. Japan 105
C. WEST AFRICA 107
LIST OF REFERENCES 109
INITIAL DISTRIBUTION LIST 111

LIST OF FIGURES

Figure 1. NOAA-17 RGB Satellite Image from 0718UTC, 26 March 2003. A large dust storm is present over southwestern Iraq (From NOAA News Online, Story 1120, 2009).....1

Figure 2. Radiance received by a satellite at the top of the atmosphere, with top of the atmosphere irradiance (E_0), solar irradiance at the Earth's surface (E_s), optical depth (δ), and reflected radiance by the target (L_t) and background (L_b) noted above. (From Durkee February 2009).....5

Figure 3. Three Persian Gulf AERONET sites used in this study (From Google Maps February 2009).....10

Figure 4. Three East Asia AERONET sites used in this study (From Google Maps February 2009).....11

Figure 5. Two West Africa AERONET sites used in this study (From Google Maps February 2009).....11

Figure 6. MODIS grid points and AERONET sites used for the Persian Gulf basin, MODIS/AERONET comparison. The numbers denote MODIS grid points, and the AERONET sites are denoted by filled circles. The six grid points in red are used to represent the over-water region near Dhabi (red circle). The seven grid points in green are used to represent the over-water region near Dhadnah (green circle) (From Google Maps February 2009).....15

Figure 7. Same as Figure 6, but for the Korea (red) and Japan (green) basins. The AERONET sites are denoted by filled circles (From Google Maps February 2009).....15

Figure 8. Same as Figure 6, but for West Africa. The AERONET site (Ilorin) is denoted by the red circle (From Google Maps February 2009).....16

Figure 9. One-year distribution of basin composite AERONET AOD (0.50μm) values for the Persian Gulf, Korea, Japan, and West Africa basins, for 2006. The histogram of AOD values (blue bars) and cumulative frequency distribution (red curve) are denoted. The sample size is listed in the upper right corner. The vertical lines (black), from left to right, denote the quartiles of the distribution, 25% (dashed), 50% (solid), 75% (dashed)...20

Figure 10. Same as Figure 9, but for 2007.....20

Figure 11. Cumulative frequency curves for the basin composite climatology for 2006-2007. The cumulative frequency curves for 2006 (blue) and 2007 (green) are are computed from the distribution for each year. The combined cumulative frequency curve (red) is computed from the combined dataset from both years.....21

Figure 12. Two-year distribution of basin composite AERONET AOD (0.50μm) values for the Persian Gulf, Korea, Japan, and West Africa basins, for 2006-2007. The histogram of AOD values (blue bars) and cumulative frequency distribution (red curve) are denoted. The sample size is listed in the upper right corner. The vertical lines (black), from left to right, denote the quartiles of the distribution, 25% (dashed), 50% (solid), 75% (dashed)...22

Figure 13. Two-year distribution of AERONET AOD (0.50 μm) values for stations Solar Village, Dhabi and Dhadnah in the Persian Gulf basin, for 2006-2007. The histogram of AOD values (blue bars) and cumulative frequency distribution (red curve) are denoted. The sample size is listed in the upper right corner. The vertical lines (black), from left to right, denote the quartiles of the distribution, 25% (dashed), 50% (solid), 75% (dashed). ..24
Figure 14. Two-year annual cumulative frequency curves for the Persian Gulf Basin for 2006-2007. The cumulative frequency curve for each individual station is compared with the cumulative frequency curve computed from the histogram distribution for the combined dataset of the three stations (Persian Gulf basin, red). 25
Figure 15. Seasonal Distribution of AERONET AOD (0.50 μm) values for the Persian Gulf basin for 2006-2007. The histogram of AOD values (blue bars) and cumulative frequency distribution (red curve) are denoted. The sample size is listed in the upper right corner. Seasons are denoted as (a) Winter (December-February), (b) Spring (March-May), (c) Summer (June-August), and (d) Fall (September-November). 26
Figure 16. Two-year distribution of AERONET AOD (0.50μm) values for Anmyon in the Korea basin, for 2006-2007. The histogram of AOD values (blue bars) and cumulative frequency distribution (red curve) are denoted. The sample size is listed in the upper right corner. The vertical lines (black), from left to right, denote the quartiles of the distribution, 25% (dashed), 50% (solid), 75% (dashed).....28
Figure 17. Same as Figure 16, but for Japan. 28
Figure 18. Two-year annual cumulative frequency curves for Korea (blue) and Japan (red) for 2006-2007. 29
Figure 19. Same as Figure 18, but for the Japan basin. 30
Figure 20. Seasonal Distribution of AERONET AOD (0.50 μm) values for the Korea basin for 2006-2007. The histogram of AOD values (blue bars) and cumulative frequency distribution (red curve) are denoted. The sample size is listed in the upper right corner. Seasons are denoted as (a) Winter (December-February), (b) Spring (March-May), (c) Summer (June-August), and (d) Fall (September-November). 31
Figure 21. Same as Figure 20 but for the Japan basin. 32
Figure 22. Two-year distribution of AERONET AOD (0.44μm) values for station Djougou in the West Africa basin, for 2006-2007. The histogram of AOD values (blue bars) and cumulative frequency distribution (red curve) are denoted. The sample size is listed in the upper right corner. The vertical lines (black), from left to right, denote the quartiles of the distribution, 25% (dashed), 50% (solid), 75% (dashed).....34
Figure 23. Same as Figure 22, but for Ilorin at 0.50μm. 34
Figure 24. Two-year annual cumulative frequency curves for the West Africa basin for 2006-2007. The Ilorin (0.50μm, blue) and Djougou (0.44μm, green) curves are denoted.....35

Figure 25. Seasonal Distribution of AERONET AOD (0.50 μm) values for Ilorin in the West Africa basin for 2006-2007. The histogram of AOD values (blue bars) and cumulative frequency distribution (red curve) are denoted. The sample size is listed in the upper right corner. Seasons are denoted as (a) Winter (December-February), (b) Spring (March-May), (c) Summer (June-August), and (d) Fall (September-November). 36
Figure 26. Annual scatter plot of daily AERONET and MODIS AOD values for the Persian Gulf basin for 2006-2007. The daily AOD values (red stars) and one-to-one line (blue) are denoted. The correlation coefficient (R) and sample size (N) are listed in the upper left corner. 38
Figure 27. Persian Gulf Basin AERONET AOD (0.50μm) versus MODIS AOD (0.55μm) scatterplots for the 2006-2007 seasons: (a) Winter, (b) Spring, (c) Summer, (d) Fall. The daily AOD values (red stars) and one-to-one line (blue) are denoted. The correlation coefficient (R) and sample size (N) are listed in the upper left corner. 39
Figure 28. Annual cumulative frequency curves for the Persian Gulf basin MODIS (red) and AERONET (blue) AOD distributions. 40
Figure 29. Annual scatter plot of daily AERONET and MODIS AOD values for the Korea basin for 2006-2007. The daily AOD values (red stars) and one-to-one line (blue) are denoted. The correlation coefficient (R) and sample size (N) are listed in the upper left corner. 42
Figure 30. Korea Basin AERONET AOD (0.50μm) versus MODIS AOD (0.55μm) scatterplots for the 2006-2007 seasons: (a) Winter, (b) Spring, (c) Summer, (d) Fall. The daily AOD values (red stars) and one-to-one line (blue) are denoted. The correlation coefficient (R) and sample size (N) are listed in the upper left corner. 43
Figure 31. Annual cumulative frequency curves for the Korea basin MODIS (red) and AERONET (blue) AOD distributions. 44
Figure 32. Annual scatter plot of daily AERONET and MODIS AOD values for Shirahama in the Japan basin for 2006-2007. The daily AOD values (red stars) and one-to-one line (blue) are denoted. The correlation coefficient (R) and sample size (N) are listed in the upper left corner. 46
Figure 33. Japan Basin AERONET AOD (0.50μm) versus MODIS AOD (0.55μm) scatterplots for the 2006-2007 seasons: (a) Winter, (b) Spring, (c) Summer, (d) Fall. The daily AOD values (red stars) and one-to-one line (blue) are denoted. The correlation coefficient (R) and sample size (N) are listed in the upper left corner. 47
Figure 34. Annual cumulative frequency curves for the Japan basin MODIS (red) and AERONET (blue) AOD distributions. 48
Figure 35. Annual scatter plot of daily AERONET and MODIS AOD values for Ilorin in the West Africa basin for 2006-2007. The daily AOD values (red stars) and one-to-one line (blue) are denoted. The correlation coefficient (R) and sample size (N) are listed in the upper left corner. 50
Figure 36. West Africa Basin AERONET AOD (0.50μm) versus MODIS AOD (0.55μm) scatterplots for the 2006-2007 seasons: (a) Winter, (b) Spring,

(c) Summer, (d) Fall. The daily AOD values (red stars) and one-to-one line (blue) are denoted. The correlation coefficient (R) and sample size (N) are listed in the upper left corner. 51
Figure 37. Annual cumulative frequency curves for the West Africa basin MODIS (red) and AERONET (blue) AOD distributions. The y-axis indicates the cumulative probability of occurrence of an AOD. The x-axis indicates the AOD values. 52
Figure 38. Two-year distribution of daily mean 0.55μm NAAPS AOD values for stations Dhabi and Dhadnah in the Persian Gulf basin, for 2006-2007. The histogram of AOD values (blue bars) and cumulative frequency distribution (red curve) corresponding to the histogram are denoted. The sample size is listed in the upper right corner. The vertical lines (black), from left to right, denote the quartiles of the distribution, 25% (dashed), 50% (solid), 75% (dashed). 54
Figure 39. Annual scatter plot of daily AERONET and NAAPS AOD values for the Persian Gulf basin for 2006-2007. The daily AOD values (red stars) and one-to-one line (blue) are denoted. The correlation coefficient (R) and sample size (N) are listed in the upper left corner. 55
Figure 40. Persian Gulf Basin AERONET AOD (0.50μm) versus NAAPS AOD (0.55μm) scatterplots for the 2006-2007 seasons: (a) Winter, (b) Spring, (c) Summer, (d) Fall. The daily AOD values (red stars) and one-to-one line (blue) are denoted. The correlation coefficient (R) and sample size (N) are listed in the upper left corner. 56
Figure 41. Two-year distribution of 0.55μm NAAPS AOD values for Anmyon in the Korea basin, for 2006-2007. The histogram of AOD values (blue bars) and cumulative frequency distribution (red curve) corresponding to the histogram are denoted. The sample size is listed in the upper right corner. The vertical lines (black), from left to right, denote the quartiles of the distribution, 25% (dashed), 50% (solid), 75% (dashed). 57
Figure 42. Annual scatter plot of daily AERONET and NAAPS AOD values for the Korea basin for 2006-2007. The daily AOD values (red stars) and one-to-one line (blue) are denoted. The correlation coefficient (R) and sample size (N) are listed in the upper left corner. 58
Figure 43. Korea Basin AERONET AOD (0.50μm) versus NAAPS AOD (0.55μm) scatterplots for the 2006-2007 seasons: (a) Winter, (b) Spring, (c) Summer, (d) Fall. The daily AOD values (red stars) and one-to-one line (blue) are denoted. The correlation coefficient (R) and sample size (N) are listed in the upper left corner. 59
Figure 44. Two-year distribution of 0.55μm NAAPS AOD values for Osaka and Shirahama in the Japan basin, for 2006-2007. The histogram of AOD values (blue bars) and cumulative frequency distribution (red curve) corresponding to the histogram are denoted. The sample size is listed in the upper right corner. The vertical lines (black), from left to right, denote the quartiles of the distribution, 25% (dashed), 50% (solid), 75% (dashed). 60

Figure 45. Annual scatter plot of daily AERONET and NAAPS AOD values for the Japan basin for 2006-2007. The daily AOD values (red stars) and one-to-one line (blue) are denoted. The correlation coefficient (R) and sample size (N) are listed in the upper left corner.....61
Figure 46. Japan Basin AERONET AOD (0.50μm) versus NAAPS AOD (0.55μm) scatterplots for the 2006-2007 seasons: (a) Winter, (b) Spring, (c) Summer, (d) Fall. The daily AOD values (red stars) and one-to-one line (blue) are denoted. The correlation coefficient (R) and sample size (N) are listed in the upper left corner. 62
Figure 47. Two-year distribution of 0.55μm NAAPS AOD values for Ilorin in the West Africa basin, for 2006-2007. The histogram of AOD values (blue bars) and cumulative frequency distribution (red curve) corresponding to the histogram are denoted. The sample size is listed in the upper right corner. The vertical lines (black), from left to right, denote the quartiles of the distribution, 25% (dashed), 50% (solid), 75% (dashed). 63
Figure 48. Annual scatter plot of daily AERONET and NAAPS AOD values for the West Africa basin for 2006-2007. The daily AOD values (red stars) and one-to-one line (blue) are denoted. The correlation coefficient (R) and sample size (N) are listed in the upper left corner. 64
Figure 49. West Africa Basin AERONET AOD (0.50μm) versus NAAPS AOD (0.55μm) scatterplots for the 2006-2007 seasons: (a) Winter, (b) Spring, (c) Summer, (d) Fall. The daily AOD values (red stars) and one-to-one line (blue) are denoted. The correlation coefficient (R) and sample size (N) are located in the upper left corner. 65
Figure 50. 14 May 2004 0630 UTC MODIS image for the Persian Gulf. Point 1 is a location with a low amount of dust, Point 2: moderate dust, and Point 3: high dust. 67
Figure 51. 14 May 2004 0730 UTC NOAA-17 image, 0.63μm, denoting retrieved AODs for the Persian Gulf basin (NRL-Monterey, 2009). Points 1, 2, and 3 are the same locations denoted in Figure 50. 69
Figure 52. Two-year distribution of AERONET AOD (0.44μm) values for Solar Village for 2006-2007. The histogram of AOD values (blue bars) and cumulative frequency distribution (red curve) corresponding to the histogram are denoted. The sample size is listed in the upper right corner. The vertical lines (black), from left to right, denote the quartiles of the distribution, 25% (dashed), 50% (solid), 75% (dashed). 73
Figure 53. Same as Figure 52, but for 0.50μm. 74
Figure 54. Same as Figure 52, but for 0.675μm. 74
Figure 55. Same as Figure 52, but for 0.870μm. 75
Figure 56. Solar Village AERONET AOD Cumulative Frequency Curves for 0.44μm, 0.50μm, 0.675μm and 0.870μm for 2006-2007. 75
Figure 57. One-year distribution of 0.50 μm AERONET AOD values for the Persian Gulf basin for 2006. The histogram of AOD values (blue bars) and cumulative frequency distribution (red curve) corresponding to the histogram are denoted. The sample size is listed in the upper right corner.

The vertical lines (black), from left to right, denote the quartiles of the distribution, 25% (dashed), 50% (solid), 75% (dashed). 77
Figure 58. Same as Figure 57, but for 2007. 78
Figure 59. Two-year Winter cumulative frequency curves for the Persian Gulf Basin for 2006-2007. The cumulative frequency curve for each individual station is compared with the cumulative frequency curve computed from the histogram distribution for the combined dataset of the three stations (red curve). 78
Figure 60. Same as Figure 59, but for Spring. 79
Figure 61. Same as Figure 59, but for Summer. 79
Figure 62. Same as Figure 59, but for Fall. 80
Figure 63. Two-year Winter cumulative frequency curves for Korea (blue) and Japan (red) for 2006-2007. 81
Figure 64. Same as Figure 63, but for Spring. 81
Figure 65. Same as Figure 63, but for Summer. 82
Figure 66. Same as Figure 63, but for Fall. 82
Figure 67. Two-year Winter cumulative frequency curves for the Japan Basin for 2006-2007. The cumulative frequency curve for each individual station is compared with the cumulative frequency curve computed from the histogram distribution for the combined dataset of the two stations (red curve). Here, no data is available from Osaka, so only Shirahama is shown. 83
Figure 68. Same as Figure 67, but for Spring. 83
Figure 69. Same as Figure 67, but for Summer. 84
Figure 70. Same as Figure 67, but for Fall. 84
Figure 71. One-year distribution of 0.50 μm AERONET AOD values for the Korea basin for 2006. The histogram of AOD values (blue bars) and cumulative frequency distribution (red curve) corresponding to the histogram are denoted. The sample size is listed in the upper right corner. The vertical lines (black), from left to right, denote the quartiles of the distribution, 25% (dashed), 50% (solid), 75% (dashed). 85
Figure 72. Same as Figure 71, but for 2007. 85
Figure 73. One-year distribution of 0.50 μm AERONET AOD values for the Japan basin for 2006. The histogram of AOD values (blue bars) and cumulative frequency distribution (red curve) corresponding to the histogram are denoted. The sample size is listed in the upper right corner. The vertical lines (black), from left to right, denote the quartiles of the distribution, 25% (dashed), 50% (solid), 75% (dashed). 86
Figure 74. Same as Figure 73, but for 2007. 86
Figure 75. One-year distribution of 0.44μm and 0.50μm AERONET AOD values for the West Africa basin for 2006. The histogram of AOD values (blue bars) and cumulative frequency distribution (red curve) corresponding to the histogram are denoted. The sample size is listed in the upper right corner. The vertical lines (black), from left to right, denote the quartiles of the distribution, 25% (dashed), 50% (solid), 75% (dashed). 87

Figure 76. Same as Figure 75, but for 2007. 88
Figure 77. Two-year Winter cumulative frequency curves for the West Africa Basin for 2006-2007. The cumulative frequency curve for each individual station is compared with the cumulative frequency curve computed from the histogram distribution for the combined dataset of the two stations (red curve). 88
Figure 78. Same as Figure 77, but for Spring. 89
Figure 79. Same as Figure 77, but for Summer....89
Figure 80. Same as Figure 77, but for Fall. 90
Figure 81. Winter distribution of AERONET AOD (0.44μm) values for station Djougou in the West Africa basin, for 2006-2007. The histogram of AOD values (blue bars) and cumulative frequency distribution (red curve) corresponding to the histogram are denoted, with AOD values ranging from 0 to 4. The vertical lines (black), from left to right, denote the quartiles of the distribution, 25% (dashed), 50% (solid), 75% (dashed). 90
Figure 82. Same as Figure 81, but for Spring. 91
Figure 83. Same as Figure 81, but for Summer....91
Figure 84. Same as Figure 81, but for Fall. 92
Figure 85. Two-year distribution of 0.55 μm MODIS AOD values for stations Solar Dhabi and Dhadnah in the Persian Gulf basin, for 2006-2007. The histogram of AOD values (blue bars) and cumulative frequency distribution (red curve) corresponding to the histogram are denoted. The sample size is listed in the upper right corner. The vertical lines (black), from left to right, denote the quartiles of the distribution, 25% (dashed), 50% (solid), 75% (dashed)....93
Figure 86. Seasonal cumulative frequency curves for the Persian Gulf basin MODIS (red) and AERONET (blue) AOD distributions for the 2006-2007 seasons: (a) Winter, (b) Spring, (c) Summer, (d) Fall. The y-axis indicates the cumulative probability of occurrence of an AOD. The x-axis indicates the AOD values....94
Figure 87. Two-year distribution of 0.55 μm MODIS AOD values for Anmyon in the Korea basin, for 2006-2007. The histogram of AOD values (blue bars) and cumulative frequency distribution (red curve) corresponding to the histogram are denoted. The sample size is listed in the upper right corner. The vertical lines (black), from left to right, denote the quartiles of the distribution, 25% (dashed), 50% (solid), 75% (dashed). 95
Figure 88. Seasonal cumulative frequency curves for the Korea basin MODIS (red) and AERONET (blue) AOD distributions for the 2006-2007 seasons: (a) Winter, (b) Spring, (c) Summer, (d) Fall. The y-axis indicates the cumulative probability of occurrence of an AOD. The x-axis indicates the AOD values....96
Figure 89. Two-year distribution of 0.55 μm MODIS AOD values for Shirahama in the Japan basin, for 2006-2007. The histogram of AOD values (blue bars) and cumulative frequency distribution (red curve) corresponding to the histogram are denoted. The sample size is listed in the upper right corner.

The vertical lines (black), from left to right, denote the quartiles of the distribution, 25% (dashed), 50% (solid), 75% (dashed). 97
Figure 90. Seasonal cumulative frequency curves for the Japan basin MODIS (red) and AERONET (blue) AOD distributions for the 2006-2007 seasons: (a) Winter, (b) Spring, (c) Summer, (d) Fall. The y-axis indicates the cumulative probability of occurrence of an AOD. The x-axis indicates the AOD values. 98
Figure 91. Two-year distribution of 0.55 μm MODIS AOD values for Ilorin in the West Africa basin, for 2006-2007. The histogram of AOD values (blue bars) and cumulative frequency distribution (red curve) corresponding to the histogram are denoted. The sample size is listed in the upper right corner. The vertical lines (black), from left to right, denote the quartiles of the distribution, 25% (dashed), 50% (solid), 75% (dashed). 99
Figure 92. Seasonal cumulative frequency curves for the West Africa basin MODIS (red) and AERONET (blue) AOD distributions for the 2006-2007 seasons: (a) Winter, (b) Spring, (c) Summer, (d) Fall. The y-axis indicates the cumulative probability of occurrence of an AOD. The x-axis indicates the AOD values. 100
Figure 93. One-year distribution of 0.55μm NAAPS AOD values for stations Solar Village, Dhabi and Dhadnah in the Persian Gulf basin, for 2006. The histogram of AOD values (blue bars) and cumulative frequency distribution (red curve) corresponding to the histogram are denoted. The sample size is listed in the upper right corner. The vertical lines (black), from left to right, denote the quartiles of the distribution, 25% (dashed), 50% (solid), 75% (dashed). 101
Figure 94. Same as Figure 93, but for 2007. 102
Figure 95. Seasonal distribution of 0.55μm NAAPS AOD values for the Persian Gulf basin, for 2006-2007. The seasons and their respective median values of the distribution are located in the upper right corner. The y-axis indicates the number of AOD samples per bin from 0 to 30, with the x-axis denoting AOD values at 0.55μm. 102
Figure 96. One-year distribution of 0.55μm NAAPS AOD values for Anmyon in the Korea basin, for 2006. The histogram of AOD values (blue bars) and cumulative frequency distribution (red curve) corresponding to the histogram are denoted. The sample size is listed in the upper right corner. The vertical lines (black), from left to right, denote the quartiles of the distribution, 25% (dashed), 50% (solid), 75% (dashed). 103
Figure 97. Same as Figure 96, but for 2007. 104
Figure 98. Seasonal distribution of 0.55μm NAAPS AOD values for the Korea basin, for 2006-2007. The seasons and their respective median values of the distribution are located in the upper right corner. The y-axis indicates the number of AOD samples per bin from 0 to 30, with the x-axis denoting AOD values at 0.55μm. 104
Figure 99. One-year distribution of 0.55μm NAAPS AOD values for Osaka and Shirahama in the Japan basin, for 2006. The histogram of AOD values

(blue bars) and cumulative frequency distribution (red curve) corresponding to the histogram are denoted. The sample size is listed in the upper right corner. The vertical lines (black), from left to right, denote the quartiles of the distribution, 25% (dashed), 50% (solid), 75% (dashed). 105
Figure 100. Same as Figure 99, but for 2007. 106
Figure 101. Seasonal distribution of 0.55μm NAAPS AOD values for the Japan basin, for 2006-2007. The seasons and their respective median AOD values of the distribution are located in the upper right corner. The y-axis indicates the number of AOD samples per bin from 0 to 30, with the x-axis denoting AOD values at 0.55μm. 106
Figure 102. One-year distribution of 0.55μm NAAPS AOD values for Ilorin in the West Africa basin, for 2006. The histogram of AOD values (blue bars) and cumulative frequency distribution (red curve) corresponding to the histogram are denoted. The sample size is listed in the upper right corner. The vertical lines (black), from left to right, denote the quartiles of the distribution, 25% (dashed), 50% (solid), 75% (dashed). 107
Figure 103. Same as Figure 102, but for 2007. 108
Figure 104. Seasonal distribution of 0.55μm NAAPS AOD values for the West Africa, for 2006-2007. The seasons and their respective median values of the distribution are located in the upper right corner. The y-axis indicates the number of AOD samples per bin from 0 to 30, with the x-axis denoting AOD values at 0.55μm. 108

THIS PAGE INTENTIONALLY LEFT BLANK

LIST OF TABLES

Table 1. MODIS/AERONET AOD Correlations for Persian Gulf basin for 2006-2007.....41

Table 2. MODIS/AERONET AOD Correlations for Korea basin for 2006-2007.....45

Table 3. MODIS/AERONET AOD Correlations for Japan basin for 2006-2007 48

Table 4. MODIS/AERONET AOD Correlations for West Africa basin for 2006-2007.....52

Table 5. MODTRAN^{TM}-Simulated TOA Radiance ($Wm^{-1}\mu m^{-1}sr^{-1}$) at 0.63μm as a function of AOD (red) and Surface Reflectance (%, blue).....67

Table 6. MODIS Top-of-the-Atmosphere Radiance Values for Points 1, 2, and 3 in Figure 50. Radiance units are $Wm^{-1}\mu m^{-1}sr^{-1}$ 68

Table 7. TOA Radiance ($Wm^{-1}\mu m^{-1}sr^{-1}$) from the MODIS image (Figure 50) and MODTRAN^{TM} simulation (Table 5) and the NOAA-17 AOD estimates from Figure 51. 69

THIS PAGE INTENTIONALLY LEFT BLANK

ACKNOWLEDGMENTS

This thesis was the culmination of lots of teamwork, assistance, and coordination involving the Naval Postgraduate School and the Naval Research Laboratory, Monterey. First, I would like to thank Professor Philip Durkee, Mary Jordan, and Kurt Nielsen of the Naval Postgraduate School for their hard work, dedication, and guidance. Second, I would like to thank Dr. Doug Westphal, Dr. Jianglong Zhang and the team at the Naval Research Laboratory for providing me with data, guidance, and support all throughout the thesis process. Third, thanks are due to Brent Holben at the Goddard Space Flight Center, whose AERONET data was used in this thesis.

Additionally, I wish to thank Professor Durkee for giving me the chance to present my thesis results at the February 2009 MEPIC Conference in Baltimore, MD. Thanks are also due to Mary Jordan for acting as a sounding board, helping me go through tons of data, and for working with me produce to literally thousands of charts over the past year.

Finally, I would like to thank Katie Wood for her patience and understanding of the work needed to complete the thesis process. Without her unwavering faith and support of me, this thesis would never have come to fruition.

THIS PAGE INTENTIONALLY LEFT BLANK

I. INTRODUCTION

A major problem for intelligence agencies that analyze satellite images is the interaction of aerosol particles with electro-optical propagation. If atmospheric aerosols obscure a target scene, image analysts will likely face difficulty in characterizing the target. As a result, depending on the aerosol contamination, satellite images may need some correction in order to be useful to the intelligence community.

An example satellite image with aerosol contamination is shown in Figure 1. The figure displays an RGB satellite image of Iraq taken by the NOAA-17 satellite on 26 March 2003 (0718UTC). A large dust storm covers much of southwestern Iraq, making target detection and target characterization difficult in this region. The degree of difficulty in target detection and characterization depends on the aerosol optical depth.

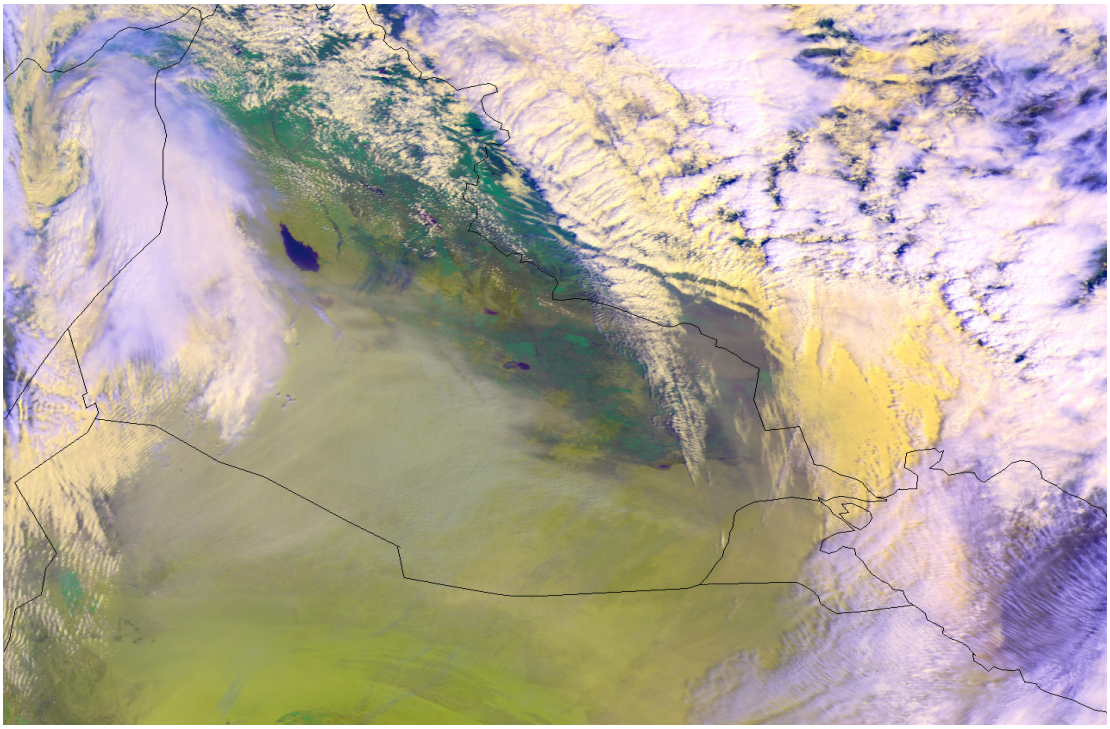

Figure 1. NOAA-17 RGB Satellite Image from 0718UTC, 26 March 2003. A large dust storm is present over southwestern Iraq (From NOAA News Online, Story 1120, 2009)

The analyst must be able to correct for any obscurations covering the target, in this case aerosols, in order to properly detect and characterize a target. Previous studies by have used Aerosol Robotic Network (AERONET) aerosol optical depth (AOD) data as "ground-truth", indicating that AERONET sites reliably provide AOD data (Zhang et al., 2006, 2008). Unfortunately, targets are not likely to be located near an AERONET site. Previous research by Misra et al. (2008), Chu et al. (2002), and Zhang et al. (2006) shows that polar orbiting satellite instruments such as the Moderate Resolution Imaging Spectroradiometer (MODIS) can also provide high quality AOD data for a target. However, satellite-retrieved AOD data is only available at the times that the satellite sensor passes over the target, which for MODIS is only twice daily during daylight hours. That leaves most targets with 22 hours per day for which no AOD data is available. The Navy Aerosol Analysis and Prediction System (NAAPS), an aerosol model, provides another assessment of AOD for targets, which may be useful when no other AOD data is available.

This thesis will first establish an AERONET AOD climatology using MODIS-retrieved and NAAPS-modeled AOD values and compare these techniques against AERONET AOD measurements. The AERONET AOD climatology will show the annual and seasonal variability for aerosol loading for each of the four basins: Persian Gulf, Korea, Japan, and West Africa. The comparison of these techniques against AERONET AOD measurements will test if each technique can be useful as a proxy for AERONET AOD measurements.

Finally, this thesis describes a radiance-based target detection matrix. To properly use this matrix, an image analyst needs information about the target and background reflectance (as a function of wavelength), and also the AOD. The radiance-based target detection matrix will help an image analyst determine whether or not a target can be detected and characterized, given an AOD and target/background reflectance as functions of wavelength.

II. BACKGROUND

A. AEROSOLS, SCATTERING, AND THE VISIBLE SPECTRUM

The focus of this thesis is visible solar radiation reflected from the Earth's surface. Before reaching the satellite, reflected solar radiation can undergo (in many directions) three processes within the atmosphere: the radiation can be absorbed, scattered by gas molecules and particles (e.g. aerosols, cloud droplets), and/or transmitted directly to the satellite. Kidder and Vonder Haar (1999) noted that the amount of reflected solar radiation by a particle is a function of: particle shape, particle size, particle index of refraction, wavelength of radiation, and viewing geometry. Additionally, in 1908, Gustav Mie showed that the scattered radiation is a function only of viewing angle, index of refraction, and the size parameter (Kidder 1999). The size parameter is defined as (equation 3.49 from Kidder and Vonder Haar):

$$\chi \equiv \frac{2\pi r}{\lambda}$$

where χ is the size parameter, r is the radius of the scattering particle, and λ is the wavelength of the radiation. The size parameter can then be used to divide scattering regimes into three types: Rayleigh, Mie, and Geometric. Mie scattering is the focus of this thesis because the study of aerosols (smoke, dust, haze) using the visible spectrum falls within the Mie regime.

Aerosol optical depth (AOD) describes the reduction of photons transmitted through the atmosphere due to interactions (i.e., scattering, absorption) with aerosols. AOD is a dimensionless quantity, and is a function of wavelength. Kidder and Vonder Haar (1999) define optical depth as (equation 3.28 from Kidder and Vonder Haar):

$$\delta\lambda(z_1, z_2) \equiv \int_{z1}^{z2} \sigma_e(\lambda, z)dz$$

where $\delta\lambda$ is the AOD for the vertical layer extending from z_1 to z_2. The right side of Equation 2 is the vertically integrated volume extinction coefficient (σ_e) as a function of

wavelength for the layer. An increase in volume extinction coefficient is indicative of increased scattering and/or absorption by aerosol particles. Thus, AOD increases as scattering and/or absorption increases. An increase in scattering/absorption occurs when more aerosol particles are in the layer, thereby increasing the probability of photon interaction with aerosol particles.

Figure 2 illustrates the top of the atmosphere radiance problem. The top of the atmosphere solar irradiance is denoted as E_0, and the solar irradiance at the Earth's surface is represented by E_s. The top of the atmosphere irradiance is greater than the amount of solar irradiance at the Earth's surface due to scattering and/or absorption of the irradiance as the photons pass through the atmosphere. The radiance reflected by the target is L_t, and the radiance reflected by the background is L_b. The amount of radiance reflected by the target and background is a function of wavelength and surface characteristics (i.e., surface color).

Photons reflected by the surface can be absorbed or scattered in many directions as they pass through the atmosphere on the way to the satellite. In order for a satellite-borne sensor to distinguish a target from its background, the difference between the target and background top of the atmosphere radiance (ΔL_T) must be greater than the sensor radiance sensitivity (ΔL_s). The difference between the target and background top of the atmosphere radiance is defined by the following equation (Durkee 2009):

$$\Delta L_T = L_{tT} - L_{bT} = (L_t - L_b)e^{-\delta}$$

The top of the atmosphere radiance from the target, L_{tT}, is the transmitted radiance reflected by the target surface and the path radiance. The top of the atmosphere radiance from the background, L_{bT}, is the transmitted radiance reflected by the background surface and the path radiance. Aerosol concentration (i.e., AOD) is important because high aerosol concentrations over a target can increase the amount of scattering and/or absorption of photons reflected by the target, thereby reducing the contrast between the target and its background. Reduced target/background contrast lowers the probability that a satellite sensor will distinguish between the target and background.

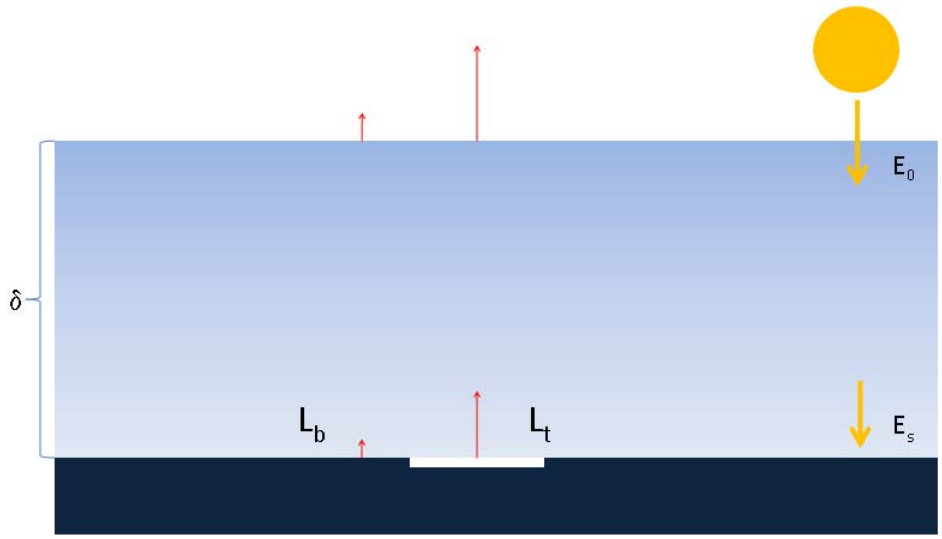

Figure 2. Radiance received by a satellite at the top of the atmosphere, with top of the atmosphere irradiance (E_0), solar irradiance at the Earth's surface (E_s), optical depth (δ), and reflected radiance by the target (L_t) and background (L_b) noted above. (From Durkee February 2009)

B. TROPOSPHERIC DUST AND SMOKE CLIMATOLOGY

Climatology narratives are included to describe seasonal variations in weather patterns for the Persian Gulf, East Asia, and West Africa. The following narratives are paraphrased from the climatology narratives produced by the Fourteenth Weather Squadron in Asheville, NC.

1. Persian Gulf

The climate of the Persian Gulf, specifically that of Saudi Arabia and the United Arab Emirates (UAE), has characteristics of a monsoon climate, because the area falls under the influence of the Near Equatorial Tradewind Convergence (NETWC) zone. The NETWC boundary stays south of the UAE, so the prevailing year-round wind flow for this region is north-northwesterly. The strength of the flow varies depending on the time of year, which effectively leads to two seasons: Winter and Summer.

The Winter season covers November through April. During Winter, restrictions to visibility occur due to the presence of dust, sand, haze, and fog (along the coast). Overall, blowing sand and dust reduces surface visibilities below seven miles approximately three times per month. However, if the flow is stronger and the dust/sand is lofted higher in the atmosphere, visibilities can be reduced for days at a time, which can hinder target detection for satellite-borne sensors.

The Summer season extends from May through October. Flow remains north-northwesterly, with prevailing surface visibilities between four and seven miles in dust, sand, or haze. Stronger flow over northern Saudi Arabia can loft so much dust into the atmosphere that the dust remains suspended for weeks at a time, further hindering target detection for satellite sensors. Often accompanying the strong northwesterly flow is a low-level Persian Gulf jet, which further enhances the amount of dust lofted over the western Persian Gulf.

Shamal winds can occur anytime during the year but are especially common during the Summer months. Shamal winds are strong northwesterly wind events that originate over the Tigris-Euphrates lowlands in Iraq. Shamal events often carry large amounts of dust and sand, lasting for periods of one to five days. However, some long lived Shamal wind storms have lasted 40 days during the summer, which can play havoc with attempts to image targets via satellite over this region. Consequently, Summer is the season with the heaviest aerosol loading over the Persian Gulf.

2. East Asia

Korea and Japan experience four distinct seasons. The first season is Winter, which stretches from November through March. During Winter, the Asiatic high over China builds in November, reaches peak strength in January, and weakens in March, with predominately northwesterly flow. The Asiatic high is the dominating feature over East Asia during the winter. Consequently, cold, dry, continental polar air flows southward from China over Korea and Japan. Clear skies and little restriction to visibility are the main results of the influence of the Asiatic high. Occasionally, however, dust storms (Yellow Wind) from China and Mongolia reduce visibility over Korea and Japan.

Yellow Wind events occur one to two times a month from December through February and two to three times per month during March, though less frequently over Japan. Smog around the cities also reduces surface visibilities during the morning. Both Yellow Wind events and smog hinder surface visibility and can negatively impact the ability of satellite sensors to detect a target on the ground.

Spring only lasts from April through May, and is the transition between the clear, cold, dry Winter season to the cloudy, warm, wet summer season. During Spring, northwesterly flow begins to weaken as the Asiatic high weakens and is displaced northwards. Also, more frontal systems move over East Asia and the flow becomes westerly. Consequently, as frontal passages become more common, so does the frequency of Yellow Wind events, especially in April, which hinders surface visibility and target detection. Again, as in winter, smog around the cities also reduces surface visibilities in the morning hours.

Summer over East Asia extends from June until mid-September. Summer is the cloudy, warm, and wet season, with the weather largely determined by the position of the monsoon frontal boundary. The monsoon frontal boundary separates the moist, warm, maritime tropical air mass from the cooler, dry, continental air mass, and brings with it lots of precipitation, cloud cover, and fog. Restrictions to visibility during the Summer months are predominately due to clouds, precipitation, and fog rather than smog and dust.

Fall covers mid-September to November and is the transition season from the cloudy, warm, wet summer season to the clear, cold, dry winter season. As the Asiatic high re-establishes itself, the flow becomes more westerly and the number of days with clouds and precipitation begins to decrease. Fog and smog are the main restrictors to surface visibility during the Fall season.

3. West Africa

The climate of Benin and Nigeria is governed by the position of the monsoon trough. The monsoon trough in this region is better known as the NETWC zone. The NETWC separates the hot, dry, continental air mass that dominates the Sahara from the

warm, moist, maritime air mass that dominates the tropics. As the NETWC moves north or south, so do these air masses, giving rise to two seasons for Benin and Nigeria. These seasons are the dry season and the wet season.

The dry season spans November through March, roughly Northern Hemisphere winter. During the dry season, the NETWC moves south towards the coastline of these two countries, and this ushers in dry Harmattan winds. Harmattan winds are northerly winds that carry Saharan dust and sand southward, which lowers visibility and obscure targets from satellite observation. In fact, Harmattan winds can reduce visibilities to one-half mile up to altitudes of 12,000 feet, though more often visibility is restricted to less than three miles up to altitudes of 8,000 feet. Consequently, the dry season is the time of year that aerosol loading is heaviest over West Africa.

The wet season spans April through October, roughly Northern Hemisphere summer. During the wet season, the NETWC moves north of Benin and Nigeria, which allows the prevailing flow to turn south-southwesterly. As the flow becomes more southerly, warm, moist, maritime air is brought into the area. Thus, any restrictions to visibility and target detections are primarily due to clouds, precipitation, and/or fog.

In addition to sand and dust, biomass burning is another source of aerosols in West Africa that can reduce visibility and target detection. Biomass burning is especially common in the savanna region, where land is burned after harvest, usually at the end of the rainy season (NASA 2009).

III. DATA AND METHODOLOGY

A. AEROSOL ROBOTIC NETWORK (AERONET)

1. Network Description

AERONET is a network of ground-based sun photometers established by NASA and the French National Center for Scientific Research (CRNS) in collaboration with many universities and agencies worldwide. The purpose of this network is to provide standard, continuous, and long-term worldwide measurements of aerosol optical depths, inversion products, and aerosol regimes. The AERONET sun photometers measure the intensity of direct sunlight and directional sky brightness throughout nine bands from 0.34μm (UV) to 1.64μm (near IR). Data are then relayed by satellite to the NASA Goddard Space Flight Center, where it is quality controlled and processed into the products listed above. For this thesis, Level 2 data are used as ground truth for eight AERONET sites throughout the West Africa, Persian Gulf, and East Asia basins. Level 2 data are the highest quality data, as a result of being both cloud screened and quality assured. AERONET AOD data has an uncertainty of 0.01 to 0.02 in AOD (GFSC 2009).

2. Site Selection

The first consideration in choosing AERONET sites for this study is the availability of Level 2 AERONET data. Data prior 2006 are not available for the AERONET sites used in this thesis. The 2006-2007 period provides sufficient data for comparisons with NAAPS and MODIS. For the Persian Gulf basin, Level 2 AERONET AOD data are available on 80% of the days during the two-year period (2006-2007). Level 2 AERONET AOD data are available only on 30% and 43% of the days for the Korea and Japan basins, respectively. For the West Africa basin, data are available on 68% of the days during the two-year period (2006-2007).

The second consideration in choosing AERONET sites for the thesis is the proximity of the AERONET sites to the coast. The MODIS AOD data used in this study is over-ocean data. In order to have valid comparisons between the AERONET and MODIS AOD data, AERONET sites need to be close to the coast. Of the eight AERONET sites this thesis includes, five of them are located along the coast. The coastal AERONET sites are: Dhabi, UAE, Dhadnah, UAE, Anmyon, South Korea, Osaka, Japan, and Shirahama, Japan. The inland AERONET sites are: Solar Village, Saudi Arabia, Djougou, Benin, and Ilorin, Nigeria.

The locations of the AERONET sites throughout the four basins are identified in Figures 3, 4 and 5. Figure 3 displays the locations of AERONET sites in the Persian Gulf basin. The Dhabi and Dhadnah AERONET sites are along the coast, while Solar Village is approximately 417 km inland. Figure 4 displays the locations of AERONET sites in East Asia. All of the East Asian AERONET sites used in this study are located along the coast. Figure 5 displays the locations of the AERONET sites in the West Africa basin. Both of the West African AERONET sites are considerably inland from the Gulf of Guinea, with Ilorin and Djougou approximately 217 km and 400 km inland, respectively.

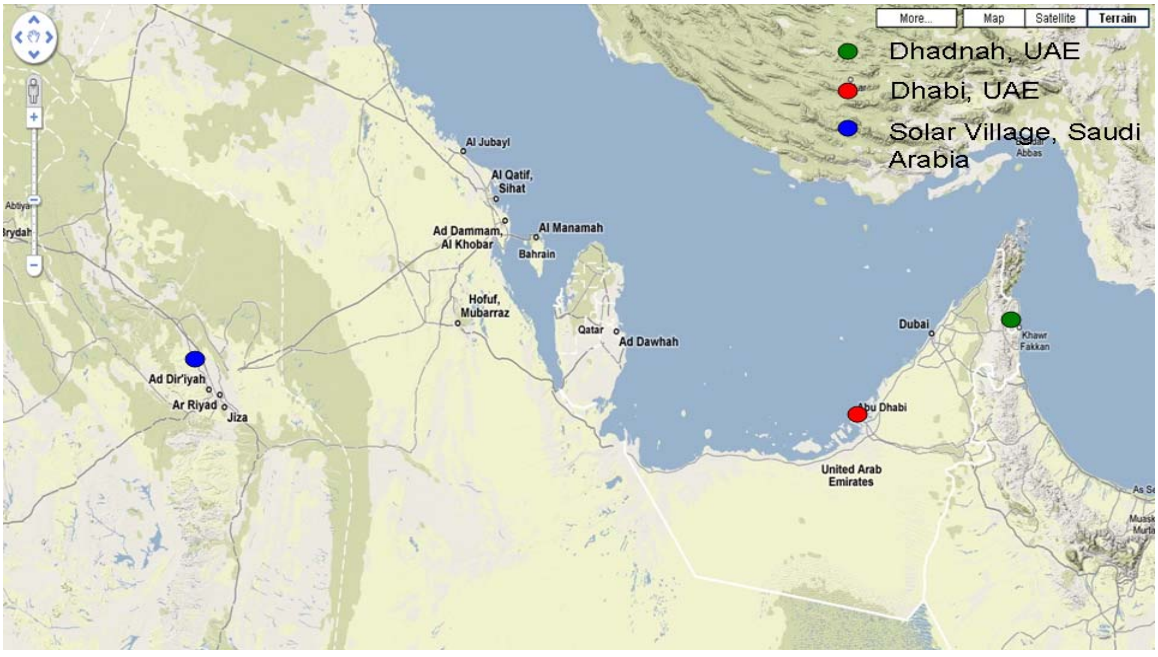

Figure 3. Three Persian Gulf AERONET sites used in this study (From Google Maps February 2009).

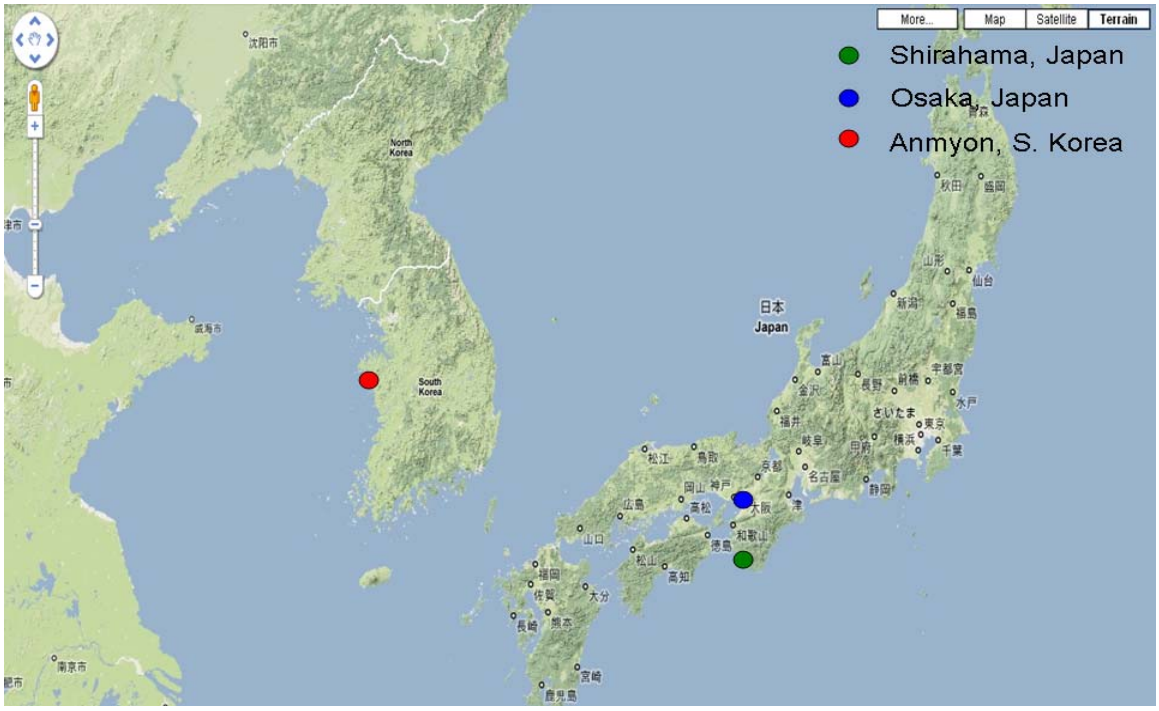

Figure 4. Three East Asia AERONET sites used in this study (From Google Maps February 2009).

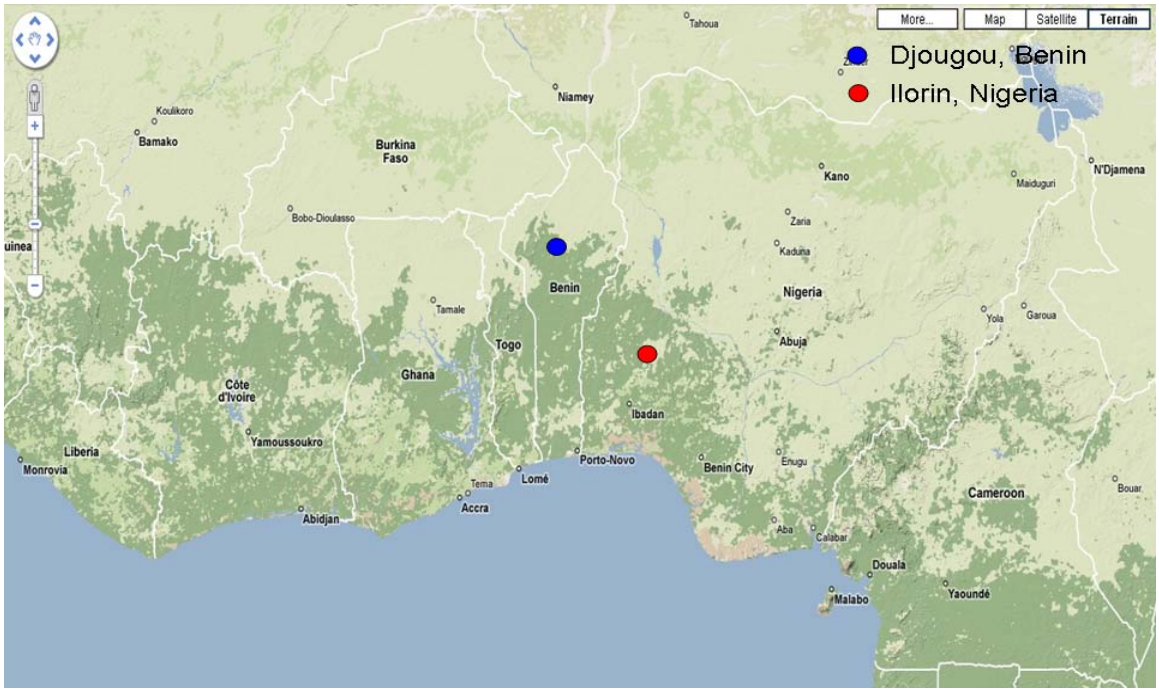

Figure 5. Two West Africa AERONET sites used in this study (From Google Maps February 2009).

3. AERONET Wavelength Variability

The NAAPS and MODIS AOD values are retrieved at 0.55μm. However, no AOD data at 0.55μm are available at any of AERONET sites. AERONET AOD data are typically available at 0.34μm, 0.38μm, 0.44μm, 0.50μm, 0.675μm, 0.87μm, 1.02μm, and 1.675μm. This thesis compares the NAAPS and MODIS AOD data to the 0.50μm, AERONET AOD data, the closest available ground-truth wavelength (note: 0.44μm wavelength is used for Djougou, since no 0.50μm AOD data are available). Figure 61 (Appendix A) displays the differences in AOD distributions by wavelength for Solar Village. Differences in AOD values between the wavelengths are small. For example, at an AOD of 0.40, the cumulative frequencies at 0.50μm and 0.675μm are 72% and 78%, respectively, only a 6% difference. Therefore, this study will use AERONET AOD measurements at 0.50μm as a proxy for AOD measurements at 0.55μm.

B. MODERATE RESOLUTION IMAGING SPECTRORADIOMETER (MODIS)

1. MODIS Data Description

MODIS is a key part of the mission of the NASA EOS program. The MODIS sensor flies on two satellites (Aqua and Terra) that together provide global coverage over a one to two day time period. Each satellite is located at an altitude of 705km, has a view swath width of 2,330km, and scans the Earth across 36 spectral bands, ranging from 0.405 to 14.385μm. Terra follows a descending orbital path, passing over the Equator at 1030LT (Local Time), while Aqua follows an ascending orbital path, passing over the Equator at 1330LT. With one morning and one afternoon pass over the same area, it is possible to detect changes in the atmosphere that occur during the day, in addition to minimizing the effects of sun-glint and shadows at the surface (GFSC 2009).

The Naval Research Laboratory, Monterey, CA, retrieves aerosol optical depth using the MOD04/MYD04 algorithm for the 0.55μm (green) spectral band (Zhang et al. 2006). The MOD04/MYD04 algorithm retrieves over-ocean AOD values and bins the

AOD values into 1° x 1° latitude/longitude grids, and does not retrieve AOD over land (Zhang et al. 2008). The MODIS AOD grid point value is the mean of the values in the 1° x 1° box. This thesis uses daily mean over-ocean AOD values retrieved by NRLMRY for 2006-07. Clouds and sun glint prevent an AOD retrieval. The NRL dataset, therefore, does not provide a daily mean value for every grid point. The uncertainty associated with the MODIS derived aerosol optical depths is $0.03 \pm 0.05\delta$ (Remer et al. 2005).

2. MODIS Climatology

Histograms of MODIS AOD are prepared for each basin for the two-year period and for each season. Clouds and sun glint prevent a daily mean AOD value to be available at the grid point closest to an AERONET station. Therefore, AOD data from several grid points near each AERONET site are used to build the MODIS AOD climatology histograms for each basin. The MODIS histograms will be compared with the AERONET histograms by basin.

3. MODIS/AERONET Comparison Methodology

In addition to comparing MODIS and AERONET basin histograms, point-to-point MODIS/AERONET comparisons are made. The first step is to make sure that the MODIS and AERONET data are matched in space. The MODIS grid point that is closest to the AERONET site is selected. The second step is to make sure that the MODIS and AERONET data are matched in time for each site. To match the time of MODIS overpasses (approximately 1030 and 1330L), AERONET measurements from 1000L to 1400L are used to calculate a mean AERONET AOD value. The daily mean MODIS AOD value is then compared with the mean AERONET AOD value for each day over the two-year period to produce seasonal and annual scatter plots.

There are days when AERONET measurements are not taken, because of cloud cover, malfunctioning equipment, etc. Additionally, there are some days for which MODIS data is unavailable. If either AERONET or MODIS data is unavailable for a specific day, that day is not included in this study.

4. MODIS Grid Locations

Figure 6 illustrates the MODIS AOD grid points in the Persian Gulf basin which are close to AERONET sites Dhabi, UAE, and Dhadnah, UAE. MODIS grid points are the numbered. The 13 grid points are used to create the Persian Gulf basin MODIS AOD climatology histograms. For the point-to-point MODIS/AERONET comparisons, MODIS AOD data from Grid Point 1 (red) in the Persian Gulf is compared to AERONET AOD data from Dhabi and MODIS AOD data from Grid Point 1 (green) in the Gulf of Oman are compared to AERONET AOD data from Dhadnah. Data from the Solar Village, Saudi Arabia AERONET site are not included because the AERONET site is too far inland (417 km) to have a valid comparison with over-ocean MODIS data.

Figure 7 illustrates the MODIS grid points for the Korea and Japan basins which are close to Anmyon, S. Korea and Shirahama, Japan AERONET sites. The nine numbered grid points (red) are used to create the Korea basin MODIS AOD climatology histograms, while the six numbered grid points (green) are used to create the Japan basin histograms. For the point-to-point MODIS/AERONET comparisons, MODIS data from Grid Point 1 (red) are compared to AERONET data from Anmyon to produce the Korea scatter plots. Similarly, MODIS data from Grid Point 1 (green) are compared to AERONET data from Shirahama to produce the Japan scatter plots. Data from the Osaka (Japan) AERONET site are not included due to its small dataset for 2006-2007.

Figure 8 illustrates the MODIS grid points for the West Africa basin which are closest to the Ilorin, Nigeria AERONET site. The 10 numbered pixels are used to create the West Africa basin MODIS AOD climatology histograms. MODIS AOD data from grid point 4 are compared to AERONET AOD data from Ilorin to produce the West Africa scatter plots. Data from the Djougou, Benin AERONET site are not included because the AERONET site is far too inland (400 km) to make any valid comparisons with over-ocean MODIS data.

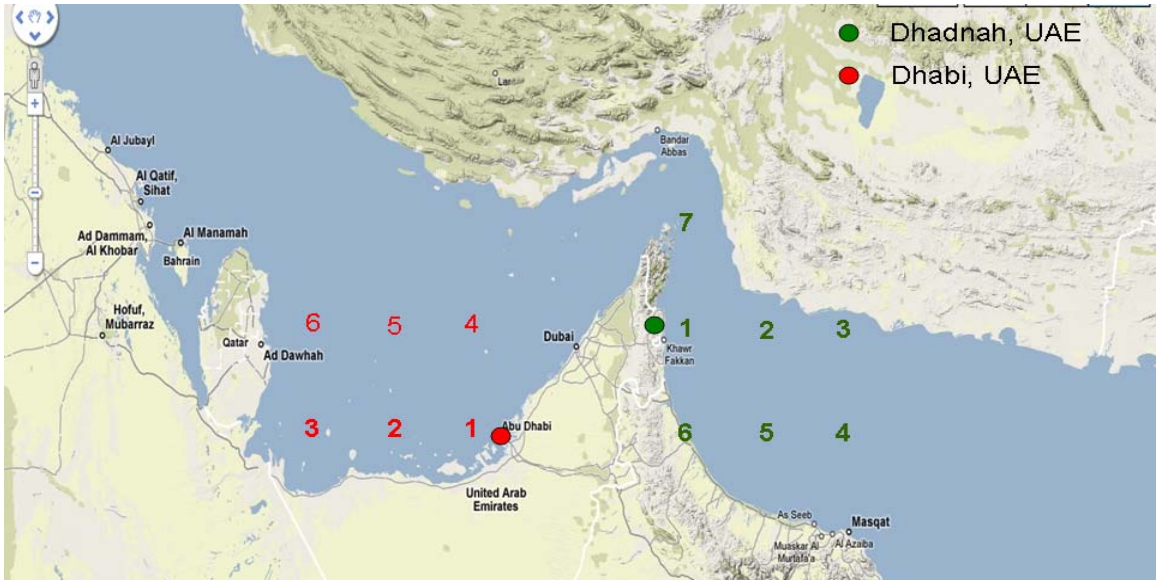

Figure 6. MODIS grid points and AERONET sites used for the Persian Gulf basin, MODIS/AERONET comparison. The numbers denote MODIS grid points, and the AERONET sites are denoted by filled circles. The six grid points in red are used to represent the over-water region near Dhabi (red circle). The seven grid points in green are used to represent the over-water region near Dhadnah (green circle) (From Google Maps February 2009).

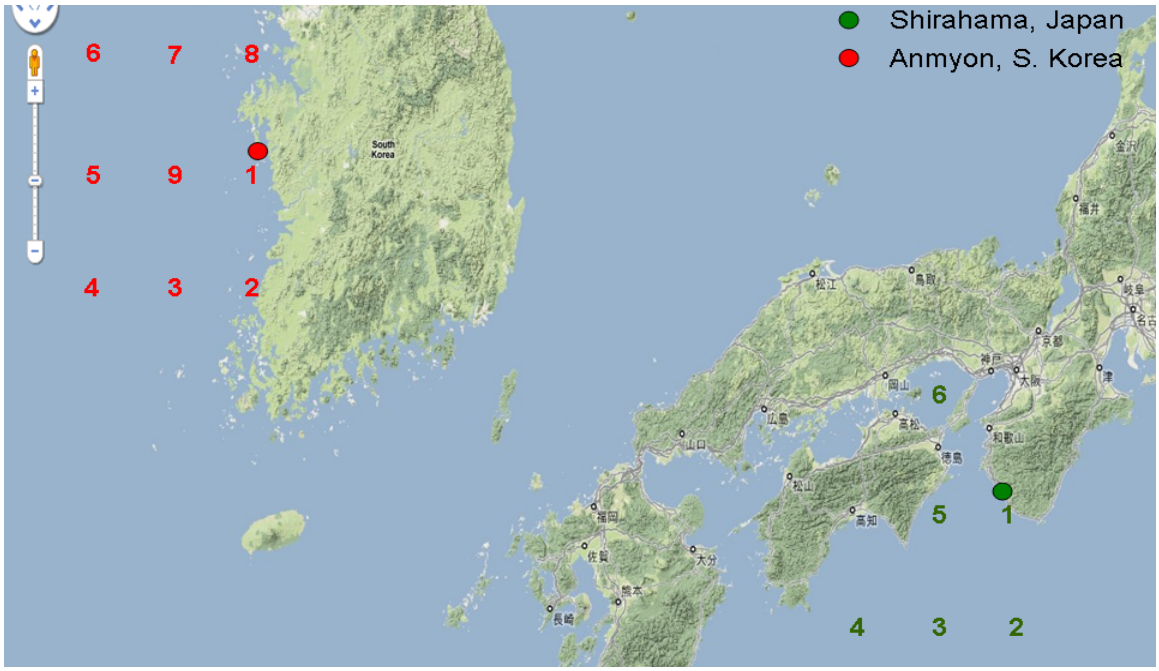

Figure 7. Same as Figure 6, but for the Korea (red) and Japan (green) basins. The AERONET sites are denoted by filled circles (From Google Maps February 2009).

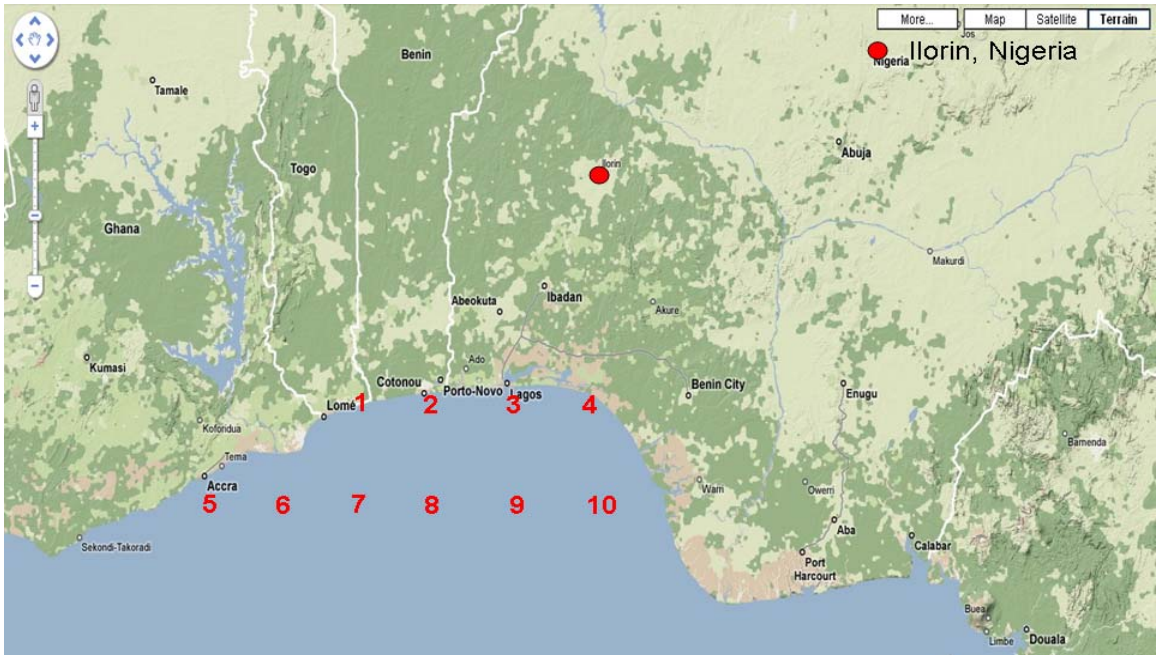

Figure 8. Same as Figure 6, but for West Africa. The AERONET site (Ilorin) is denoted by the red circle (From Google Maps February 2009)

C. NAVY AEROSOL ANALYSIS AND PREDICTION SYSTEM (NAAPS)

1. NAAPS AOD Description

NAAPS is the model developed by the Naval Research Laboratory (NRL) in Monterey, CA, and is used to predict the distribution of tropospheric aerosols. NAAPS uses the Navy Operational Global Atmospheric Prediction System (NOGAPS) to provide global meteorological fields. Twice daily, NAAPS produces analyses and forecasts of aerosol concentrations at six hour intervals for a five-day forecast period on 1° x 1° latitude/longitude grids (NAAPS 2009 and Zhang et al. 2008). Aerosol optical depth is not directly calculated by NAAPS. Aerosol optical depth is produced by the Forecast of Aerosol Radiative Optical Properties (FAROP) optical model. NAAPS uses the FAROP optical model as a post-processor, which takes the aerosol concentration data from NAAPS model runs and computes optical properties of aerosols, i.e., aerosol optical depth.

This thesis uses the AOD product produced from NAAPS with assimilated over-ocean MODIS AOD data using the Navy Atmospheric Variational Data Assimilation System (NAVDAS). NAVDAS assimilates over-ocean MODIS AOD data at 0.55μm by first mapping the MODIS data to 1° x 1° grids. To prevent AOD errors introduced by the presence of clouds, two quality control procedures are applied to the MODIS AOD data. First, when the cloud fraction is larger than 30% for a grid box, the grid point is excluded from the dataset. Second, bins with less than five data entries and bins isolated from continuous aerosol features are removed (Zhang et al. 2008).

The NAAPS AOD product used in this thesis is an analysis on a 1° x 1° grid at 00, 06, 12 and 18 UTC for each day in 2006-07. NAAPS AOD values are available for over-ocean points only. There is a NAAPS AOD grid point within 30km of AERONET sites Dhabi, UAE, Anmyon, South Korea, Osaka and Shirahama, Japan. The closest grid point to AERONET site Dhadnah, UAE, is 1.0° longitude due east of the site. The Ilorin, Nigeria AERONET site is inland from the coast. The over-ocean NAAPS AOD grid point used to compare with Ilorin is 2.8° latitude due south of the AERONET site. The NAAPS AOD product provides an AOD value for each over-ocean grid point at each analysis time. The NAAPS AOD grid point closest to the six AERONET sites will be used in annual and seasonal histograms and also in point-to-point comparisons with AERONET. Two AERONET sites, Djougou, Benin, and Solar Village, Saudi Arabia, are not included in the NAAPS/AERONET comparisons because both sites are too far inland.

2. NAAPS/AERONET Comparison Methodology

Histograms of NAAPS AOD are prepared for each basin for the two-year period and for each season. In addition to comparing NAAPS and AERONET basin histograms, point-to-point NAAPS/AERONET comparisons are made. For each AERONET site, a daily mean AERONET AOD value is computed. Using the closest NAAPS grid point to each AERONET site, the daily mean NAAPS AOD value is also computed. On days when both AERONET and NAAPS daily mean values are available, a point-to-point comparison is performed.

D. RADIANCE-BASED TARGET DETECTION

1. MODTRAN ™ Model Runs

MODTRAN™ is the U.S. Air Force moderate spectral resolution radiative transport model for wavelengths in the ultraviolet to thermal IR. In this thesis, MODTRAN™ is used to compute the top-of-the-atmosphere (TOA) radiance for an input vertical profile of atmospheric temperature, moisture and dust aerosols typical of a desert environment. The surface reflectance is an input to MODTRAN™. To simulate ground-based targets of different reflectance characteristics, multiple MODTRAN™ runs are made, each with a different surface reflectance value and the same amount of dust aerosols. To simulate the radiative effects of different aerosol loading, multiple MODTRAN™ runs are made, each with a different amount of dust aerosols and the same surface reflectance. In all, the MODTRAN™ model is run 260 times with different surface reflectance values and dust aerosol loading. The model runs simulate the TOA radiance expected to be detected by a satellite sensor for AOD values ranging from 0.0-3.5 and surface reflectance values ranging from 0-99%.

2. MODTRAN™ Radiance Comparison with MODIS Imagery

This study compares MODTRAN™ TOA radiance estimates with TOA radiance in MODIS imagery. The MODIS radiance values are treated as ground truth for the comparison. The purpose of the MODTRAN/MODIS comparison is to establish the reliability MODTRAN™ TOA radiance values. Then, MODTRAN™ can be used to create a radiance-based target detection matrix. Results of this analysis are discussed in Chapter IV, Section D.

IV. RESULTS

A. AERONET CLIMATOLOGY

1. Basin Composite

This thesis establishes a basin composite AERONET climatology. The purpose is to determine how the different geographic regions rank in terms of aerosol optical depth. First, this study needs to determine if there are any significant differences in the basin composite AERONET AOD distributions for 2006 and 2007. Figure 9 is the one-year AERONET AOD (0.50μm) distribution for 2006 using data from the Persian Gulf, Korea, Japan, and West Africa basins. The figure contains both a histogram of AOD values and cumulative frequency distribution corresponding to the histogram. Half of the AOD distribution lies between values of 0.21 and 0.56, with the median of the distribution at 0.35.

Figure 10 is the one-year AERONET 0.50μm wavelength AOD distribution for 2007 using data from the four basins of interest. The figure contains both a histogram of AOD values and cumulative frequency distribution corresponding to the histogram. Half of the AOD distribution lies between values of 0.21 and 0.59, with the median of the distribution at 0.39.

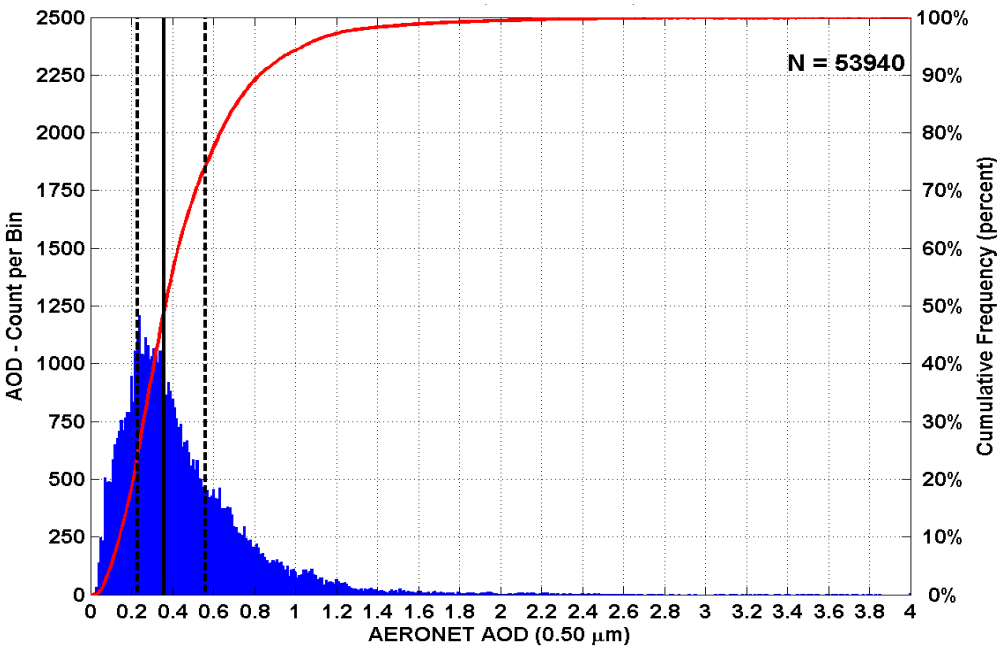

Figure 9. One-year distribution of basin composite AERONET AOD (0.50μm) values for the Persian Gulf, Korea, Japan, and West Africa basins, for 2006. The histogram of AOD values (blue bars) and cumulative frequency distribution (red curve) are denoted. The sample size is listed in the upper right corner. The vertical lines (black), from left to right, denote the quartiles of the distribution, 25% (dashed), 50% (solid), 75% (dashed).

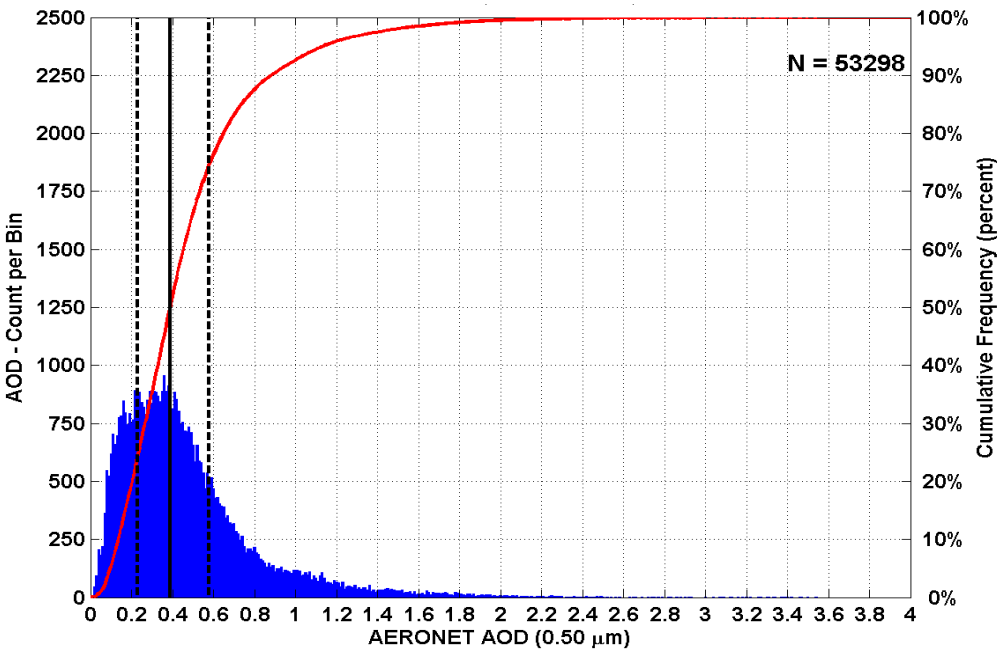

Figure 10. Same as Figure 9, but for 2007.

Figure 11 illustrates the differences between the AERONET AOD distributions for 2006 and 2007. The cumulative frequency curve for each individual year is shown. The cumulative frequency curve for 2006 closely mirrors the cumulative frequency curve from 2007, indicating no significant differences in the distributions for each year. Therefore, the 2006 and 2007 AERONET AOD datasets can be safely combined to produce a basin composite AOD climatology.

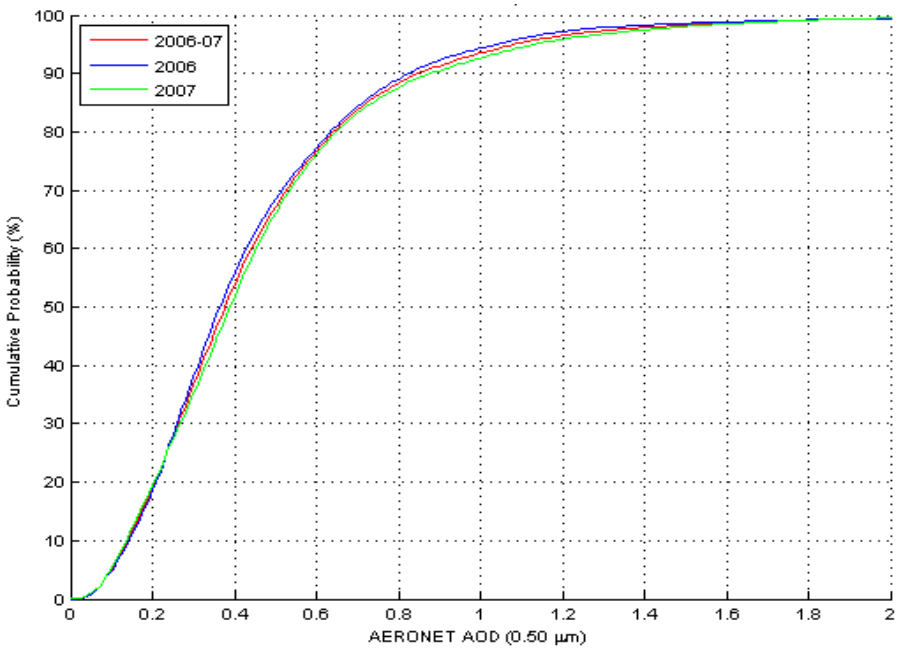

Figure 11. Cumulative frequency curves for the basin composite climatology for 2006-2007. The cumulative frequency curves for 2006 (blue) and 2007 (green) are are computed from the distribution for each year. The combined cumulative frequency curve (red) is computed from the combined dataset from both years.

Figure 12 is the two-year composite AERONET 0.50µm AOD distribution for 2006-2007 using AERONET AOD data from the four basins. The figure contains both a histogram of AOD values and cumulative frequency distribution corresponding to the histogram. Half of the AOD distribution lies between AOD values of 0.21 and 0.59, with the median of the distribution at 0.38. In 6% of the cases, AOD values are greater than 1.0.

To demonstrate why the 2006-2007 distribution could be useful for an image analyst, assume an AOD equal to or greater than 0.50 makes an image uncorrectable. Figure 12, therefore, suggests that aerosol loading may be light enough to allow for scene correction in approximately 65% of the cases.

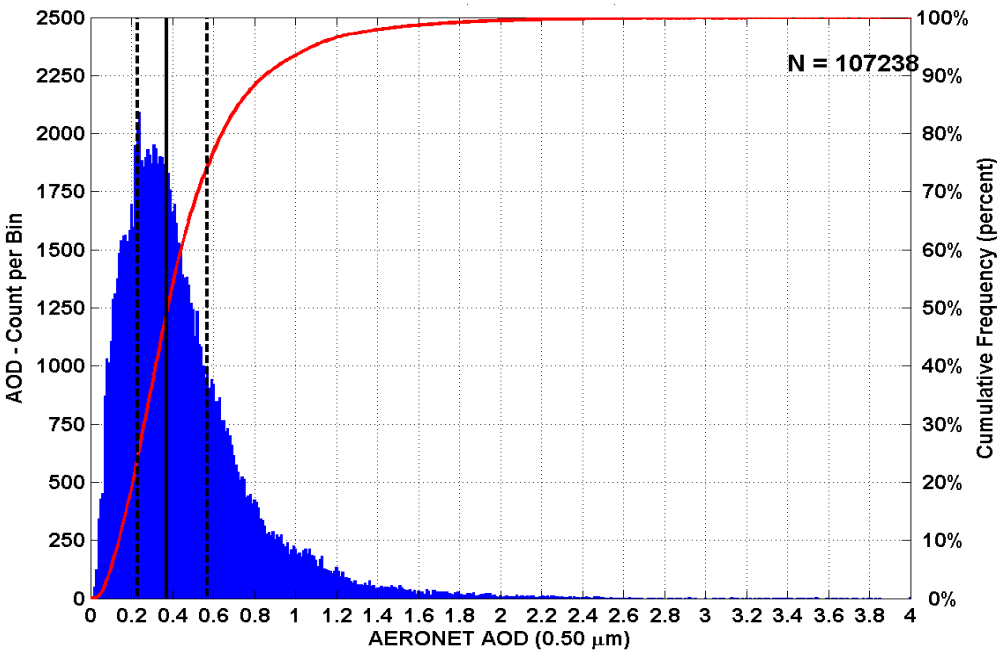

Figure 12. Two-year distribution of basin composite AERONET AOD (0.50μm) values for the Persian Gulf, Korea, Japan, and West Africa basins, for 2006-2007. The histogram of AOD values (blue bars) and cumulative frequency distribution (red curve) are denoted. The sample size is listed in the upper right corner. The vertical lines (black), from left to right, denote the quartiles of the distribution, 25% (dashed), 50% (solid), 75% (dashed).

In terms of relative contributions to the composite dataset, the Persian Gulf ranks first with 63.3% of all AERONET AOD measurements used in this thesis originating in this basin. West Africa is the source of 22% of AERONET AOD measurements, followed by the Japan and Korea basins at 11.5% and 3.2%, respectively. Therefore, the composite climatology is heavily weighted towards the Persian Gulf basin. However, even with most of the AERONET AOD measurements for the 2006-2007 period originating in the Persian Gulf basin, the West Africa basin carries, on average, the

heaviest aerosol loading. The Persian Gulf basin ranks second, followed by the Korea and Japan basins. The following sections will examine the details behind the aerosol loading for each basin.

2. Persian Gulf

This thesis includes AOD data from all three Persian Gulf AERONET sites (Dhabi, Dhadnah, and Solar Village) to produce an AERONET AOD climatology for the Persian Gulf basin. If this study only includes data from Dhabi and Dhadnah, UAE, the AOD climatology will be heavily biased towards conditions at the southern end of the Persian Gulf. Solar Village, Saudi Arabia is northwest of Dhabi and Dhadnah, and by including data from Solar Village, the AOD climatology becomes more representative of the Persian Gulf basin as a whole.

Because the AERONET stations are geographically separated, there will be some subtle differences in AOD data. For example, while all three AERONET sites are located near dust source regions, only Dhabi and Dhadnah are located near sources of industrial pollution and maritime aerosols. Solar Village, on the other hand, is located inland on the Arabian Peninsula (refer to Figure 3), generally upwind from sources of industrial pollution (e.g., Riyadh) and maritime aerosols. Consequently, on an annual basis, Solar Village should have lower mean AOD values than Dhabi and Dhadnah.

Figure 13 is the two-year AERONET 0.50μm AOD distribution for the Persian Gulf basin for 2006-2007 using the three stations Solar Village, Dhabi and Dhadnah. The figure contains both a histogram of AOD values and cumulative frequency distribution. Half of the AOD values lie between 0.20 and 0.50, with the median of the distribution at 0.35. In 75% of the cases, the aerosol loading may be light enough to allow for scene correction, using an AOD of 0.50 as a baseline.

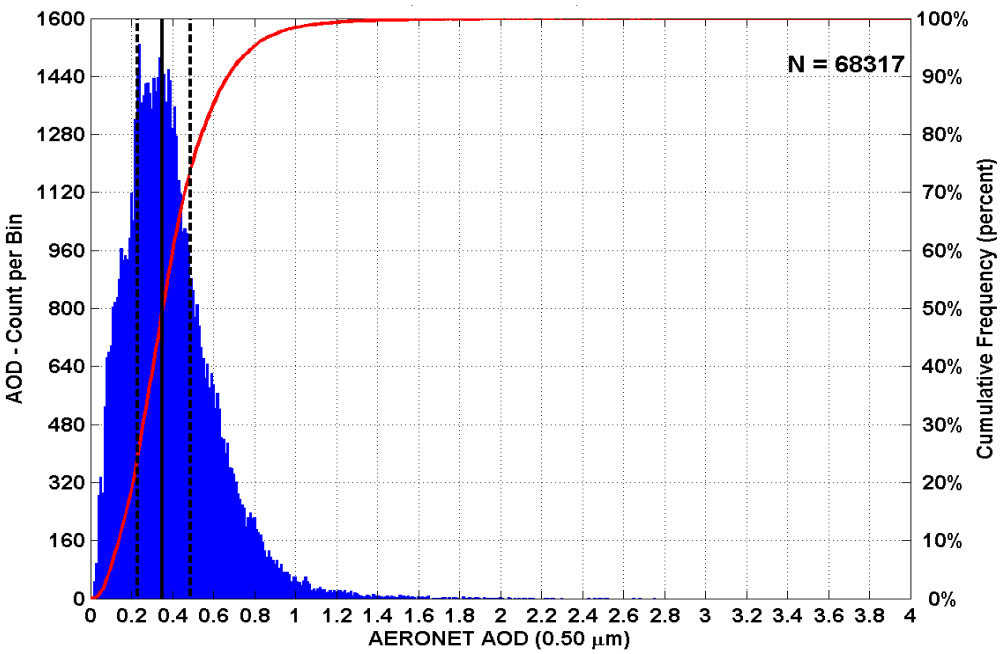

Figure 13. Two-year distribution of AERONET AOD (0.50 μm) values for stations Solar Village, Dhabi and Dhadnah in the Persian Gulf basin, for 2006-2007. The histogram of AOD values (blue bars) and cumulative frequency distribution (red curve) are denoted. The sample size is listed in the upper right corner. The vertical lines (black), from left to right, denote the quartiles of the distribution, 25% (dashed), 50% (solid), 75% (dashed).

Figure 14 illustrates the differences between Persian Gulf basin stations for 2006-2007. The cumulative frequency curve for each individual station is compared with the cumulative frequency curve for the combined dataset of the three stations. On an annual basis, aerosol concentration tends to be less at Solar Village than at Dhabi and Dhadnah. This may occur because Solar Village is located upwind of industrial pollution sources and also sees less maritime aerosols. There is no significant difference in the annual distribution of AERONET AOD values for Dhabi and Dhadnah, most likely due to relatively close proximity to each other. Effects from the Shamal are likely more pronounced over the Persian Gulf than inland over the Arabian Peninsula, offering another explanation why aerosol concentration tends to be less over Solar Village.

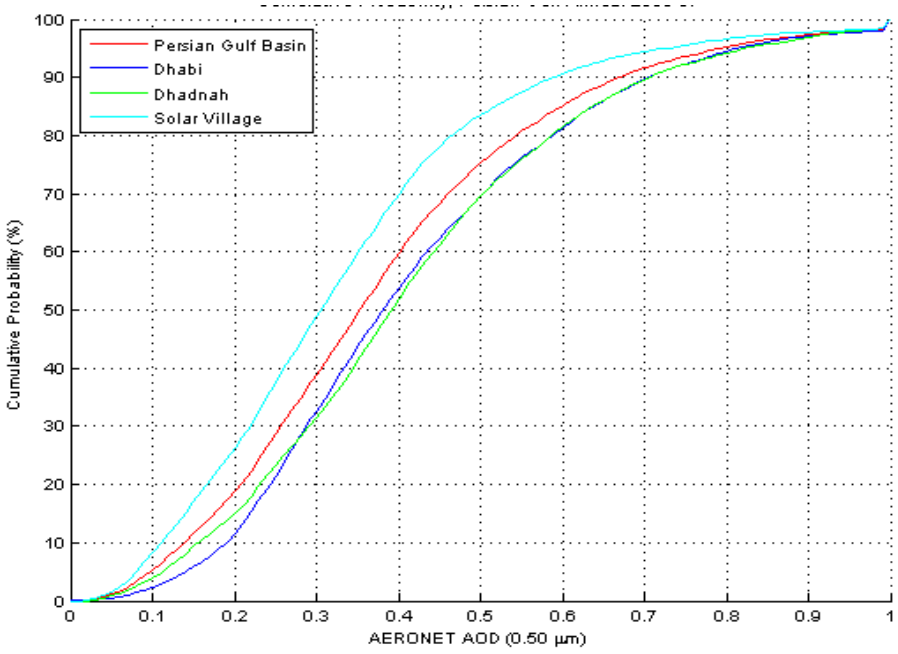

Figure 14. Two-year annual cumulative frequency curves for the Persian Gulf Basin for 2006-2007. The cumulative frequency curve for each individual station is compared with the cumulative frequency curve computed from the histogram distribution for the combined dataset of the three stations (Persian Gulf basin, red).

To best illustrate seasonal differences in AOD distributions, this thesis divides each year into four seasons, each lasting three months. The seasons boundaries are: Winter (December-February), Spring (March-May), Summer (June-August), and Fall (September-November). Figure 15 contains the Persian Gulf basin histograms of AERONET AOD distributions by season for 2006-2007. Figure 15a represents Winter, 15b is Spring, 15c is Summer, and 15d is Fall. Figures 15a and 15d indicate that aerosol concentrations are lowest over the Persian Gulf basin from September through February (Fall and Winter), with approximately 92.5% of cases having sufficiently low aerosol loading to allow for scene correction. Figures 15b and 15c suggest that aerosol concentrations are highest from March through August (Spring and Summer), with approximately 68% of cases having sufficiently low aerosol loading to allow for scene correction (with 0.50 as the baseline for correctability). The results from Figure 15 are consistent with the Fourteenth Weather Squadron climatology for the Persian Gulf basin

(Chapter II, Section B, Para. 1), which found that dust storms are more frequent in Spring and Summer than in Winter and Fall. Consequently, image analysts should expect more uncorrectable images in Spring and Summer versus Fall and Winter.

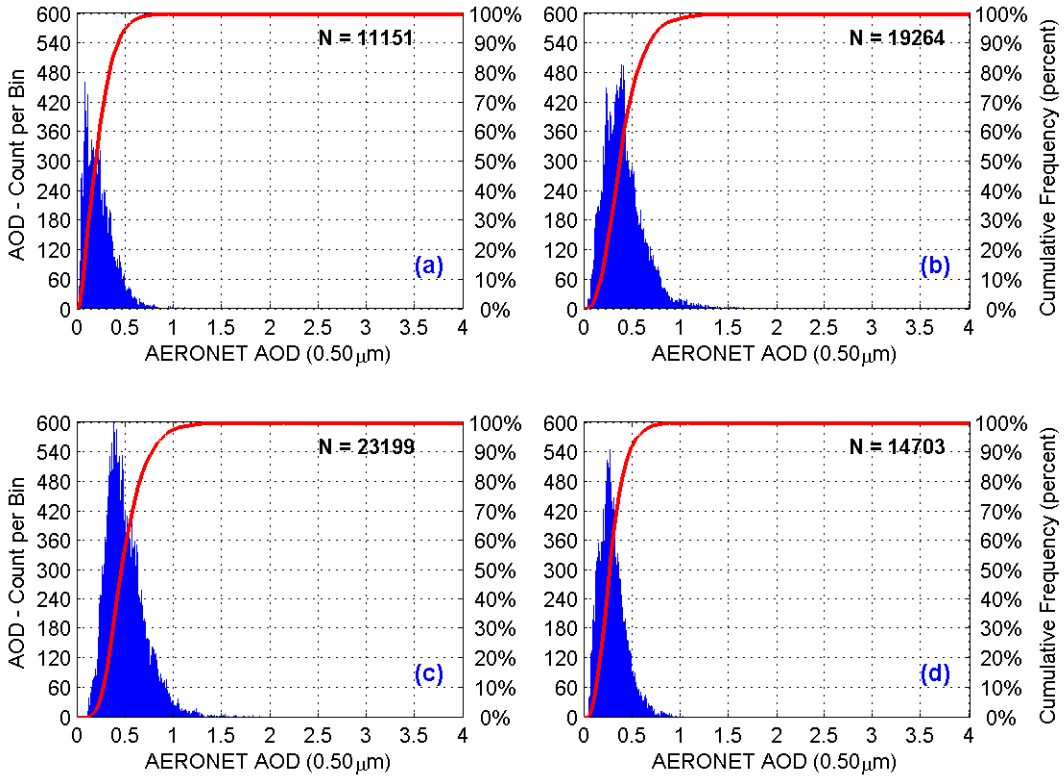

Figure 15. Seasonal Distribution of AERONET AOD (0.50 μm) values for the Persian Gulf basin for 2006-2007. The histogram of AOD values (blue bars) and cumulative frequency distribution (red curve) are denoted. The sample size is listed in the upper right corner. Seasons are denoted as (a) Winter (December-February), (b) Spring (March-May), (c) Summer (June-August), and (d) Fall (September-November).

3. East Asia

A single basin AERONET AOD climatology for East Asia is impractical for two reasons. First, there is a large geographic separation between western Korea and southeastern Japan. Second, Korea is much closer than Japan to dust and pollution source regions in China and Mongolia (see Figure 4), leading to the hypothesis that, on

an annual basis, AERONET AOD measurements will be higher over Korea than Japan. As a result, two basin climatologies are created, one for Korea, and another for Japan. Only one station (Anmyon) is used in creating the aerosol climatology for Korea, while two stations are used for Japan (Osaka and Shirahama).

Figure 16 is the two-year AERONET AOD (0.50μm) distribution for Korea for 2006-2007 using Anmyon. Figure 17 illustrates the same for Japan, using Shirahama and Osaka. For Korea, fifty percent of the AOD values lie between 0.14 and 0.49, with the median of the distribution at 0.26. In 75% of the cases in Korea, the aerosol loading may be light enough to allow for scene correction, using an AOD of 0.50 as a baseline. Meanwhile, for Japan, 50% of the AOD values lie between 0.14 and 0.36, with the median of the distribution at 0.21. Additionally, in Japan, the aerosol may be sufficiently light to allow for scene correction in approximately 87% of the cases. Furthermore, Figures 16 and 17 also suggest that, on an annual basis, Korea has higher aerosol concentrations than Japan. Therefore, image analysts will have more uncorrectable imagery over Korea than Japan.

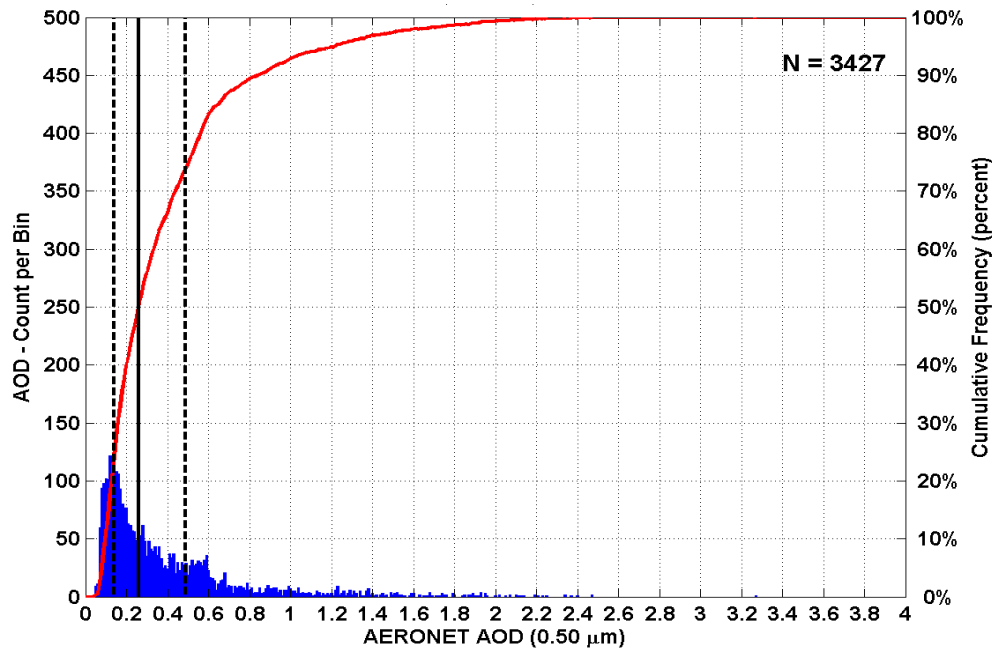

Figure 16. Two-year distribution of AERONET AOD (0.50μm) values for Anmyon in the Korea basin, for 2006-2007. The histogram of AOD values (blue bars) and cumulative frequency distribution (red curve) are denoted. The sample size is listed in the upper right corner. The vertical lines (black), from left to right, denote the quartiles of the distribution, 25% (dashed), 50% (solid), 75% (dashed).

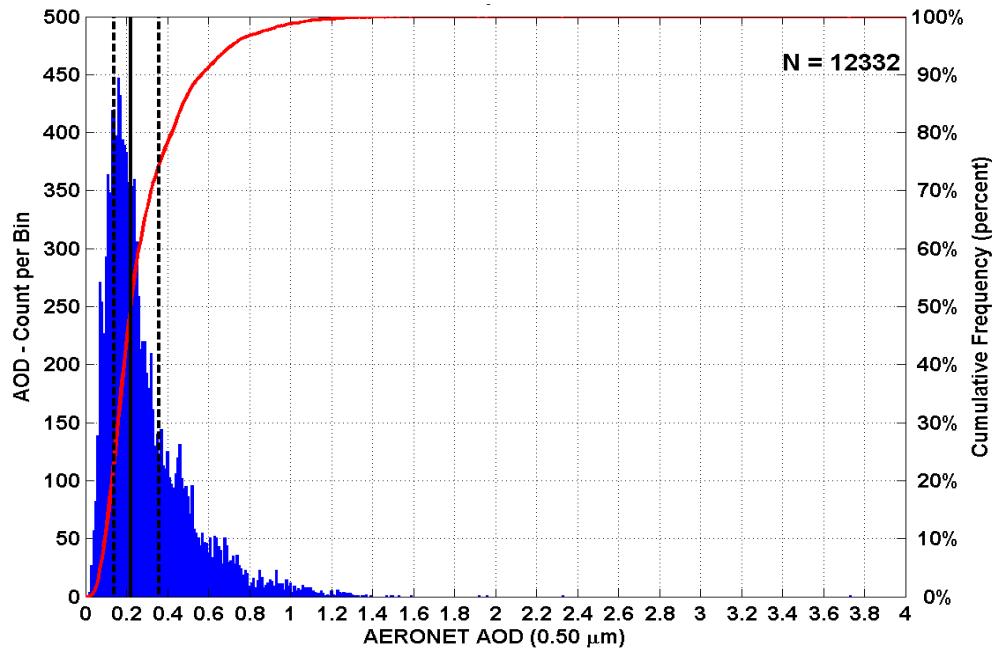

Figure 17. Same as Figure 16, but for Japan.

Figure 18 illustrates the differences between the AERONET AOD distributions for the Korea and Japan basins for 2006-2007. The cumulative frequency curve for Korea basin is compared with the cumulative frequency curve from Japan (see Figures 16 and 17). Each cumulative frequency curve is computed from the histogram distribution for the each basin. Figure 18 indicates that the AERONET AOD distributions are very different for Korea and Japan, with Korea clearly carrying a heavier aerosol load than Japan. For example, for Korea, 74% of the AERONET AOD distribution has an AOD less than 0.50. However, for Japan, 86% of the AERONET AOD distribution has an AOD less than 0.50. Additionally, the Korea basin has 7% of the AOD distribution greater than 1.0, while the Japan basin only has 1% of the AOD distribution greater than 1.0. Therefore, the Korea and Japan AERONET AOD datasets cannot be combined to produce one single East Asia basin AERONET AOD climatology.

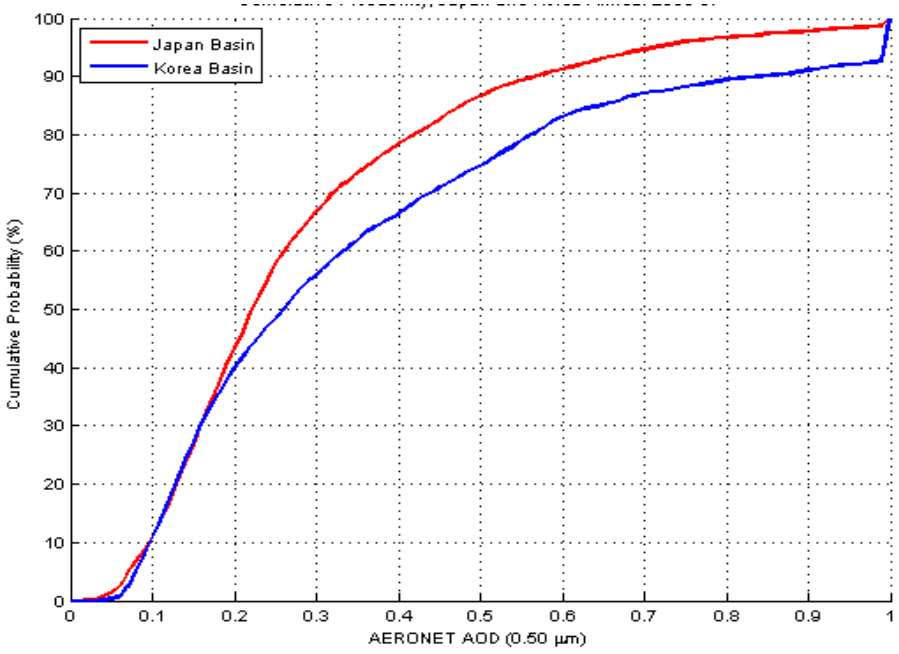

Figure 18. Two-year annual cumulative frequency curves for Korea (blue) and Japan (red) for 2006-2007.

Figure 19 illustrates the differences between Japan basin stations for 2006-2007. There are differences in the annual distribution of AERONET AOD values between Osaka and Shirahama. Osaka is located next to a sheltered bay, surrounded by mountains

on three sides, while Shirahama is directly on the Pacific coast. However, Shirahama may be exposed to more dust/pollution from sources in China, since there are no mountains that block flow from China, and also is likely sees more maritime aerosols than Osaka. Therefore, it stands to reason that aerosol loading over Shirahama is greater than Osaka. Also, many fewer AERONET AOD measurements are available for Osaka than Shirahama, which explains why the Japan basin composite cumulative frequency curve closely mirrors the Shirahama curve.

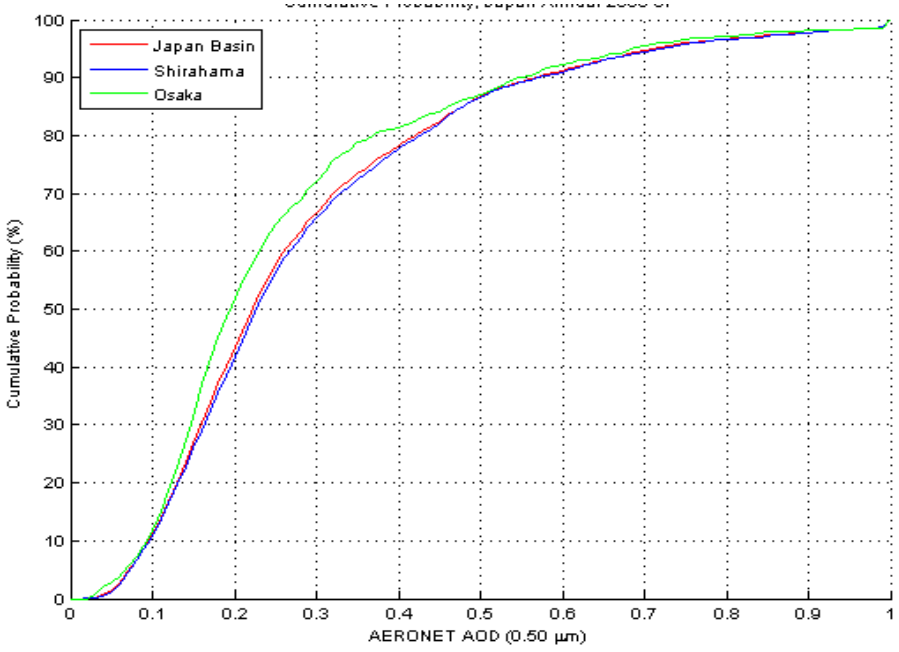

Figure 19. Same as Figure 18, but for the Japan basin.

Figure 20 contains the seasonal distributions of AERONET AOD values for Korea. Figures 20a and 20d indicate that aerosol concentrations are lowest over Korea from September through February (Fall and Winter), with approximately 90% of cases having sufficiently low aerosol loading to allow for scene correction. Figures 20b and 20c suggest that aerosol concentrations are highest from March through August (Spring and Summer), with approximately 58% of cases having sufficiently low aerosol loading to allow for scene correction. The results from Figure 20 agree with the Fourteenth Weather Squadron climatology (Chapter II, Section B, Para. 2), that dust storms are more frequent in Spring and Summer than in Winter and Fall.

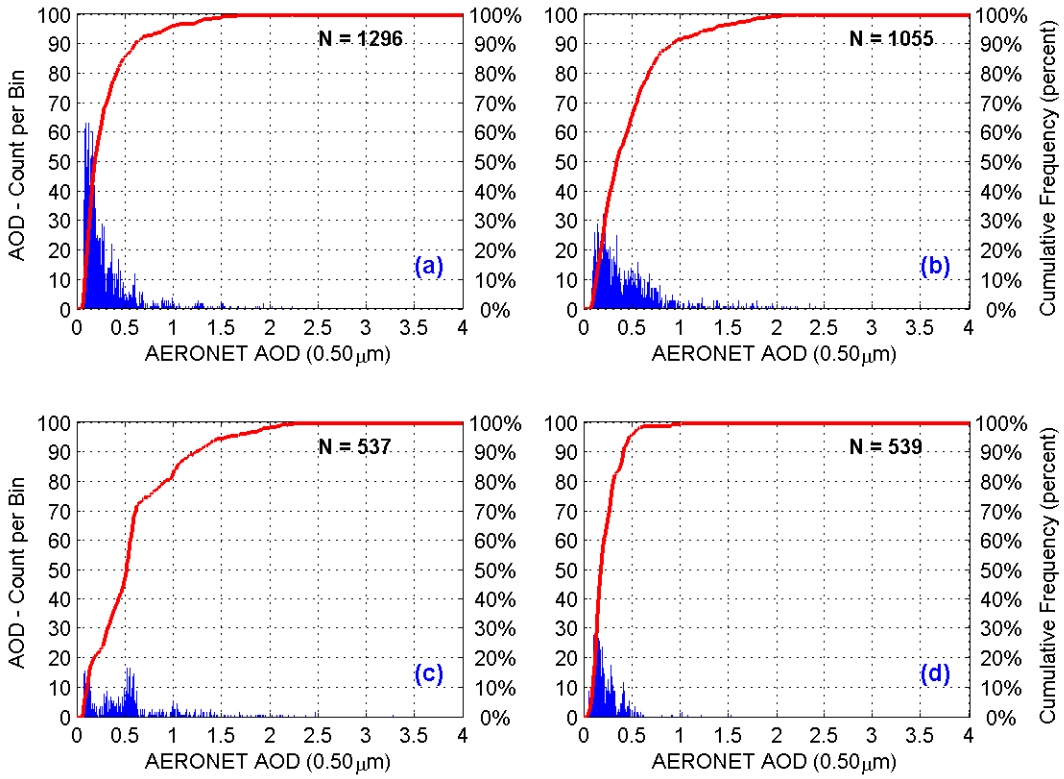

Figure 20. Seasonal Distribution of AERONET AOD (0.50 μm) values for the Korea basin for 2006-2007. The histogram of AOD values (blue bars) and cumulative frequency distribution (red curve) are denoted. The sample size is listed in the upper right corner. Seasons are denoted as (a) Winter (December-February), (b) Spring (March-May), (c) Summer (June-August), and (d) Fall (September-November).

Figure 21 contains the seasonal distributions of AERONET AOD values for Japan. Figures 21a and 21d indicate that aerosol concentrations are lowest over Japan from September through February (Fall and Winter), with more than 95% of cases having sufficiently low aerosol loading to allow for scene correction (with 0.50 as the baseline for correctability). Figures 21b and 21c suggest that aerosol concentrations are highest from March through August (Spring and Summer), with approximately 80% percent of cases having sufficiently low aerosol loading to allow for scene correction. The results

from Figure 21 are consistent with the Fourteenth Weather Squadron climatology (Chapter II, Section B, Para. 2), that dust storms are more frequent in Spring and Summer than in Winter and Fall over Japan.

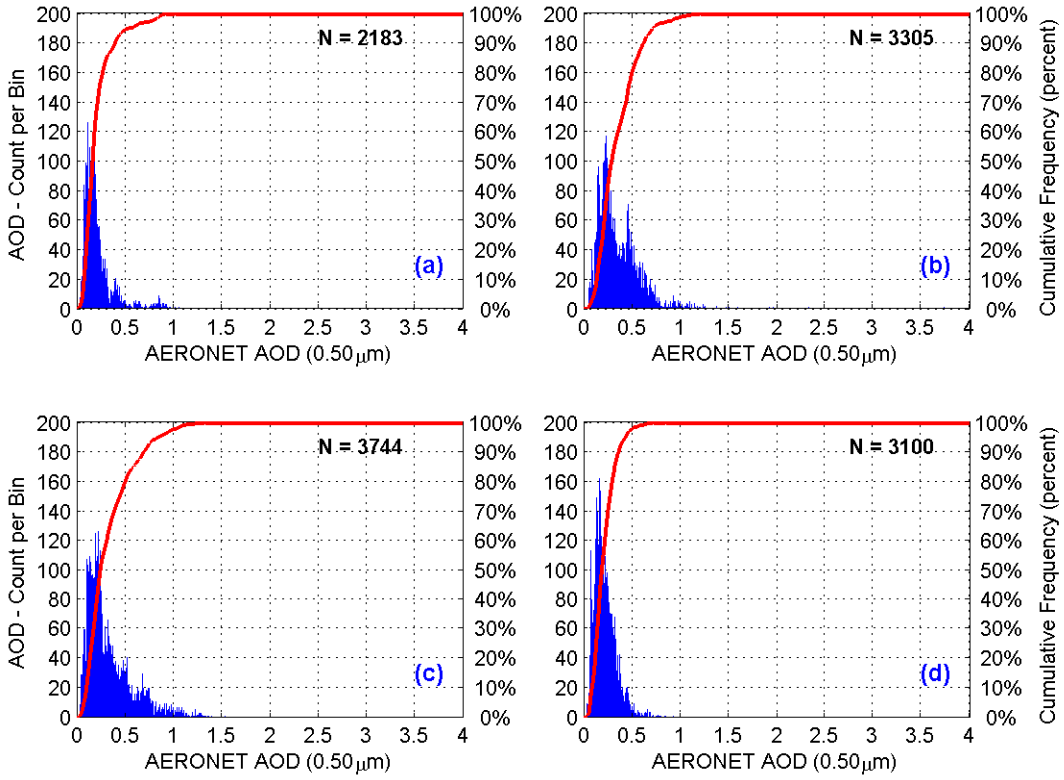

Figure 21. Same as Figure 20 but for the Japan basin.

Additionally, aerosol loading appears to be higher over Korea than Japan. As Korea is closer to dust and pollution sources in China and Mongolia, Korea should have a heavier aerosol load than Japan. When analyzing imagery over East Asia, an analyst should expect more aerosol loading over Korean imagery versus Japanese imagery, with most uncorrectable images occurring during Spring and Summer.

4. West Africa

AOD data from both West Africa AERONET sites is used to produce an AOD climatology for the West African basin. If data from only Ilorin, Nigeria are included, for

example, the AOD climatology will be heavily biased towards conditions at the Ilorin. Djougou, Benin is northwest of Ilorin, and by including data from Djougou, the AOD climatology becomes more representative of the West African basin as a whole, which helps verify the significant basin differences compared to the Persian Gulf and East Asia.

Because the AERONET stations are geographically separated, there will be some subtle differences in AOD data. Additionally, no AOD data is available at 0.50μm for Djougou. Instead, this thesis uses AERONET AOD data at 0.44μm for Djougou. Since AOD generally increases with decreasing wavelength, we expect the Djougou results to be biased toward slightly higher values.

Figures 22 and 23 are the two-year AERONET AOD distributions for the two West Africa stations. Overall aerosol loading in West Africa is quite high. For Djougou, half of the AOD values lie between 0.42 and 0.89, with the median of the distribution at 0.61. For Ilorin, half of the AOD values lie between 0.40 and 1.05, with the median of the distribution at 0.70. The aerosol loading may be light enough to allow for scene correction in only 35% of the cases in West Africa, using an AOD of 0.50 as a baseline.

Additionally, Figures 22 and 23 suggest that annual aerosol concentrations over West Africa are much higher than for the Persian Gulf and East Asia. For example, for West Africa, 22.5% of AERONET AOD measurements taken during 2006-2007 are greater than 1.0, versus 3% of AERONET AOD measurements for the Persian Gulf basin. Aerosol loading over West Africa is greater than aerosol loading for the Persian Gulf and East Asia because of the proximity of Djougou and Ilorin to the Sahara Desert. Because both stations are located in the Sahel region of Africa, Djougou and Ilorin are subject to strong Harmattan winds that blow over West Africa during the dry season (roughly November through March). These winds blanket the region with high concentrations of dust and sand from the Sahara Desert, and are a major source of aerosols over West Africa (Westphal 1988). The other major source of aerosols during the dry season is biomass burning, generally advected from the regions south and east of the West Africa stations.

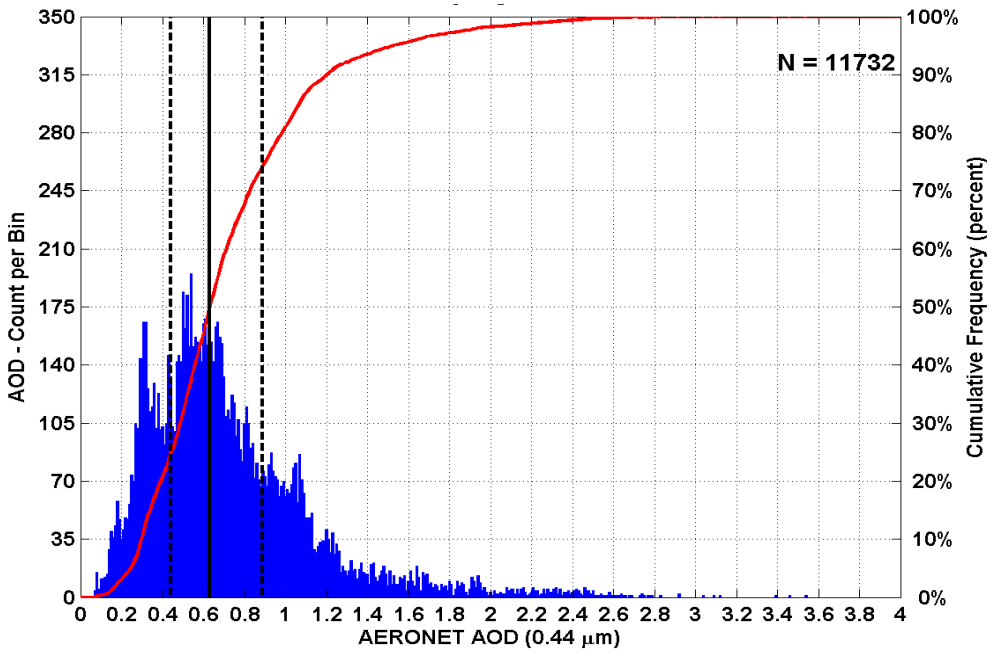

Figure 22. Two-year distribution of AERONET AOD (0.44μm) values for station Djougou in the West Africa basin, for 2006-2007. The histogram of AOD values (blue bars) and cumulative frequency distribution (red curve) are denoted. The sample size is listed in the upper right corner. The vertical lines (black), from left to right, denote the quartiles of the distribution, 25% (dashed), 50% (solid), 75% (dashed).

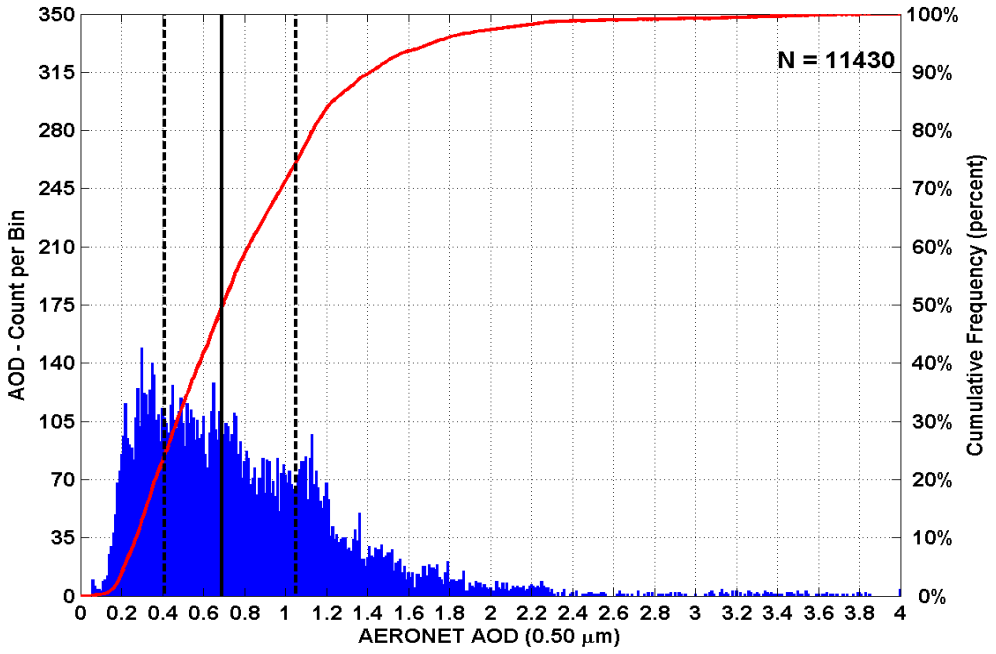

Figure 23. Same as Figure 22, but for Ilorin at 0.50μm.

Figure 24 illustrates the differences between West Africa basin stations for 2006-2007. At AODs below 0.55, there is little difference in AOD distributions between Djougou and Ilorin. This implies that aerosol source differences are larger than the effect of the shorter wavelength used for Djougou. At AODs above 0.55, there is a greater difference in AOT distributions. Ilorin is much closer to Lake Chad, which is a major dust source region in West Africa. It is possible that Ilorin, given its proximity to Lake Chad, receives more dust than Djougou. Thus, the AOD distribution for Ilorin shows a heavier aerosol concentration as compared to Djougou.

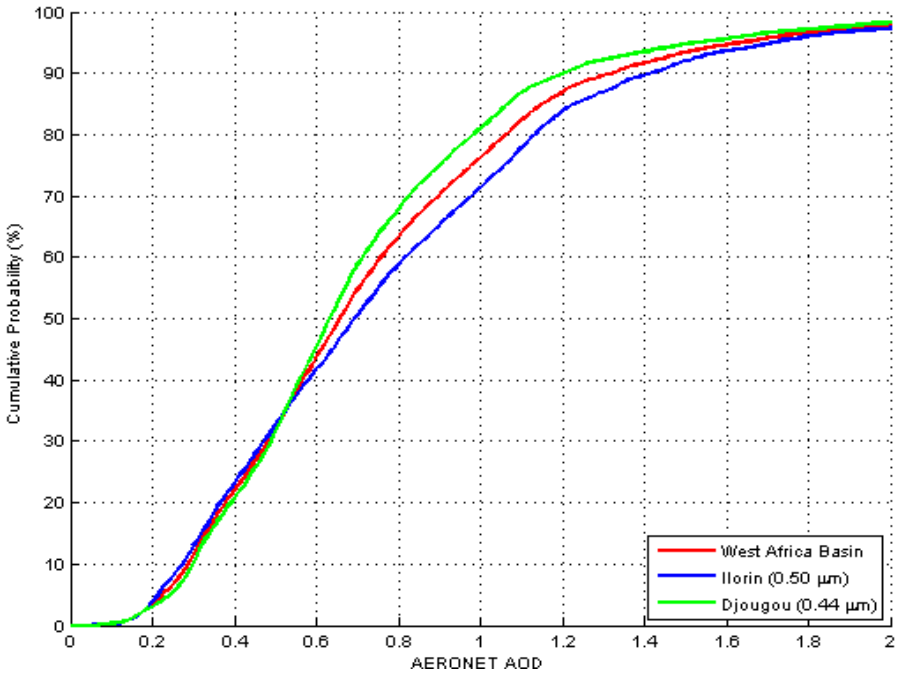

Figure 24. Two-year annual cumulative frequency curves for the West Africa basin for 2006-2007. The Ilorin (0.50µm, blue) and Djougou (0.44µm, green) curves are denoted.

Figure 25 contains seasonal West Africa basin histograms for Ilorin, which illustrate AERONET AOD distributions by season for 2006-2007. Figures 25c and 25d indicate that aerosol concentrations are lowest over Ilorin from June through November (wet season), with approximately 75% of cases having sufficiently low aerosol loading to allow for scene correction, using an AOD value of 0.50 as a baseline for image correctability. Figures 25a and 25b suggest that aerosol concentrations are highest from

December through May (dry season), with only approximately 20% of cases having sufficiently low aerosol loading to allow for scene correction. The results from Figure 25 are consistent with the climatology produced by the Fourteenth Weather Squadron, that dust storms are more frequent in the dry season than in the wet season for the West Africa basin. Seasonal AERONET AOD histograms for Djougou are included in Appendix B (Figures 81-84), and display the same trends as Ilorin.

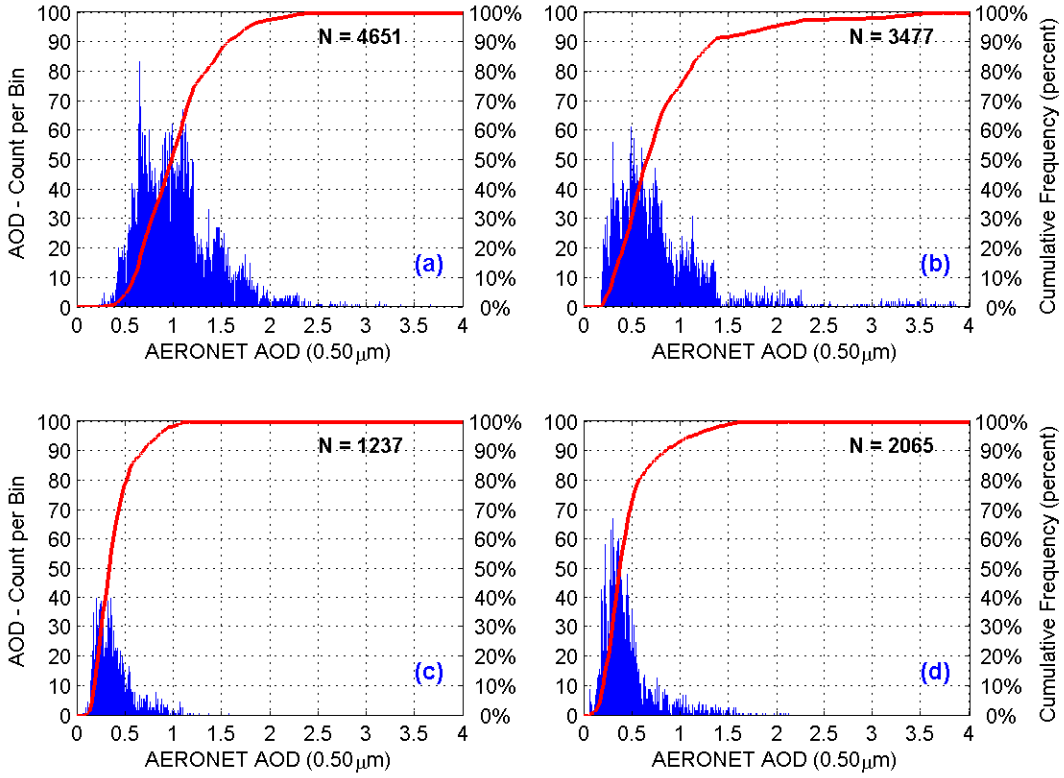

Figure 25. Seasonal Distribution of AERONET AOD (0.50 µm) values for Ilorin in the West Africa basin for 2006-2007. The histogram of AOD values (blue bars) and cumulative frequency distribution (red curve) are denoted. The sample size is listed in the upper right corner. Seasons are denoted as (a) Winter (December-February), (b) Spring (March-May), (c) Summer (June-August), and (d) Fall (September-November).

As shown in Figures 25a and 25b, AERONET AOD distributions are shifted towards the high end of the AOD spectrum during the dry season (Winter and Spring). Based on climatology, West Africa stations should see higher aerosol concentrations

during the dry season, and that is exactly what is shown by the AERONET AOD distributions. With the approach of the rainy season (Summer and Fall), the Harmattan winds die down, and the AERONET AOD distributions shift towards lower values. Also, the number of cloudy days increases, reducing the frequency that AERONET measurements are taken, and thus, lowering the sample sizes.

In summary, an analyst viewing targets over West Africa will have to apply the greatest amount of corrections in the dry season, due to the increased frequency of dust storms over the region. However, during the rainy season, while there will be more correctable imagery, there will be fewer images to work with because of increased cloud cover.

B. MODIS/AERONET COMPARISON

1. Persian Gulf

The purpose of the MODIS/AERONET comparison is to establish that MODIS-retrieved AOD values at 0.55μm are representative of ground-truth AOD values throughout each geographic basin. AOD data from only two Persian Gulf AERONET sites are included in the MODIS/AERONET comparison for the Persian Gulf basin. MODIS-retrieved AOD values are from over the ocean only. Solar Village, Saudi Arabia is approximately 417 km inland from the Persian Gulf, so there are no MODIS-retrieved AOD values in the vicinity of Solar Village. Consequently, AERONET AOD data from Solar Village are not used in the MODIS/AERONET comparison. The Dhabi, UAE and Dhadnah, UAE AERONET sites are both located along the coast, so this study is able to make point-to-point MODIS/AERONET AOD comparisons for both sites (see Figure 6). The datasets from Dhabi and Dhadnah are combined to produce the Persian Gulf basin MODIS/AERONET AOD comparison.

MODIS and AERONET AOD values need to be coincident in time and space for proper comparison. The MODIS grid point closest to each AERONET site is used (see Figure 6). Each MODIS AOD value is a daily mean of the AOD values for a 1° x 1° grid box. MODIS overpass times for the Persian Gulf basin are approximately 1030LT

(0630UTC) and 1330LT (0930UTC). For each AERONET site, AOD data is averaged between 1000LT (0600UTC) and 1400LT (1000UTC) to be consistent with the time span of the MODIS satellite passes. On each day when both MODIS and AERONET AOD values are available for the time window, a one-to-one comparison of AOD values is performed.

Figure 26 contains a scatter plot of AERONET and MODIS AOD values for the Persian Gulf basin for the two-year period from 2006 through 2007. Agreement between the MODIS and AERONET values is quite good. The correlation coefficient is 0.90, and the scatter does not imply bias in the comparison. At an AOD greater than 0.50, the spread increases slightly with increasing AOD. The spread may increase because of greater differences in time and space between the observation techniques.

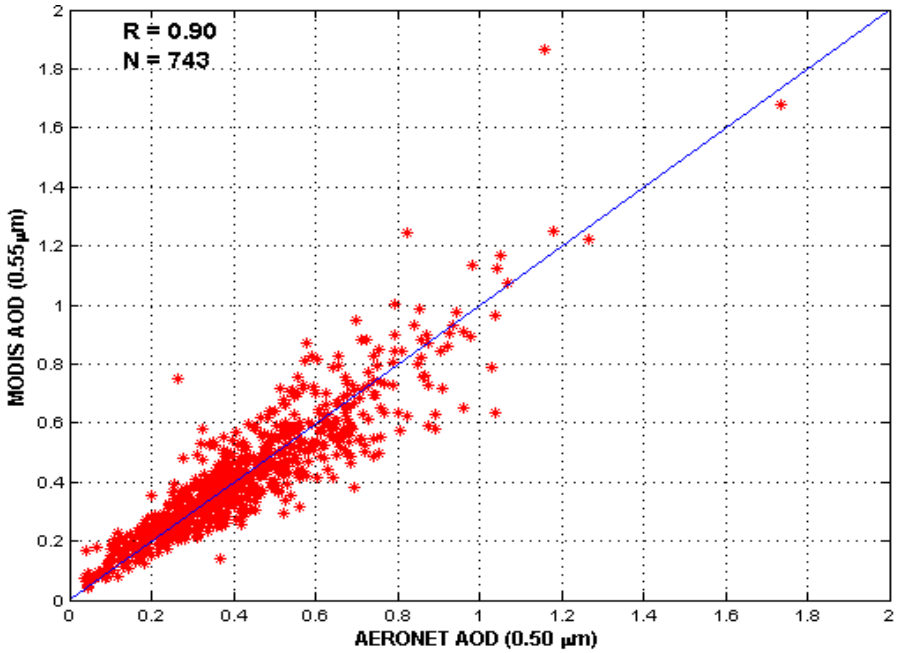

Figure 26. Annual scatter plot of daily AERONET and MODIS AOD values for the Persian Gulf basin for 2006-2007. The daily AOD values (red stars) and one-to-one line (blue) are denoted. The correlation coefficient (R) and sample size (N) are listed in the upper left corner.

Figure 27 contains scatter plots of AERONET and MODIS AOD values by season for the 2006-2007 timeframe. There is good correlation for all seasons. As before, the spread increases as AOD increases. Spring and Summer display higher

average AOD values, reinforcing that Spring and Summer are the seasons with higher aerosol loading over the Persian Gulf basin. The implications are that for Spring and Summer over the Persian Gulf basin, an analyst should have a higher percentage of images that are uncorrectable. Additionally, Fall and Winter are the seasons of the year that may allow for more images to be corrected. Finally, Figure 27 confirms that, on a seasonal basis, MODIS-retrieved AOD values are representative of the land-based AERONET AOD values for the Persian Gulf basin.

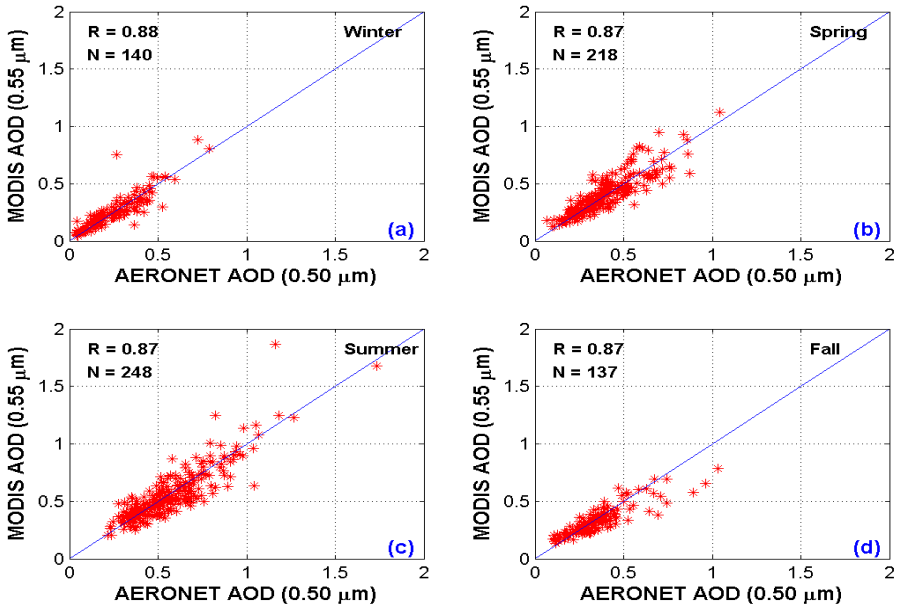

Figure 27. Persian Gulf Basin AERONET AOD (0.50μm) versus MODIS AOD (0.55μm) scatterplots for the 2006-2007 seasons: (a) Winter, (b) Spring, (c) Summer, (d) Fall. The daily AOD values (red stars) and one-to-one line (blue) are denoted. The correlation coefficient (R) and sample size (N) are listed in the upper left corner.

Figure 28 displays MODIS and AERONET annual cumulative frequency curves from the Persian Gulf basin for the two-year period (2006-2007). The MODIS cumulative frequency curve is derived from the two-year Persian Gulf basin MODIS AOD distribution (0.55μm) histogram, located in Appendix B (Figure 85). The AERONET cumulative frequency curve is taken from the two-year basin AERONET AOD distribution (0.50μm) histogram (Figure 13). The MODIS cumulative frequency

curve closely mirrors the AERONET AOD curve, suggesting that on an annual basis there is little difference in the distribution of AOD values for both MODIS and AERONET. For example, 40% of both MODIS and AERONET AOD values are less than an AOD of 0.30. The region of most spread between the MODIS and AERONET curves is between AODs of 0.05 to 0.25, with the MODIS curve indicating slightly higher AODs than AERONET. At AODs from 0.05 to 0.25, MODIS portrays heavier aerosol loading compared to what is actually occurring. Turbid waters in the Persian Gulf add TOA radiance, influencing the MODIS AOD retrieval, resulting in an overestimate of the AOD values over water. For optical depths above about 0.25, aerosol radiance contribution may dominate the contribution from the surface.

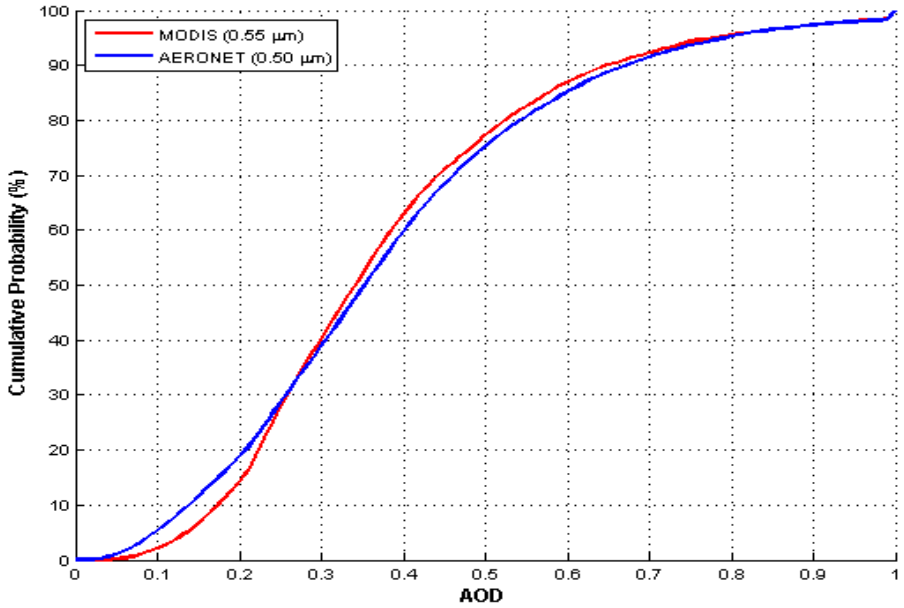

Figure 28. Annual cumulative frequency curves for the Persian Gulf basin MODIS (red) and AERONET (blue) AOD distributions.

Table 1 provides a summary of the statistical results for the MODIS/AERONET AOD comparison for the Persian Gulf basin. Sample sizes are sufficiently large such that valid conclusions can be drawn from the data. Correlation coefficients range from 0.87 to 0.90, which suggest a high degree of correlation between MODIS and AERONET AOD values. Thus, the implication is that the MODIS AOD values for the Persian Gulf basin can be used with a high degree of confidence in areas lacking AERONET sites.

Table 1. MODIS/AERONET AOD Correlations for Persian Gulf basin for 2006-2007

	R (correlation)	N (sample size)
Annual	0.90	743
Winter	0.88	140
Spring	0.87	218
Summer	0.87	248
Fall	0.87	137

In summary, the MODIS AOD retrieval at 0.55μm can provide reliable estimates of AOD values in the Persian Gulf basin for areas not located near AERONET sites. While the AERONET sites used here are along coasts, they are still located on land and are located closer to dust and pollution sources. The proximity to the aerosol sources may account for some of the slight differences between MODIS and AERONET AOD measurements for the basin. Additionally, local weather conditions at the AERONET sites (i.e., sea and land breezes) no doubt affect aerosol loading. In turn, some of the differences between MODIS and AERONET AOD measurements may come about due to local weather conditions at the AERONET sites.

2. East Asia

a. Korea

Only data from the Anmyon, South Korea AERONET site is included in the MODIS/AERONET comparison for the Korea basin. AOD values from the MODIS grid point closest to Anmyon is used in this comparison (see Figure 7). As previously described, AERONET AOD values are averaged over a time span to match the time frame of the mean MODIS AOD value. The MODIS satellites image the Korea basin at approximately 1030LT (0130UTC) and 1330LT (0430UTC). The mean AERONET AOD value is computed for the time period from 1000-1400LT (0100-0500UTC), for each cloud-free day for which MODIS AOD values are available.

Figure 29 contains a scatter plot of AERONET and MODIS AOD values for the Korea basin for the two-year period from 2006 through 2007. Agreement between the MODIS and AERONET values is quite good. The scatter does not imply bias in the comparison, and the correlation coefficient is 0.91.

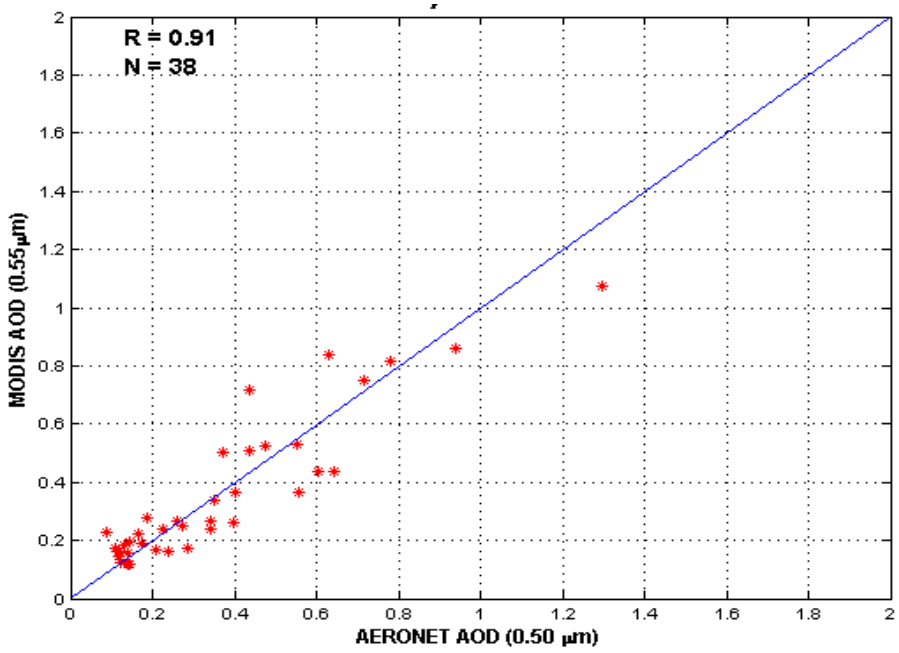

Figure 29. Annual scatter plot of daily AERONET and MODIS AOD values for the Korea basin for 2006-2007. The daily AOD values (red stars) and one-to-one line (blue) are denoted. The correlation coefficient (R) and sample size (N) are listed in the upper left corner.

Figure 30 contains scatter plots of AERONET and MODIS AOD values by season for the 2006-2007 time period. The correlation is high for all seasons. Spring and Summer display higher average AOD values, reinforcing that Spring and Summer are the seasons with higher aerosol loading over the Korea basin. The implications are that for Spring and Summer over the Korea basin, an analyst should have a higher percentage of images that are uncorrectable, with fewer correctable images. Additionally, Fall and Winter are the seasons of the year that may allow for more images to be corrected.

Figure 30 also shows that sample size is small for the Korea basin. The small sample size serves to increase the uncertainty behind the MODIS AOD retrieval. One possible reason for small sample size is the amount of cloud cover over Korea. In comparison to the Persian Gulf, Korea is, on average, much cloudier, resulting in fewer days on which MODIS and AERONET AOD retrievals can be made. Equipment shutoff or failure may also contribute to the small sample size for the Korea basin.

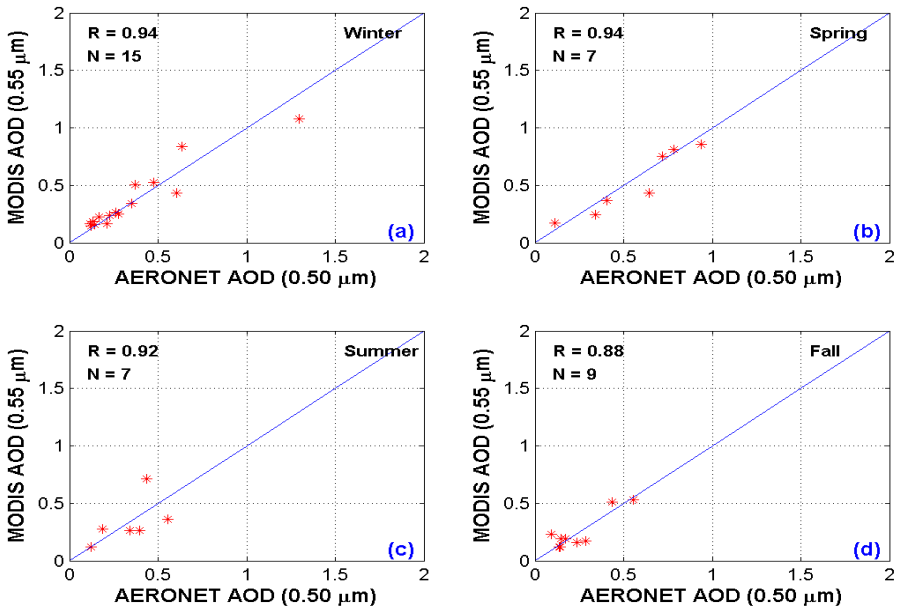

Figure 30. Korea Basin AERONET AOD (0.50μm) versus MODIS AOD (0.55μm) scatterplots for the 2006-2007 seasons: (a) Winter, (b) Spring, (c) Summer, (d) Fall. The daily AOD values (red stars) and one-to-one line (blue) are denoted. The correlation coefficient (R) and sample size (N) are listed in the upper left corner.

Figure 31 displays MODIS and AERONET annual cumulative frequency curves from the Korea basin for the two-year period (2006-2007). The MODIS cumulative frequency curve is derived from the two-year Korea basin MODIS AOD distribution (0.55μm) histogram, located in Appendix B (Figure 87). The AERONET cumulative frequency curve is taken from the two-year basin AERONET AOD distribution (0.50μm) histogram (Figure 16). The MODIS curve is far to the right of the AERONET curve, indicating that on an annual basis, MODIS displays a tendency to

portray heavier aerosol loading compared to AERONET. Turbid, shallow waters in the Yellow Sea and a small AERONET dataset for Korea may explain why MODIS displays a tendency to overestimate aerosol loading.

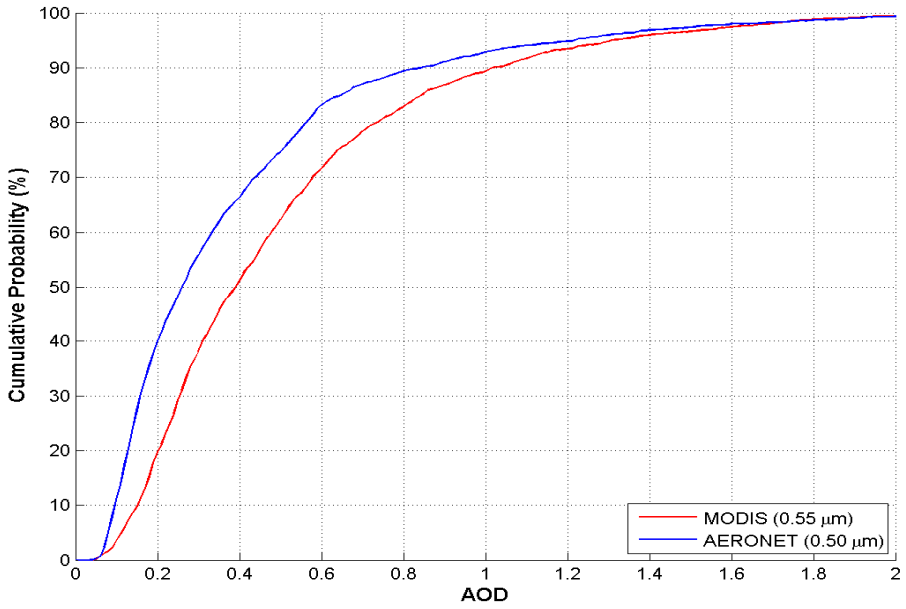

Figure 31. Annual cumulative frequency curves for the Korea basin MODIS (red) and AERONET (blue) AOD distributions.

Table 2 provides a summary of the statistical results for the MODIS/AERONET AOD comparison for the Korea basin. Correlation coefficients range from 0.91 to 0.94. Table 2, in addition to Figures 29-31; indicate that the MODIS AOD retrieval at 0.55μm may provide close to ground truth AOD values in the Korea basin for areas not located near AERONET sites. Larger AERONET and MODIS AOD sample sizes will help narrow down the uncertainty as to whether or not MODIS can reliably provide AOD measurements over the Korea basin.

Table 2. MODIS/AERONET AOD Correlations for Korea basin for 2006-2007

	R (correlation)	N (sample size)
Annual	0.91	38
Winter	0.94	15
Spring	0.94	7
Summer	0.92	7
Fall	0.88	9

b. Japan

Shirahama MODIS AOD data are included in the MODIS/AERONET comparison for the Japan basin. Osaka MODIS AOD data are not included because limited MODIS data are available in the proximity of Osaka. AOD values from the MODIS grid point closest to Shirahama are used in this comparison (see Figure 7). As previously described, AERONET AOD values are averaged over time to match the mean MODIS AOD values. The MODIS satellites image the Japan basin at approximately 1030L (0130UTC) and 1330L (0430UTC). The mean AERONET AOD value is computed for 1000-1400L (0100-0500UTC), for each cloud-free day for which MODIS AOD values are available.

Figure 32 contains a scatter plot of AERONET and MODIS AOD values for the Japan basin for the two-year period (2006-2007). Agreement between the MODIS and AERONET values is very good, with the correlation coefficient equal to 0.86.

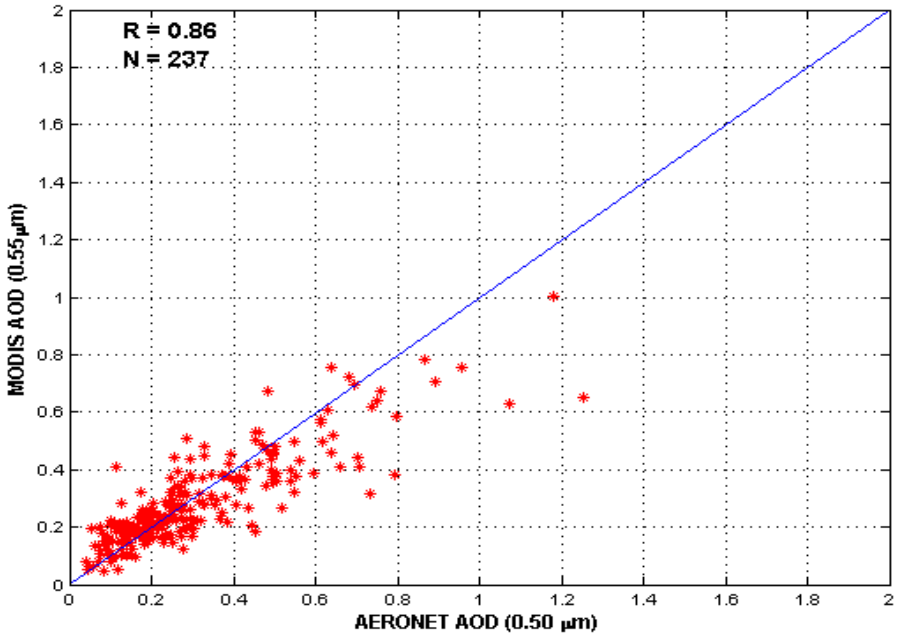

Figure 32. Annual scatter plot of daily AERONET and MODIS AOD values for Shirahama in the Japan basin for 2006-2007. The daily AOD values (red stars) and one-to-one line (blue) are denoted. The correlation coefficient (R) and sample size (N) are listed in the upper left corner.

Figure 33 contains scatter plots of AERONET and MODIS AOD values by season for 2006-2007. The correlation is not consistent across the seasons. One possible reason may be the low sample size. Further explanation of the differences in correlation by season is beyond the scope of this thesis.

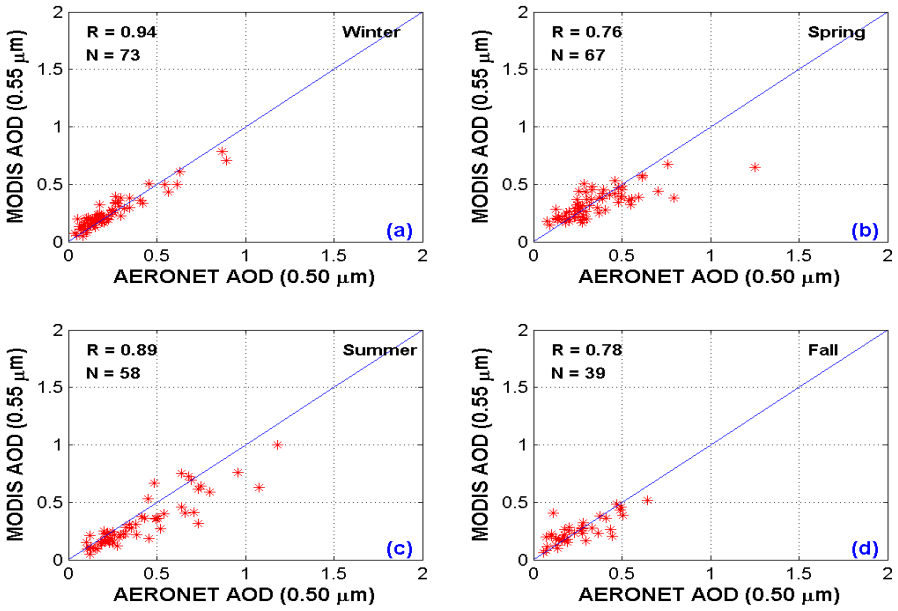

Figure 33. Japan Basin AERONET AOD (0.50μm) versus MODIS AOD (0.55μm) scatterplots for the 2006-2007 seasons: (a) Winter, (b) Spring, (c) Summer, (d) Fall. The daily AOD values (red stars) and one-to-one line (blue) are denoted. The correlation coefficient (R) and sample size (N) are listed in the upper left corner.

Figure 34 displays MODIS and AERONET annual cumulative frequency curves from the Japan basin for the two-year period (2006-2007). The MODIS cumulative frequency curve is derived from the two-year Japan basin MODIS AOD distribution (0.55μm) histogram, located in Appendix B (Figure 89). The AERONET cumulative frequency curve is taken from the two-year basin AERONET AOD distribution (0.50μm) histogram (Figure 17). The MODIS cumulative frequency curve, in general, closely mirrors the AERONET AOD curve, suggesting that on an annual basis there are only slight differences in the distribution of AOD values for both MODIS and AERONET. Below an AOD of 0.30, the MODIS curve is slightly to the right of the AERONET curve, implying that MODIS slightly overestimates AOD values when the actual AOD is less than or equal to 0.30 (possibly because of turbid waters). Above an

AOD of 0.30, the MODIS curve is slightly to the left of the AERONET curve, suggesting that MODIS slightly underestimates AOD values when the actual AOD is less than or equal to 0.30.

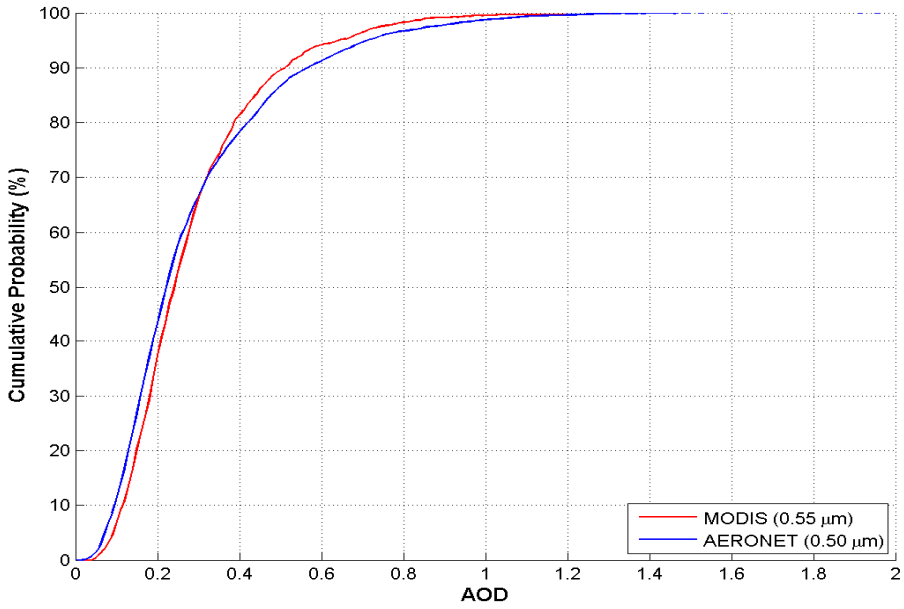

Figure 34. Annual cumulative frequency curves for the Japan basin MODIS (red) and AERONET (blue) AOD distributions.

Table 3 summarizes the statistical results for the MODIS/AERONET AOD comparison for the Japan basin. Correlation coefficients range from 0.76 to 0.94, which suggest a high degree of correlation between MODIS and AERONET AOD values.

Table 3. MODIS/AERONET AOD Correlations for Japan basin for 2006-2007

	R (correlation)	N (sample size)
Annual	0.86	237
Winter	0.94	73
Spring	0.76	67
Summer	0.89	58
Fall	0.78	39

In summary, like the Persian Gulf basin, the MODIS AOD retrieval at 0.55μm can provide a good estimate of AOD values in the Japan basin for areas not located near AERONET sites. While the AERONET site used in this thesis is along the coast, the site is still located on land, and is located closer to dust and pollution sources. The proximity to the aerosol sources may account for some of the slight differences between MODIS and AERONET AOD measurements for the basin. Additionally, local weather conditions at the AERONET site (i.e., sea and land breezes) no doubt affect aerosol loading. In turn, some of the differences between MODIS and AERONET AOD measurements may come about due to local weather conditions at the AERONET sites.

3. West Africa

Only AOD data from Ilorin, Nigeria are included in the MODIS/AERONET comparison for the West Africa basin. The MODIS AOD retrieval is an over water retrieval. A more accurate MODIS/AERONET comparison will result using only Ilorin because Djougou, Benin is more than 167 km further inland than Ilorin. AOD values from the MODIS grid point closest to Ilorin are used in this comparison (see Figure 8). As previously described, AERONET AOD values are averaged over time to match the mean MODIS AOD values. The MODIS satellites image the West Africa basin at approximately 1030L (0930UTC) and 1330L (1230UTC). The mean AERONET AOD value is computed for 1000-1400L (0900-1300UTC), for each cloud-free day for which MODIS AOD values are available.

Figure 35 contains a scatter plot of AERONET and MODIS AOD values for the West Africa basin for the two-year period from 2006 through 2007. Agreement between the MODIS and AERONET values is not nearly as good for West Africa as it is for the Persian Gulf and Japan basins. MODIS AOD values have a significant low bias. The source of the low bias may be due to the distance between the Ilorin AERONET station and the coast. Ilorin is over 217 km inland, and is much closer to dust and pollution sources than the over-ocean values of the MODIS AOD retrieval. Consequently, AOD values measured over Ilorin should be greater than over-ocean MODIS AOD values.

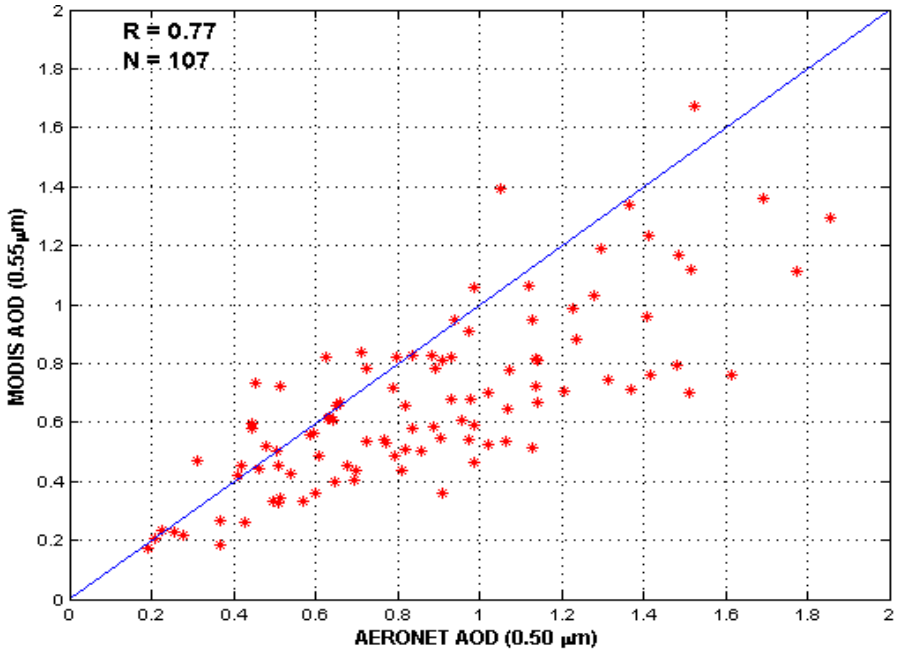

Figure 35. Annual scatter plot of daily AERONET and MODIS AOD values for Ilorin in the West Africa basin for 2006-2007. The daily AOD values (red stars) and one-to-one line (blue) are denoted. The correlation coefficient (R) and sample size (N) are listed in the upper left corner.

Figure 36 contains scatter plots of AERONET and MODIS AOD values by season for the 2006-2007 timeframe. A low bias exists in the seasonal comparisons. The MODIS retrieval regularly underestimates AOD values, especially in the dry season (Winter and Spring). Sample size is small during Summer and Fall. The Summer and Fall encompasses the cloudy, wet season in West Africa, so the number of cloud-free days on which MODIS can make retrievals is low. Even with a low sample size, Figure 36 suggests that the MODIS AOD retrieval may not provide representative AOD values for the West Africa basin, due to the proximity of the AERONET sites to the dust and pollution sources.

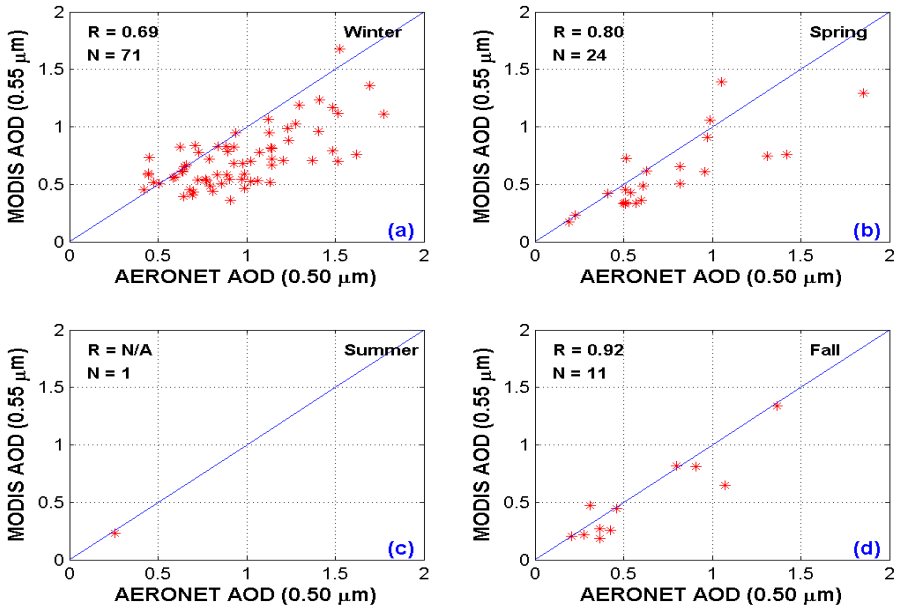

Figure 36. West Africa Basin AERONET AOD (0.50μm) versus MODIS AOD (0.55μm) scatterplots for the 2006-2007 seasons: (a) Winter, (b) Spring, (c) Summer, (d) Fall. The daily AOD values (red stars) and one-to-one line (blue) are denoted. The correlation coefficient (R) and sample size (N) are listed in the upper left corner.

Figure 37 displays MODIS and AERONET annual cumulative frequency curves from the West Africa basin for the two-year period (2006-2007). The MODIS cumulative frequency curve is derived from the two-year West Africa basin MODIS AOD distribution histogram, located in Appendix B (Figure 91). The AERONET cumulative frequency curve is taken from the two-year basin AERONET AOD distribution histogram (Figure 23). The MODIS cumulative frequency curve remains to the left of the AERONET curve, suggesting that on an annual basis the MODIS AOD retrieval underestimates aerosol loading over West Africa. Due to the distance between the MODIS grid point and aerosol sources, it is reasonable that on an annual basis, the MODIS AOD retrieval underestimates aerosol loading. The implication from Figure 37 is that analysts should expect MODIS to underestimate aerosol loading over the West Africa basin.

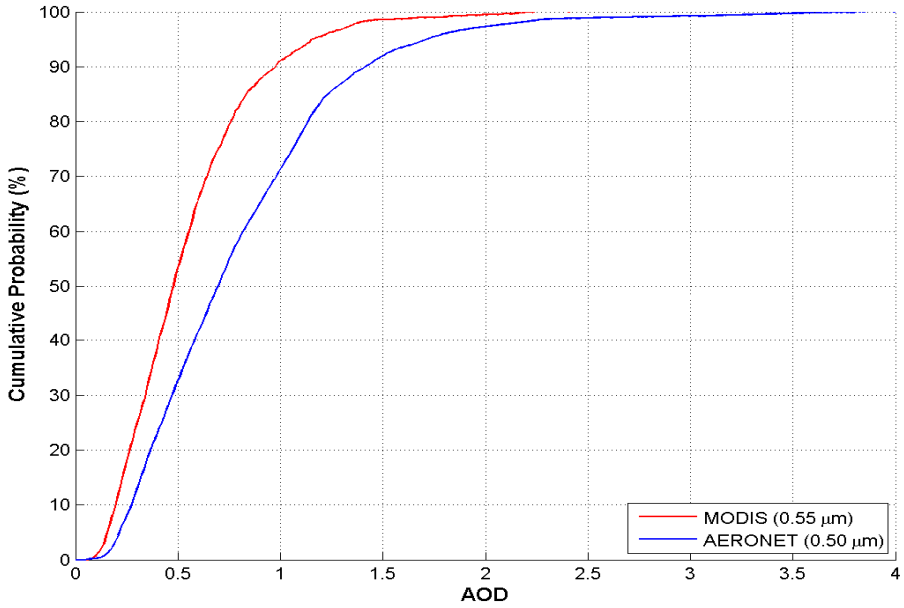

Figure 37. Annual cumulative frequency curves for the West Africa basin MODIS (red) and AERONET (blue) AOD distributions. The y-axis indicates the cumulative probability of occurrence of an AOD. The x-axis indicates the AOD values.

Table 4 provides a summary of the statistical results for the MODIS/AERONET AOD comparison for the West Africa basin. Correlation coefficients range from 0.69 to 0.92. MODIS AOD results from the Fall season appear to be more reliable than for the other seasons.

Table 4. MODIS/AERONET AOD Correlations for West Africa basin for 2006-2007

	R (correlation)	N (sample size)
Annual	0.77	107
Winter	0.69	71
Spring	0.80	24
Summer	N/A	1
Fall	0.92	11

In summary, MODIS-retrieved AOD values consistently underestimate aerosol loading throughout the West Africa basin. As such, over-water MODIS-retrieved AOD values are not a reliable proxy for AERONET AOD values over West Africa.

4. Summary

The MODIS AOD retrieval at 0.55μm consistently provides accurate AOD values for the Persian Gulf and Japan basins. The MODIS AOD retrieval is not as accurate for the Korea and West Africa basins. The disparity between MODIS-retrieved and AERONET AOD values over Korea may be due to the small sample sizes over the Korean Peninsula. West Africa, on the other hand, has more MODIS and AERONET AOD data. However, the MODIS results are verified against an AERONET approximately 217 km from the Atlantic coast, which naturally introduces error into the comparison.

C. NAAPS/AERONET COMPARISON

1. Persian Gulf

The purpose of the NAAPS/AERONET comparison is to consider if the NAAPS-modeled AOD values at 0.55μm are representative of ground-based AOD measurements throughout each geographic basin. Because NAAPS AOD values are provided only over water, no AERONET data from Solar Village, Saudi Arabia are included. The NAAPS AOD grid point closest to each coastal station, Dhabi and Dhadnah, UAE, are used for the comparison. Both stations are combined to produce the Persian Gulf basin NAAPS/AERONET comparison.

Figure 38 is the two-year NAAPS 0.55μm AOD distribution for the Persian Gulf basin for 2006-2007. Half of the AOD values lie between 0.25 and 0.45, with the median of the distribution at 0.32. In nearly 80% of the cases the aerosol loading may be light enough to allow for scene correction, using an AOD of 0.50 as a baseline. In comparison, Persian Gulf basin AERONET AOD data (Figure 13) shows that (a) the median of the distribution is 0.35 and (b) 75% of the cases show light enough aerosol loading to allow for scene correction. Therefore, the comparison between Figures 13 and 38 suggests that for the two-year period (2006-2007), the NAAPS aerosol loading over the Persian Gulf basin closely matches the AERONET aerosol loading.

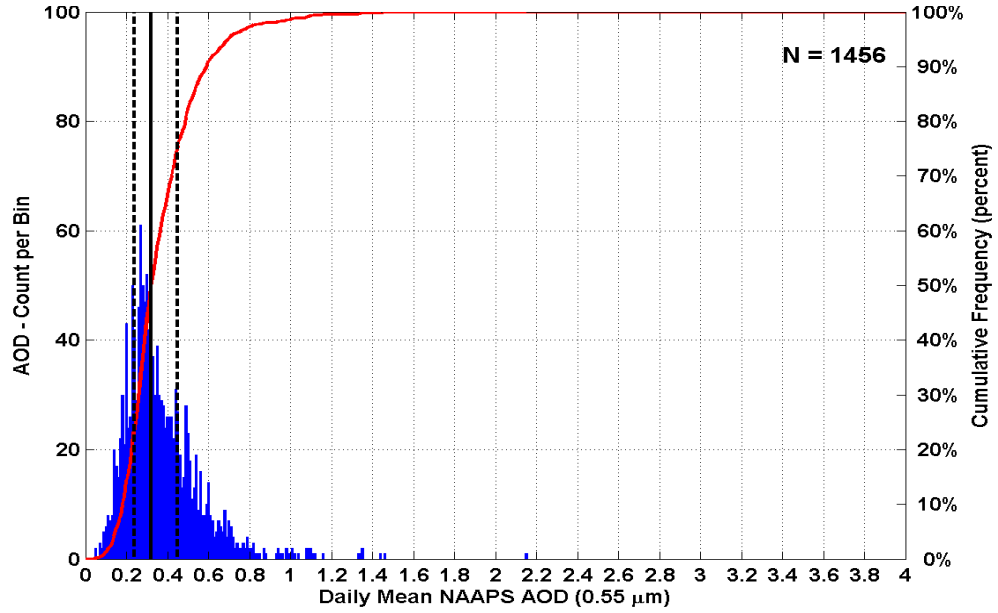

Figure 38. Two-year distribution of daily mean 0.55μm NAAPS AOD values for stations Dhabi and Dhadnah in the Persian Gulf basin, for 2006-2007. The histogram of AOD values (blue bars) and cumulative frequency distribution (red curve) corresponding to the histogram are denoted. The sample size is listed in the upper right corner. The vertical lines (black), from left to right, denote the quartiles of the distribution, 25% (dashed), 50% (solid), 75% (dashed).

Figure 39 contains a scatter plot of AERONET and NAAPS AOD values for the Persian Gulf basin for the two-year period from 2006 through 2007. Agreement between the NAAPS and AERONET values is good. The scatter implies no bias in the comparison. The amount of scatter does increase at higher AOD values (i.e. above 0.60), suggesting that the uncertainty of NAAPS estimates for the Persian Gulf increases with AOD. The uncertainty of NAAPS estimates may increase with AOD due to errors in the modeled wind field, aerosol type, and dust source. Additionally, the uncertainty of the MODIS AOD retrieval assimilated into NAAPS may contribute to the uncertainty of the NAAPS AOD product. However, even with the increase in uncertainty at high AODs, Figure 39 reveals that NAAPS provides accurate AOD values, on an annual basis, for the Persian Gulf basin.

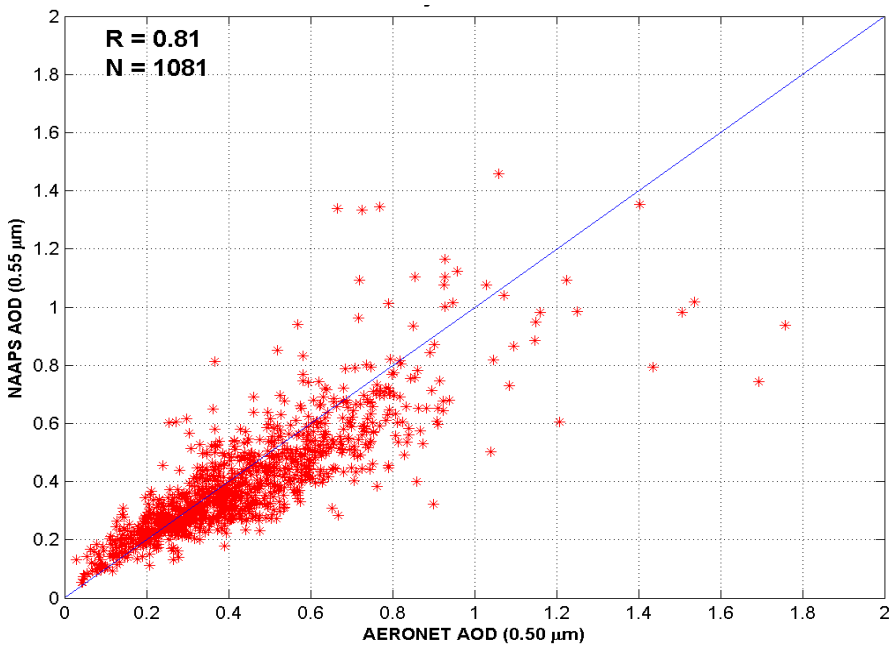

Figure 39. Annual scatter plot of daily AERONET and NAAPS AOD values for the Persian Gulf basin for 2006-2007. The daily AOD values (red stars) and one-to-one line (blue) are denoted. The correlation coefficient (R) and sample size (N) are listed in the upper left corner.

Figure 40 contains scatter plots of AERONET and NAAPS AOD values by season for the 2006-2007 timeframe. The correlation is consistent across seasons, indicating that the accuracy of NAAPS AOD forecasts varies little by season.

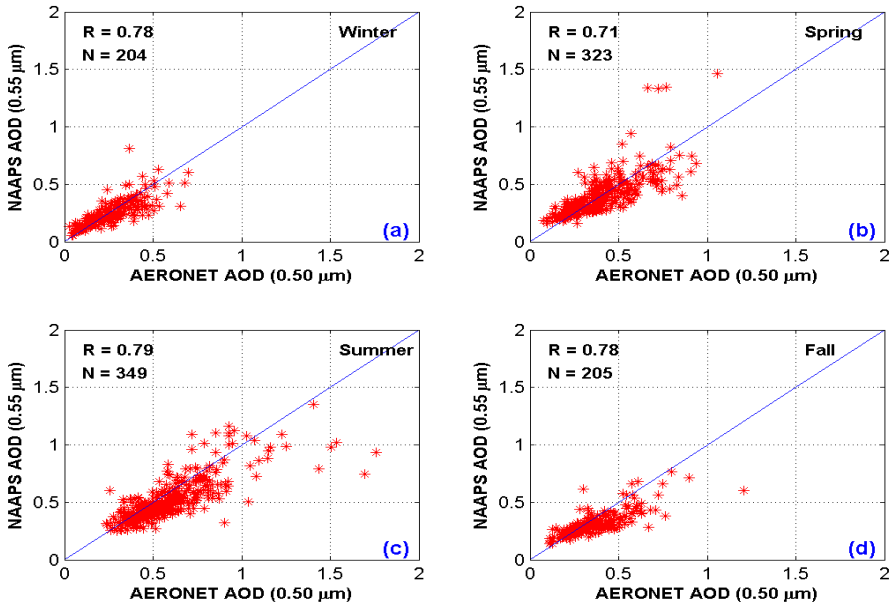

Figure 40. Persian Gulf Basin AERONET AOD (0.50µm) versus NAAPS AOD (0.55µm) scatterplots for the 2006-2007 seasons: (a) Winter, (b) Spring, (c) Summer, (d) Fall. The daily AOD values (red stars) and one-to-one line (blue) are denoted. The correlation coefficient (R) and sample size (N) are listed in the upper left corner.

In conclusion, the results for the Persian Gulf basin NAAPS/AERONET comparison are very promising. Figures 38, 39, and 40 suggest that the NAAPS with assimilated MODIS AOD data does provide representative AOD values for the Persian Gulf basin.

2. East Asia

a. Korea

The NAAPS AOD grid point closest to Anmyon, South Korea is used for the Korea basin comparison. Figure 41 is the two-year NAAPS 0.55µm AOD distribution for the Korea basin for 2006-2007. Half of the AOD values lie between 0.20 and 0.45, with the median of the distribution at 0.30. In 75% of the cases, the aerosol loading may be light enough to allow for scene correction, using an AOD of 0.50 as a

baseline. In comparison, Korea basin AERONET AOD data (Figure 16) shows that (a) the median of the distribution is 0.28 and (b) 75% of the cases show light enough aerosol loading to allow for scene correction. The comparison between Figures 16 and 41 suggests that for the two-year period, the NAAPS aerosol loading over the Korea basin closely matches the AERONET aerosol loading.

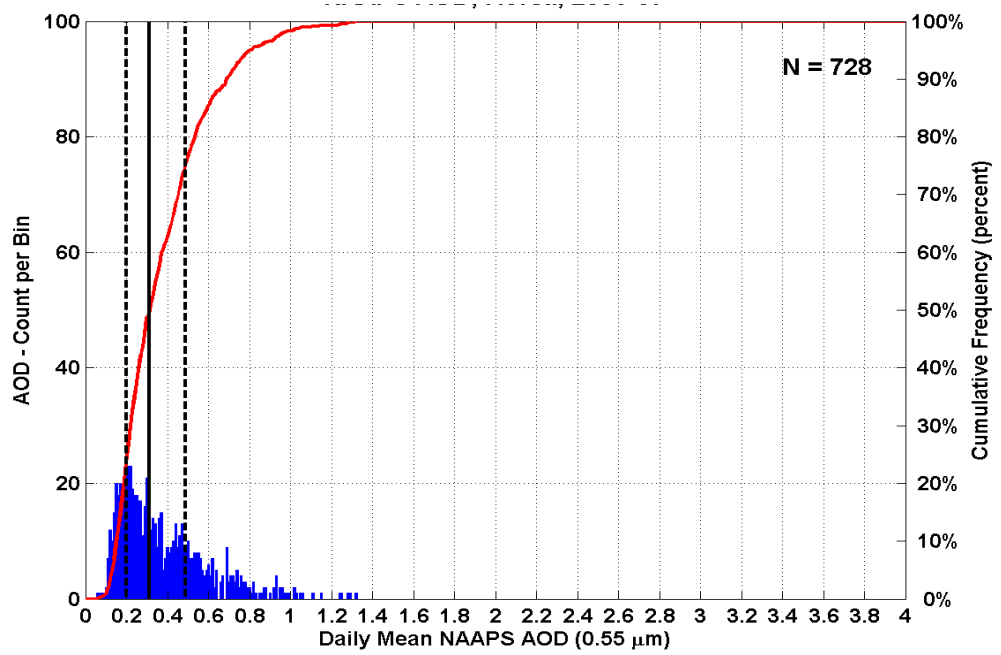

Figure 41. Two-year distribution of 0.55μm NAAPS AOD values for Anmyon in the Korea basin, for 2006-2007. The histogram of AOD values (blue bars) and cumulative frequency distribution (red curve) corresponding to the histogram are denoted. The sample size is listed in the upper right corner. The vertical lines (black), from left to right, denote the quartiles of the distribution, 25% (dashed), 50% (solid), 75% (dashed).

Figure 42 contains a scatter plot of AERONET and NAAPS AOD values for the Korea basin for the two-year period from 2006 through 2007. The scatter is not symmetric around the one-to-one line for AOD values above 0.80. Figure 42 appears to show a tendency for NAAPS to underestimate high AOD events, especially when the AOD is greater than 0.80.

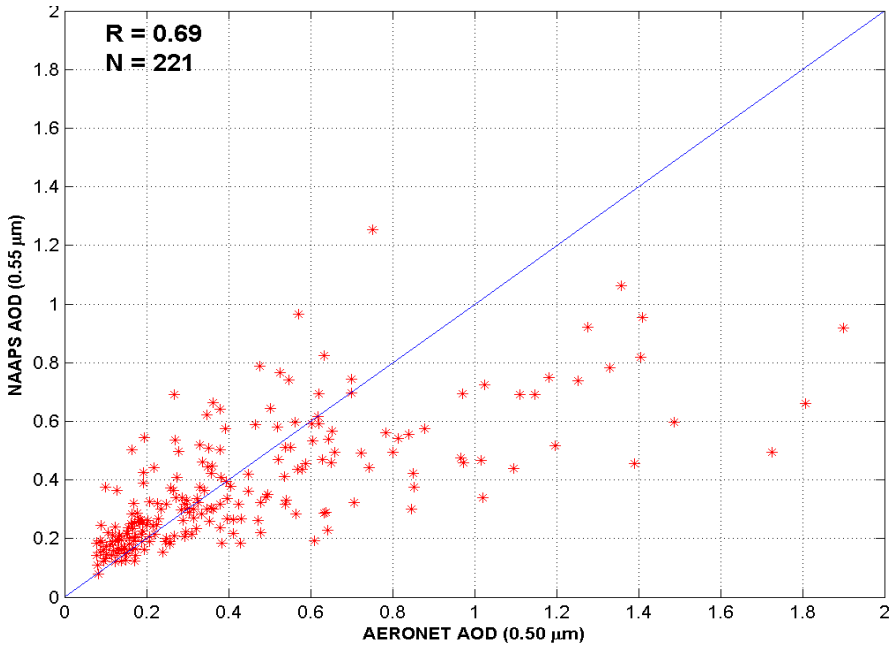

Figure 42. Annual scatter plot of daily AERONET and NAAPS AOD values for the Korea basin for 2006-2007. The daily AOD values (red stars) and one-to-one line (blue) are denoted. The correlation coefficient (R) and sample size (N) are listed in the upper left corner.

Figure 43 contains scatter plots of AERONET and NAAPS AOD values by season for the 2006-2007 timeframe. Correlation coefficients range from 0.59 to 0.78. Figure 43 suggests a lower correlation between NAAPS and AERONET AOD values for the Korea basin than the Persian Gulf. Additionally, Fall and Winter show much less scatter than Spring and Summer, indicating less uncertainty in NAAPS AOD estimates in Fall and Winter. Finally, the correlation is highest in the Winter.

In summary, Figures 41, 42, and 43 indicate mixed results for the Korea basin. The NAAPS distribution over the two-year period (Figure 41) compared well with the AERONET distribution for the basin (Figure 16). The point-to-point daily mean NAAPS and AERONET comparison indicates a tendency for NAAPS to underestimate AOD on days with AOD values greater than 0.80.

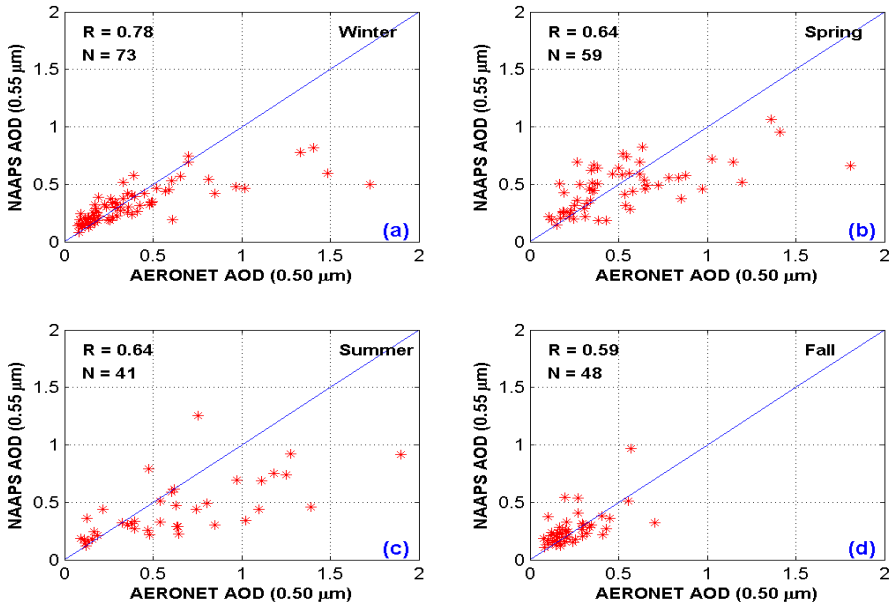

Figure 43. Korea Basin AERONET AOD (0.50µm) versus NAAPS AOD (0.55µm) scatterplots for the 2006-2007 seasons: (a) Winter, (b) Spring, (c) Summer, (d) Fall. The daily AOD values (red stars) and one-to-one line (blue) are denoted. The correlation coefficient (R) and sample size (N) are listed in the upper left corner.

b. Japan

The NAAPS AOD grid point closest to each of the two Japan stations, Shirahama and Osaka is used in the Japan basin comparison. Figure 44 is the two-year NAAPS 0.55µm AOD distribution for the Japan basin for 2006-2007. Half of the AOD values lie between 0.15 and 0.30, with the median of the distribution at 0.21. In 95% of the cases, the aerosol loading may be light enough to allow for scene correction, using an AOD value of 0.50 as a baseline. In comparison, Japan basin AERONET AOD data (Figure 17) shows that (a) the median of the distribution is also 0.21 and (b) 87% of the cases show light enough aerosol loading to allow for scene correction. The comparison between Figures 17 and 44 suggests that for the two-year period, the NAAPS estimates of aerosol loading over the Japan basin closely matches the AERONET aerosol loading.

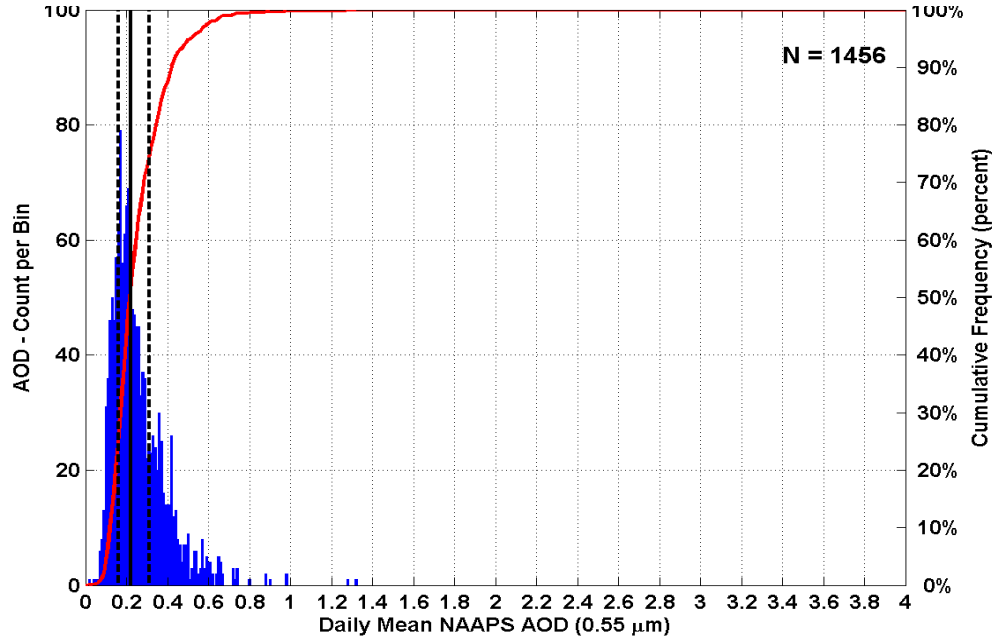

Figure 44. Two-year distribution of 0.55μm NAAPS AOD values for Osaka and Shirahama in the Japan basin, for 2006-2007. The histogram of AOD values (blue bars) and cumulative frequency distribution (red curve) corresponding to the histogram are denoted. The sample size is listed in the upper right corner. The vertical lines (black), from left to right, denote the quartiles of the distribution, 25% (dashed), 50% (solid), 75% (dashed).

Figure 45 contains a scatter plot of AERONET and NAAPS AOD values for the Japan basin for the two-year period from 2006 through 2007. The correlation is 0.73. NAAPS AOD values display a low bias at higher AOD values greater than 0.40. Consequently, NAAPS AOD values for the Japan basin are likely to be low when aerosol loading is heavy. Otherwise, there is good agreement between the NAAPS and AERONET AOD values.

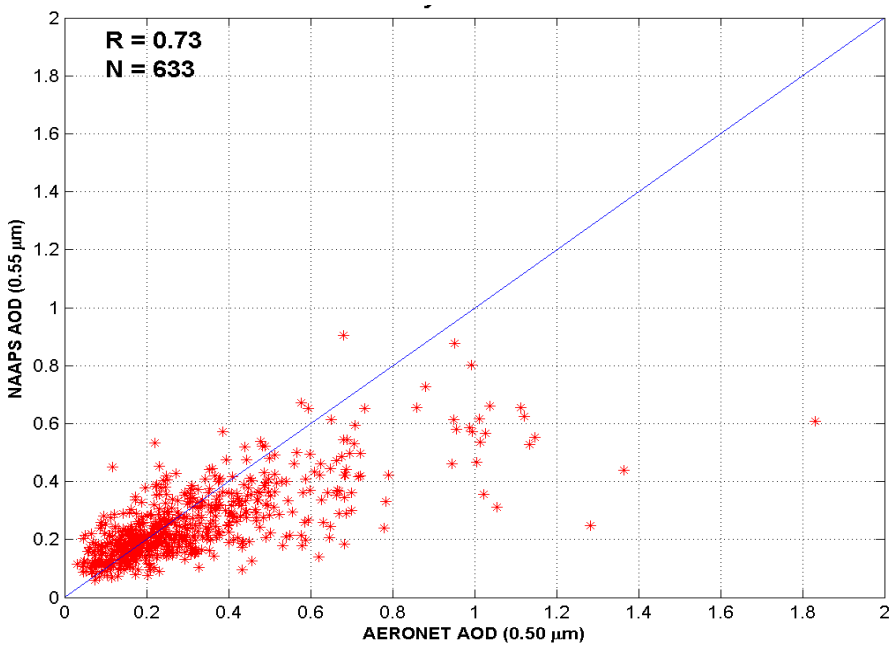

Figure 45. Annual scatter plot of daily AERONET and NAAPS AOD values for the Japan basin for 2006-2007. The daily AOD values (red stars) and one-to-one line (blue) are denoted. The correlation coefficient (R) and sample size (N) are listed in the upper left corner.

Figure 46 contains scatter plots of AERONET and NAAPS AOD values by season for 2006-2007. The tendency to underestimate higher AOD values, seen in Figure 45, is also seen in the seasonal scatter plots. The underestimation is most prominent in the Spring and Summer seasons when aerosol loading is highest. In the Fall season, which has a lighter aerosol load than Spring and Summer, the underestimation occurs for AOD values greater than 0.25. NAAPS estimates have the highest correlation for the Winter season. Overall, Figure 46 suggests that NAAPS performs best over the Japan basin when aerosol loading is low.

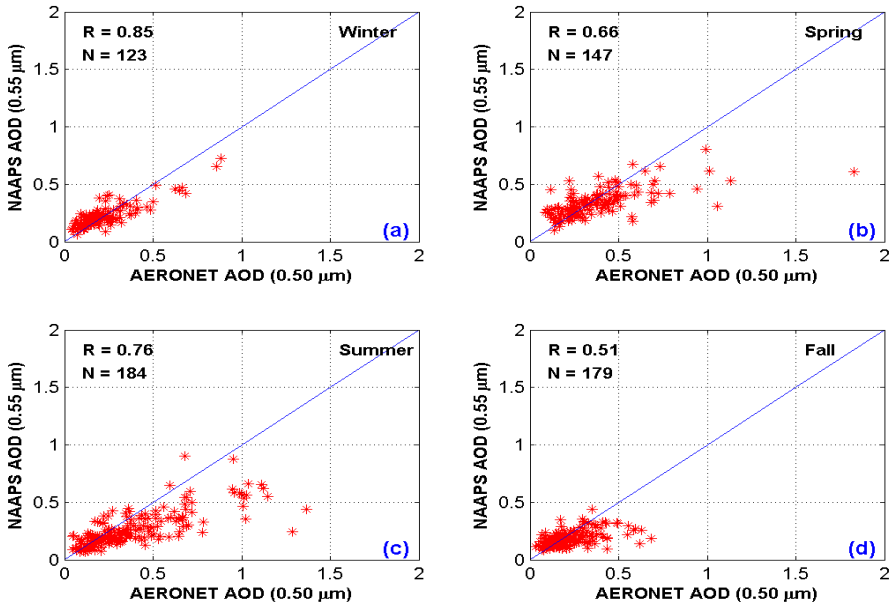

Figure 46. Japan Basin AERONET AOD (0.50µm) versus NAAPS AOD (0.55µm) scatterplots for the 2006-2007 seasons: (a) Winter, (b) Spring, (c) Summer, (d) Fall. The daily AOD values (red stars) and one-to-one line (blue) are denoted. The correlation coefficient (R) and sample size (N) are listed in the upper left corner.

In summary, the results for the Japan NAAPS/AERONET comparison are promising. Figures 44, 45, and 46 show that the NAAPS does provide representative AOD values for the Japan basin when the aerosol loading is low.

3. West Africa

The NAAPS AOD grid point closest to Ilorin, Nigeria is used for the West Africa basin comparison, but this grid point is over water approximately 350 km due south of Ilorin. Figure 47 is the two-year NAAPS 0.55µm AOD distribution for the West Africa basin for 2006-2007. Half of the AOD values lie between 0.20 and 0.40, with the median of the distribution at 0.30. In 82% of the cases, the aerosol loading may be light enough to allow for scene correction, using an AOD of 0.50 as a baseline. In comparison, West Africa basin AERONET AOD data (Figure 23) shows that (a) the median of the distribution is 0.70 and (b) only 35% of the cases show light enough aerosol loading to

allow for scene correction. Therefore, the comparison between Figures 23 and 47 suggest that on an annual basis, the NAAPS aerosol loading over the West Africa basin is significantly less than the AERONET aerosol loading.

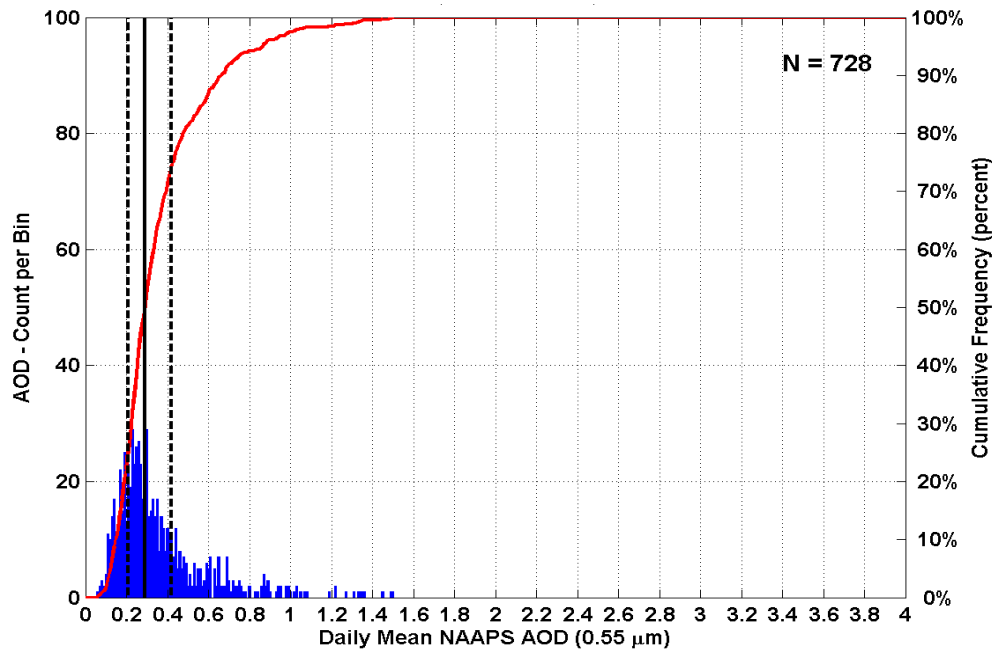

Figure 47. Two-year distribution of 0.55μm NAAPS AOD values for Ilorin in the West Africa basin, for 2006-2007. The histogram of AOD values (blue bars) and cumulative frequency distribution (red curve) corresponding to the histogram are denoted. The sample size is listed in the upper right corner. The vertical lines (black), from left to right, denote the quartiles of the distribution, 25% (dashed), 50% (solid), 75% (dashed).

Figure 48 contains a scatter plot of AERONET and NAAPS AOD values for the West Africa basin for the two-year period from 2006 through 2007. The scatter implies a low bias in the NAAPS AOD values. The MODIS/AERONET comparison similarly reveals a low bias for West Africa. Consequently, the NAAPS AOD estimates for the West Africa basin are likely to be lower than AERONET AOD measurements.

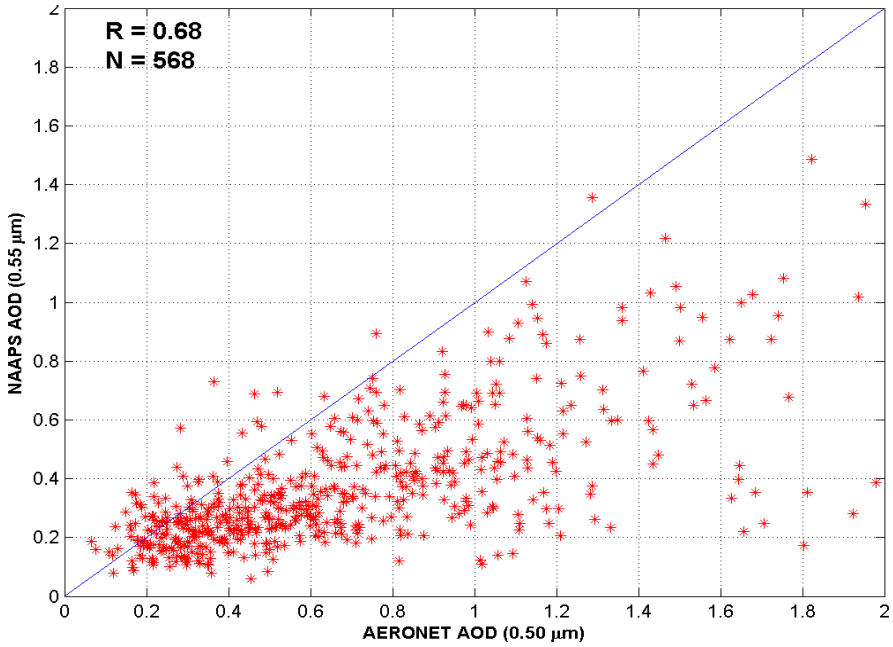

Figure 48. Annual scatter plot of daily AERONET and NAAPS AOD values for the West Africa basin for 2006-2007. The daily AOD values (red stars) and one-to-one line (blue) are denoted. The correlation coefficient (R) and sample size (N) are listed in the upper left corner.

Figure 49 contains scatter plots of AERONET and NAAPS AOD values by season for 2006-2007. All seasons display the tendency for NAAPS to underestimate AOD values. The correlation is not consistent across seasons, and all seasons display a low bias.

In summary, NAAPS AOD estimates consistently underestimate aerosol loading in the West Africa basin. The comparison of MODIS and AERONET in the West Africa basin provided similar results. With both the NAAPS and MODIS datasets, the over-water grid point is more than 300 km away from the AERONET station and dust and pollution sources. It is reasonable that on an annual basis NAAPS will underestimate aerosol loading.

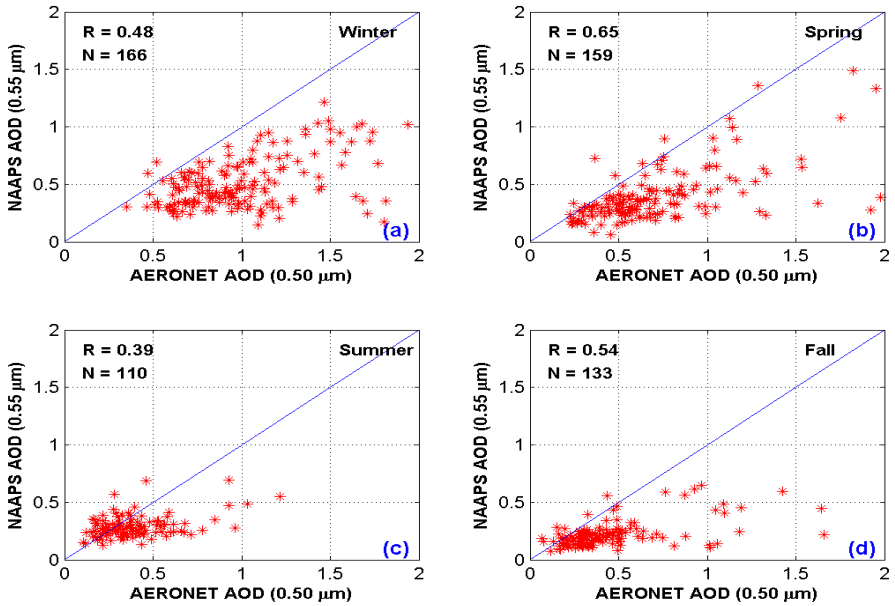

Figure 49. West Africa Basin AERONET AOD (0.50µm) versus NAAPS AOD (0.55µm) scatterplots for the 2006-2007 seasons: (a) Winter, (b) Spring, (c) Summer, (d) Fall. The daily AOD values (red stars) and one-to-one line (blue) are denoted. The correlation coefficient (R) and sample size (N) are located in the upper left corner.

4. Summary

The results from the NAAPS/AERONET comparison indicate that the NAAPS AOD estimates are a reliable proxy for AERONET AOD data over the Persian Gulf and Japan basins, especially when aerosol loading is light. The comparison results for the Korea and West Africa basins are less conclusive, due to low sample size (Korea) and distance from the coast (West Africa). Errors in the modeled wind field, aerosol types, and aerosol sources no doubt account for some of the uncertainty associated with the NAAPS estimates. Additionally, there is uncertainty in the MODIS AOD retrievals which are assimilated into NAAPS. Limitations of the MODIS AOD retrievals are beyond the scope of this thesis and are not investigated here.

D. RADIANCE-BASED TARGET DETECTION

This thesis creates a sample radiance-based target detection matrix, Table 5, as described in Chapter III, Section D. The matrix simulates the form of information decision-makers require to estimate the probability that a satellite sensor can distinguish a ground-based target during high AOD events. The matrix is constructed using MODTRAN^{TM} calculations, and displays simulated TOA radiance values by AOD and surface reflectance for a specific wavelength (0.63μm in this study).

To validate the MODTRAN^{TM} radiance values in Table 5, this study uses the TOA radiance measurements from a MODIS image at three locations in the image. For each location, the AOD and surface reflectance are estimated. Figure 50 is a MODIS image for 0630 UTC 14 May 2004, which contains a large dust plume extending from southern Iraq down to western portions of United Arab Emirates. Point 1 in Figure 50 represents a location with a low amount of dust. Point 2 is a location with a moderate amount of dust, and Point 3 is a location with a high amount of dust. Using the TeraVision satellite image display software, TOA radiance values are measured at each point for the following wavelengths: 0.44μm, 0.55μm, 0.65μm, 0.86μm, and 1.60μm. The measured MODIS TOA radiation values at Points 1, 2, and 3 are listed in Table 6.

Table 5. MODTRAN^{TM}-Simulated TOA Radiance ($Wm^{-1}\mu m^{-1}sr^{-1}$) at 0.63µm as a function of AOD (red) and Surface Reflectance (%, blue).

AOD/Surface Reflectance (%)	0	1	5	10	20	30	40
0.00	7.40	10.50	22.90	38.40	69.70	101.00	133.00
0.05	8.10	11.10	23.20	38.30	69.00	100.00	131.00
0.10	8.70	11.70	23.50	38.30	68.30	98.60	129.00
0.20	10.20	13.00	24.20	38.30	66.90	96.00	126.00
0.30	11.80	14.40	25.10	38.50	65.80	93.60	122.00
0.40	13.40	15.90	26.00	38.80	64.70	91.30	118.00
0.50	15.10	17.50	27.10	39.20	63.80	89.10	115.00
0.57	16.30	18.60	27.80	39.50	63.30	87.70	113.00
0.60	16.80	19.10	28.20	39.60	63.10	87.10	112.00
0.70	18.60	20.70	29.30	40.20	62.40	85.30	109.00
0.80	20.30	22.40	30.50	40.80	61.80	83.60	106.00
0.90	22.10	24.00	31.70	41.40	61.30	82.00	103.00
1.00	23.80	25.60	32.90	42.10	60.90	80.50	101.00
1.25	27.90	29.50	35.80	43.80	60.20	77.20	94.90
1.50	31.80	33.10	38.50	45.50	59.70	74.50	90.00
1.75	35.30	36.40	41.10	47.10	59.40	72.30	85.70
2.00	38.40	39.40	43.50	48.60	59.30	70.40	82.10
2.50	43.70	44.50	47.50	51.30	59.20	67.50	76.20
3.00	47.80	48.30	50.50	53.40	59.30	65.40	72.00
3.50	50.80	51.30	52.90	55.00	59.40	64.00	68.80

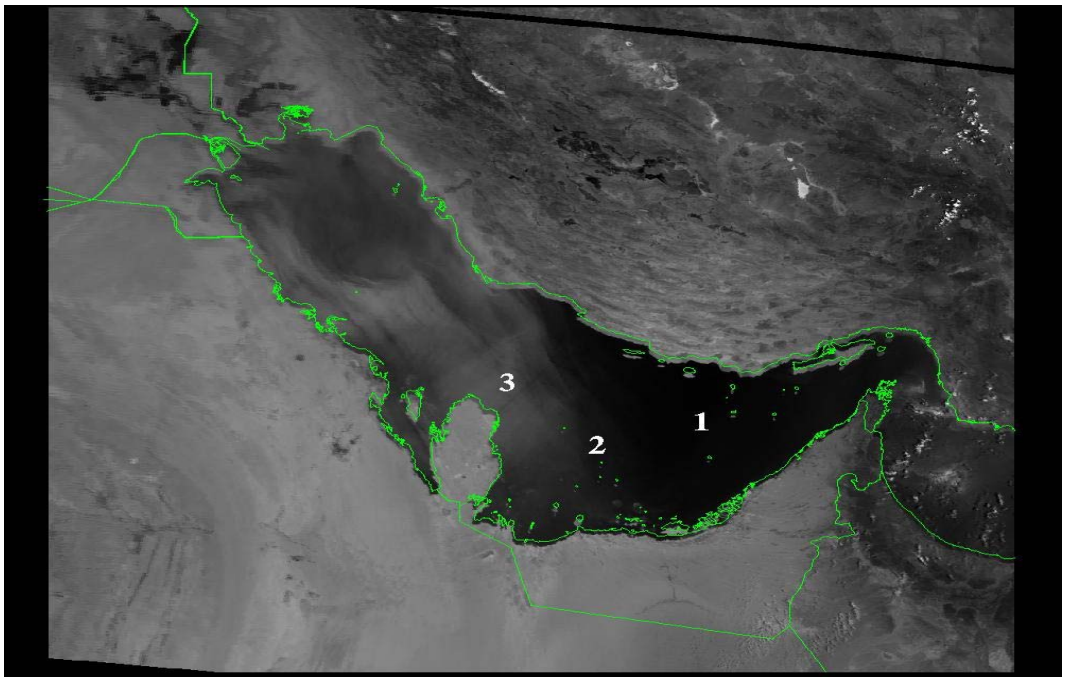

Figure 50. 14 May 2004 0630 UTC MODIS image for the Persian Gulf. Point 1 is a location with a low amount of dust, Point 2: moderate dust, and Point 3: high dust.

Table 6. MODIS Top-of-the-Atmosphere Radiance Values for Points 1, 2, and 3 in Figure 50. Radiance units are $Wm^{-1}\mu m^{-1}sr^{-1}$.

Wavelength (μm)	Point 1 Radiance (Low dust)	Point 2 Radiance (Moderate dust)	Point 3 Radiance (High dust)
0.44	80.40	98.88	140.35
0.55	43.91	69.01	141.92
0.65	27.14	49.30	126.91
0.86	12.85	25.81	77.99
1.60	2.39	4.45	15.30

Comparison of the radiance values for Points 1, 2, and 3 reveals that as atmospheric aerosol (dust) content increases, so does the TOA radiance received by the satellite. The dust in the atmosphere scatters incoming solar radiation, much of which is reflected back to the satellite. Therefore, the TOA radiance values increase as atmospheric aerosol content increases.

Figure 51 provides AOD estimates at 0.63μm for the Persian Gulf using NOAA-17 imagery at 0730 UTC 14 May 04 (Durkee et al. 1991; NRL-Monterey 2009). The AOD values in Figure 51 are an estimate of the AOD values in the MODIS image in Figure 50. The image contains AOD values for the eastern half of the Persian Gulf. No AOD values for the western Persian Gulf are available because the dust is so thick that the AOD retrieval algorithm interprets the dust as cloud cover (Martins et al. 2002). The color-coded legend on the left side of the image lists the AOD values. The AOD values at Point 1, 2, and 3 are respectively: 0.5, 1.5, and 2.4.

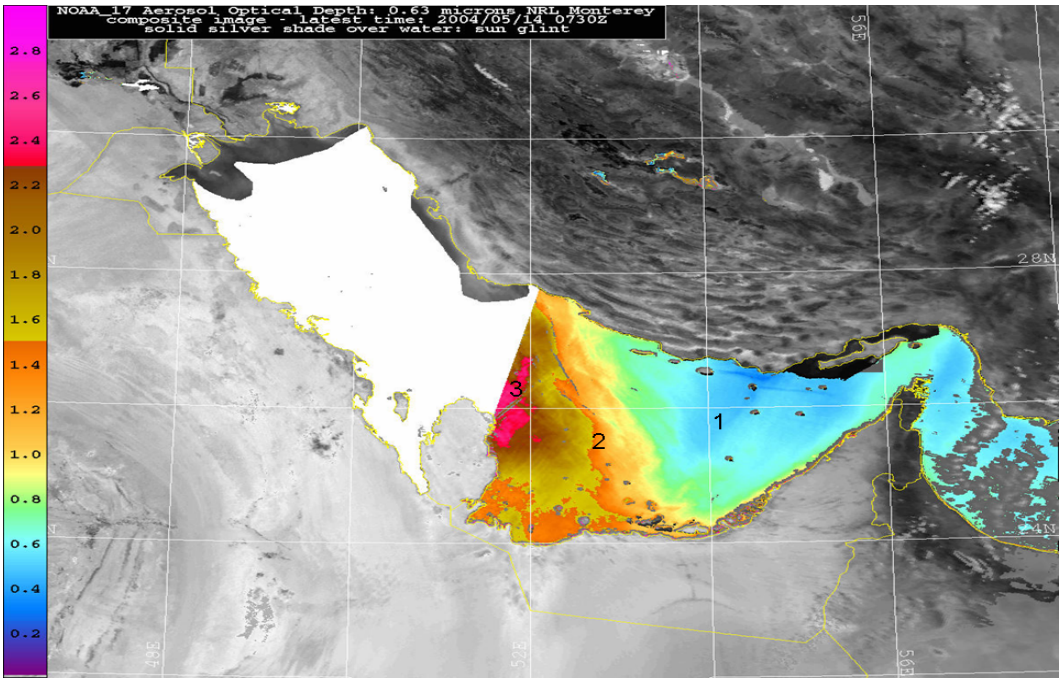

Figure 51. 14 May 2004 0730 UTC NOAA-17 image, 0.63µm, denoting retrieved AODs for the Persian Gulf basin (NRL-Monterey, 2009). Points 1, 2, and 3 are the same locations denoted in Figure 50.

A representative ocean surface reflectance for Points 1-3 is five percent (ASTER Spectral Library 2009). Using the five percent surface reflectance column in Table 5 and the AOD values corresponding to Points 1-3, the MODTRAN™-estimated TOA radiance values are extracted from Table 5. The MODIS TOA radiance measurements at 0.65 µm and the MODTRAN™ TOA radiance estimates at 0.63 µm are displayed in Table 7.

Table 7. TOA Radiance ($Wm^{-1}\mu m^{-1}sr^{-1}$) from the MODIS image (Figure 50) and MODTRAN™ simulation (Table 5) and the NOAA-17 AOD estimates from Figure 51.

Point	NOAA-17 AOD (0.63 µm)	MODIS (0.65 µm)	MODTRAN™ (0.63 µm)
1	0.50	27.14	27.10
2	1.50	49.30	38.50
3	2.40	126.91	47.50

At Point 1, there is little difference between the measured and simulated TOA radiance values. At Point 2, with moderate dust, the MODIS TOA radiance is higher than the simulated radiance. At Point 3, with high dust loading, significantly more radiance is detected by the MODIS sensor than MODTRAN™ simulates. As AOD increases above approximately 0.5, MODTRAN™ may not fully account for the amount of multiple scatter interactions with the aerosols, which would reduce the simulated TOA radiance. Consequently, MODTRAN™ estimates of TOA radiance are currently insufficient to produce a matrix for operational use.

V. CONCLUSIONS AND RECOMMENDATIONS FOR FUTURE RESEARCH

A. CONCLUSIONS

The MODIS data used in this study is reliable in retrieving AOD values at 0.55μm for the Persian Gulf and Japan basins, when compared to AERONET data at 0.50μm. Consequently, data from this MODIS retrieval may be used with confidence over the Persian Gulf and Japan. For the Korea basin, the MODIS AOD retrieval at 0.55μm may provide close to ground truth AOD values. Larger AERONET and MODIS AOD sample sizes will help reduce uncertainty and increase the reliability of MODIS AOD measurements over the Korea basin. As for West Africa, MODIS-retrieved AOD values consistently underestimate aerosol loading. As such, over-water MODIS-retrieved AOD values are not a reliable proxy for AERONET AOD values over continental West Africa.

Likewise, the NAAPS with NAVDAS-AOD model used in this study is reliable in forecasting AOD values at 0.55μm for the Persian Gulf and Japan basins, when compared to AERONET data at 0.50μm. Consequently, data from this model may be used with confidence over the Persian Gulf and Japan. The accuracy of NAAPS forecasts for Korea and West Africa is less certain. NAAPS estimates show some skill for Korea, but larger sample sizes should improve accuracy over Korea. The low bias over West Africa is most likely due to the distance between the NAAPS AOD grid point and the AERONET station.

This thesis is unable to validate the MODTRAN^{TM} TOA radiance calculation because of the large disparity between the MODTRAN^{TM} radiances and MODIS radiances. Consequently, MODTRAN^{TM} estimates of TOA radiance are currently insufficient to produce a matrix for operational use.

B. RECOMMENDATIONS FOR FUTURE RESEARCH

This study uses NAAPS and MODIS data at only one wavelength. More research needs to be done to determine how well each system characterizes aerosols at other wavelengths and thereby determine the impacts of different particle sizes.

Additionally, lack of data was a problem over Korea. In the future, data from eastern China needs to be used to help account for conditions on the east coast of the Yellow Sea. Also, if new AERONET stations happen to be set up along the Atlantic Coast in West Africa, their data needs to be included in future studies for this region.

APPENDIX A: AOD VARIATION BY WAVELENGTH

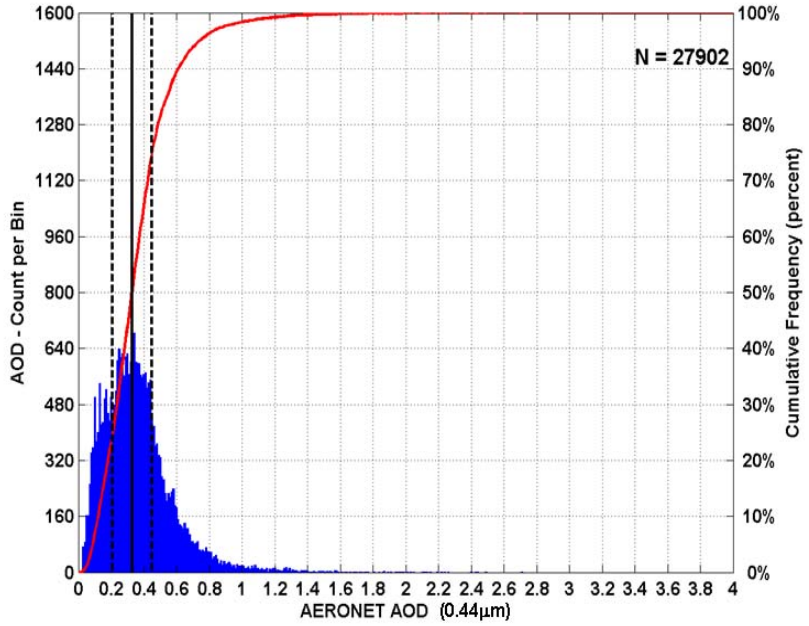

Figure 52. Two-year distribution of AERONET AOD (0.44µm) values for Solar Village for 2006-2007. The histogram of AOD values (blue bars) and cumulative frequency distribution (red curve) corresponding to the histogram are denoted. The sample size is listed in the upper right corner. The vertical lines (black), from left to right, denote the quartiles of the distribution, 25% (dashed), 50% (solid), 75% (dashed).

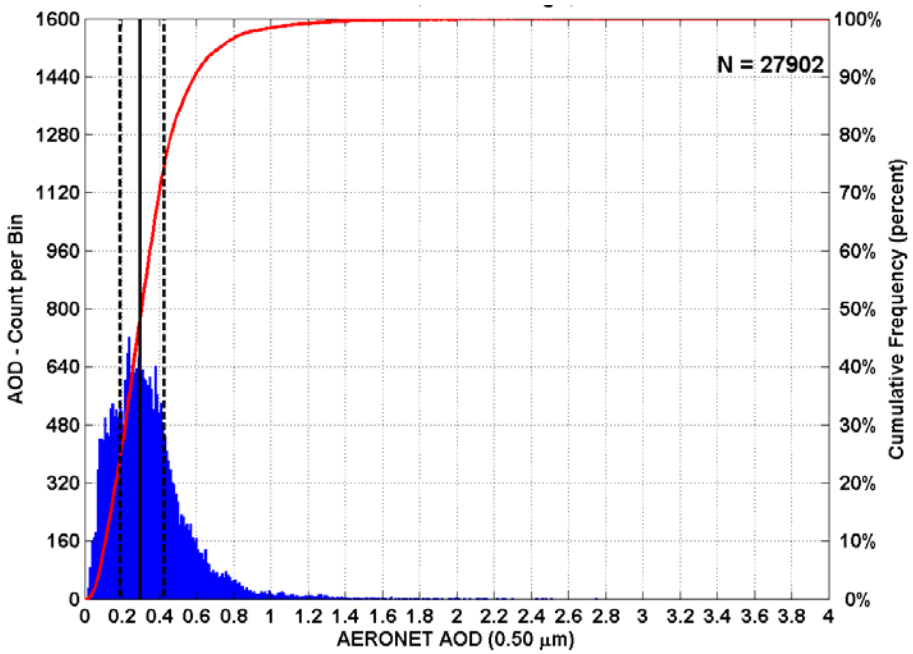

Figure 53. Same as Figure 52, but for 0.50µm.

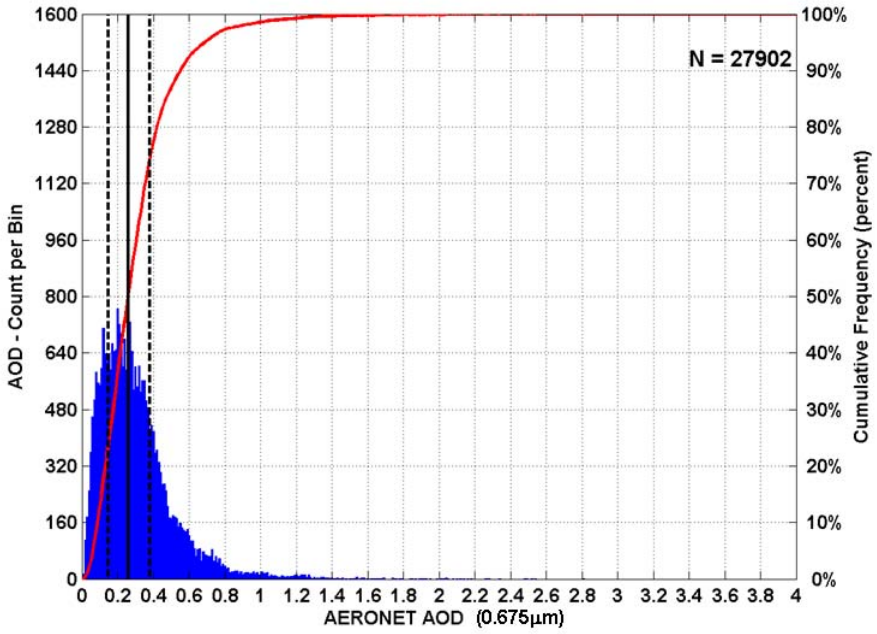

Figure 54. Same as Figure 52, but for 0.675µm.

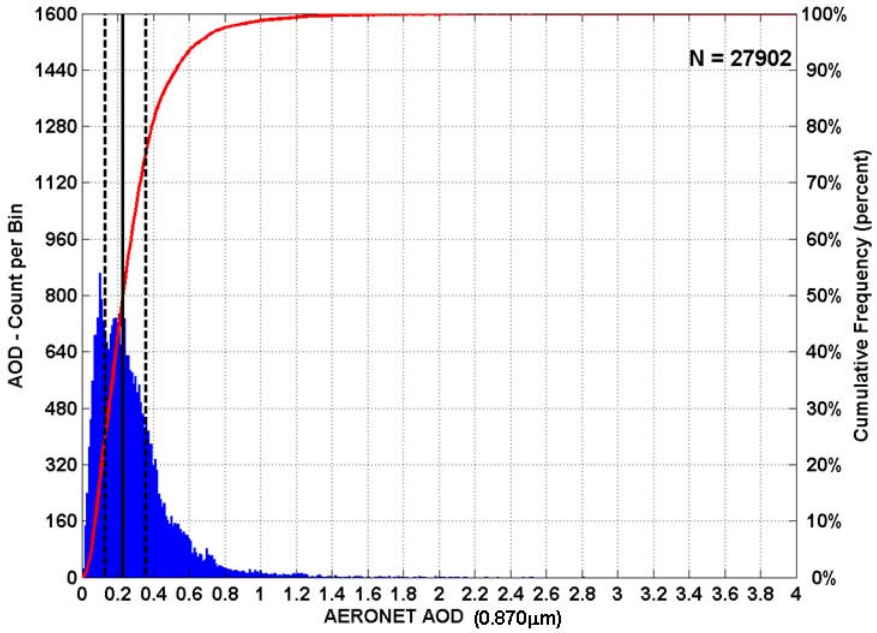

Figure 55. Same as Figure 52, but for 0.870µm.

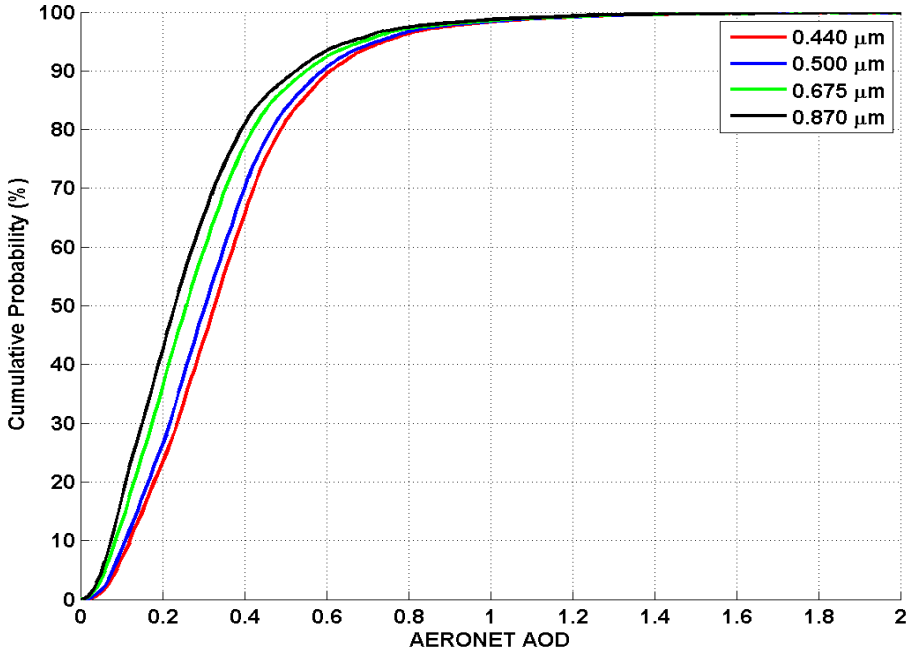

Figure 56. Solar Village AERONET AOD Cumulative Frequency Curves for 0.44µm, 0.50µm, 0.675µm and 0.870µm for 2006-2007.

THIS PAGE INTENTIONALLY LEFT BLANK

APPENDIX B: AERONET CLIMATOLOGY

A. PERSIAN GULF

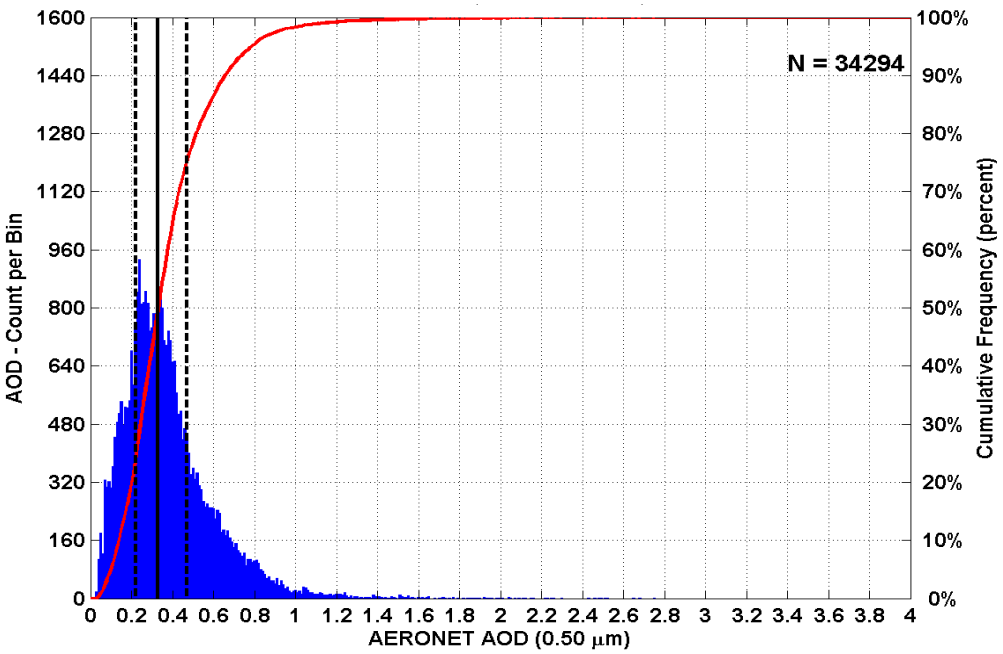

Figure 57. One-year distribution of 0.50 μm AERONET AOD values for the Persian Gulf basin for 2006. The histogram of AOD values (blue bars) and cumulative frequency distribution (red curve) corresponding to the histogram are denoted. The sample size is listed in the upper right corner. The vertical lines (black), from left to right, denote the quartiles of the distribution, 25% (dashed), 50% (solid), 75% (dashed).

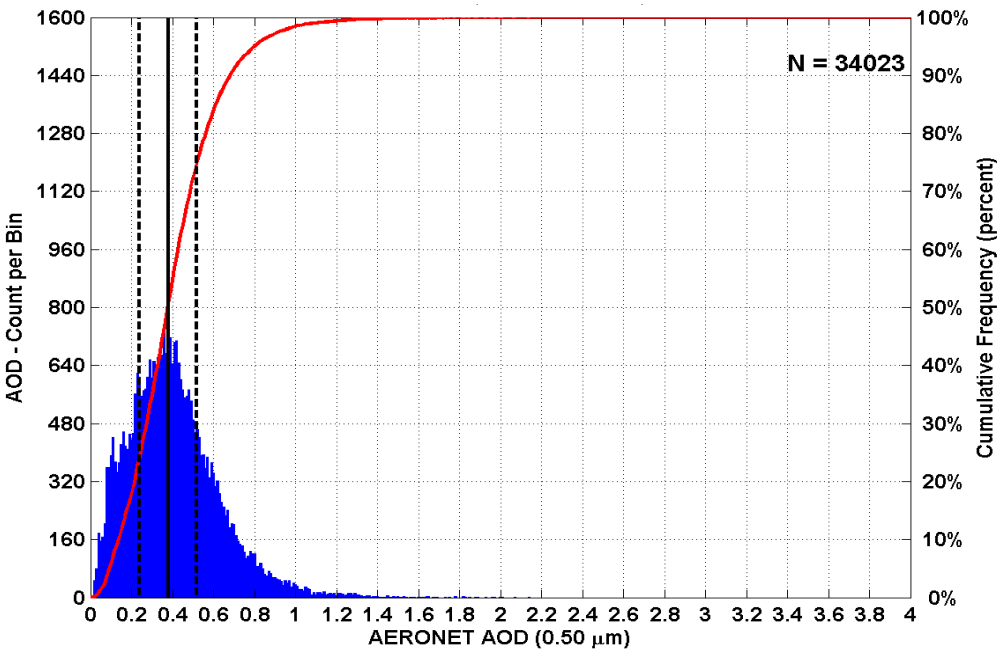

Figure 58. Same as Figure 57, but for 2007.

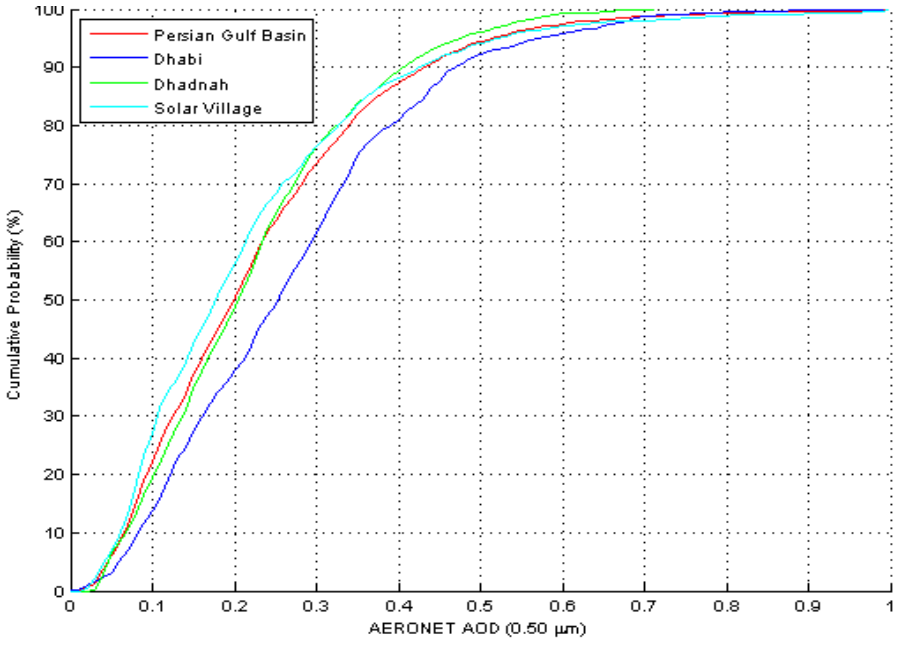

Figure 59. Two-year Winter cumulative frequency curves for the Persian Gulf Basin for 2006-2007. The cumulative frequency curve for each individual station is compared with the cumulative frequency curve computed from the histogram distribution for the combined dataset of the three stations (red curve).

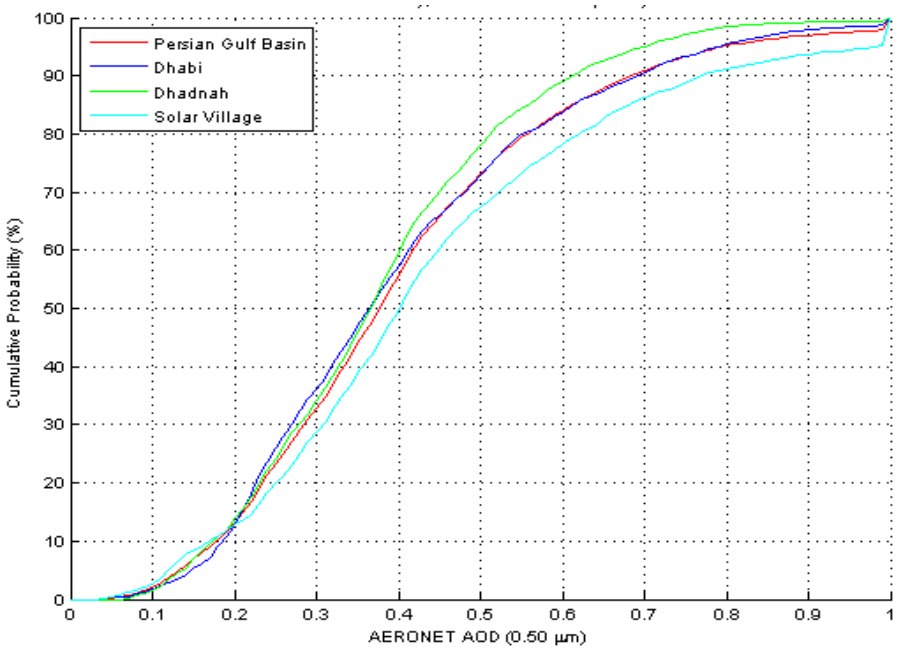

Figure 60. Same as Figure 59, but for Spring.

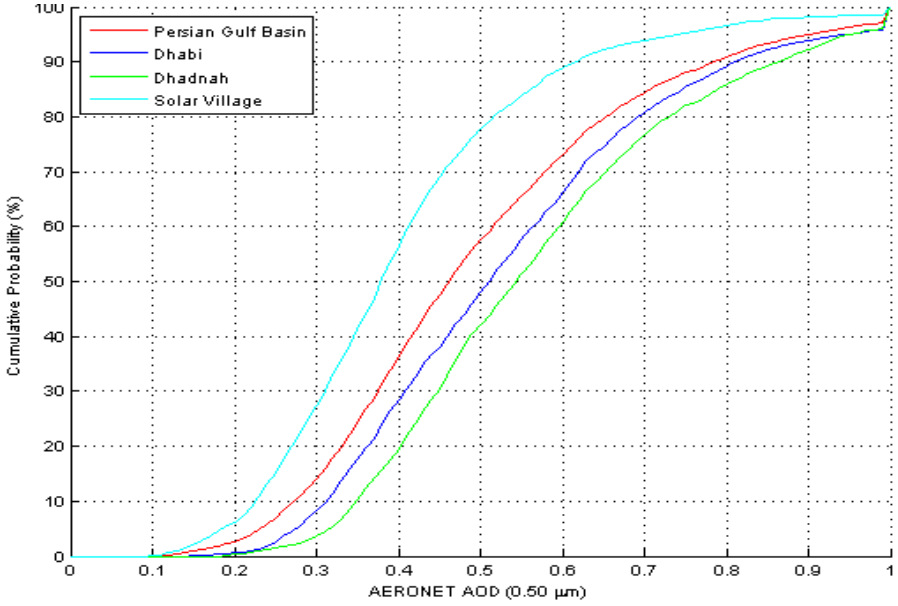

Figure 61. Same as Figure 59, but for Summer.

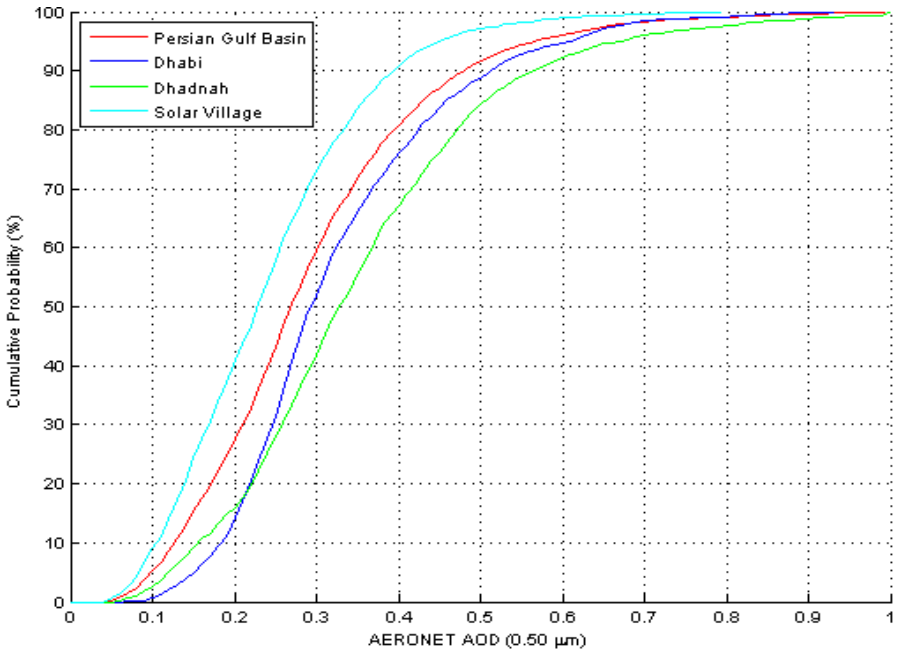

Figure 62. Same as Figure 59, but for Fall.

B. EAST ASIA

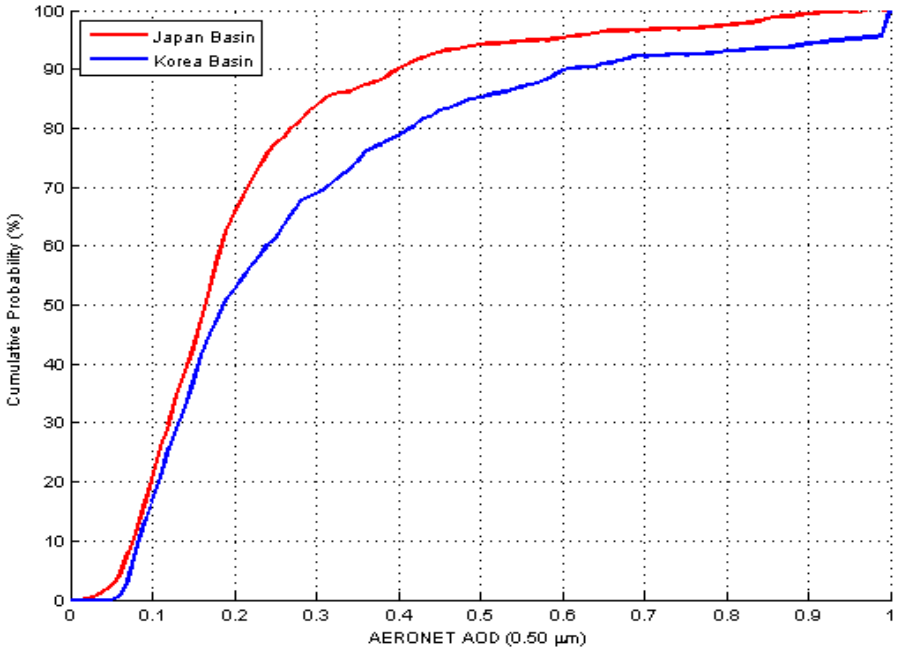

Figure 63. Two-year Winter cumulative frequency curves for Korea (blue) and Japan (red) for 2006-2007.

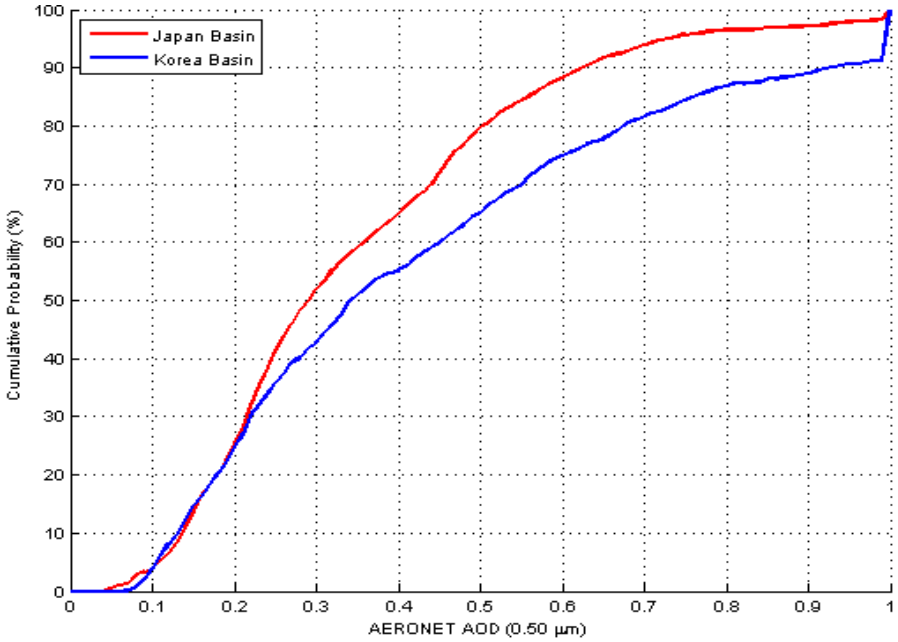

Figure 64. Same as Figure 63, but for Spring.

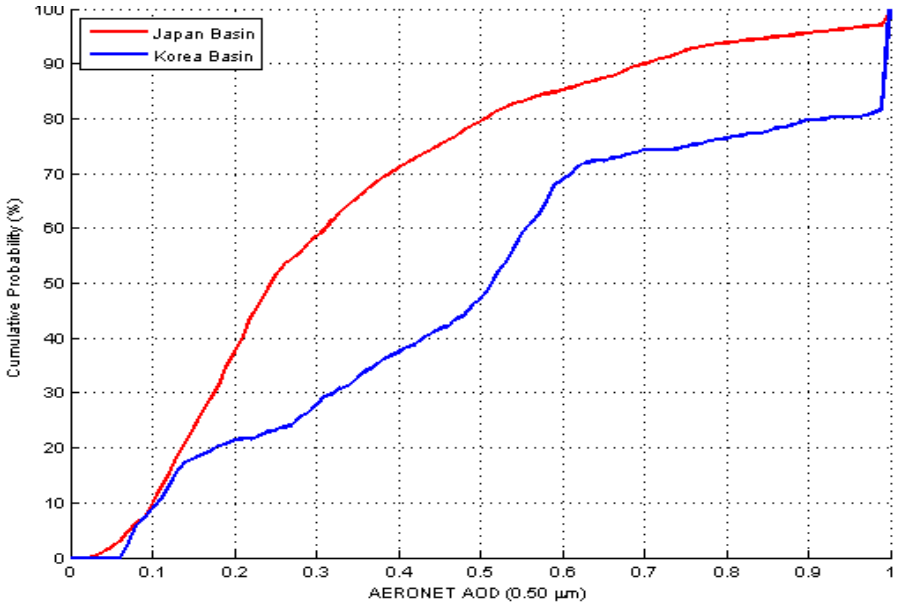

Figure 65. Same as Figure 63, but for Summer.

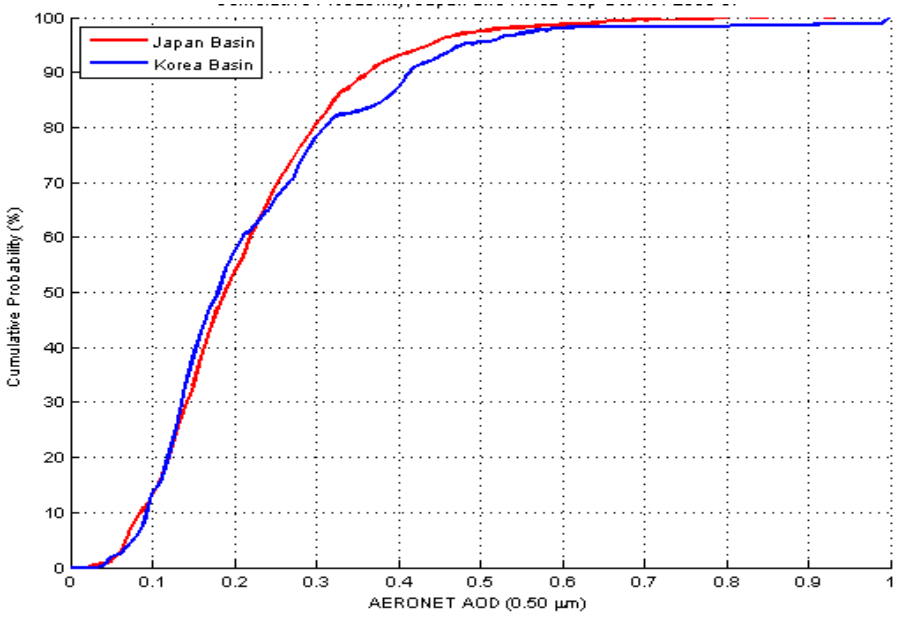

Figure 66. Same as Figure 63, but for Fall.

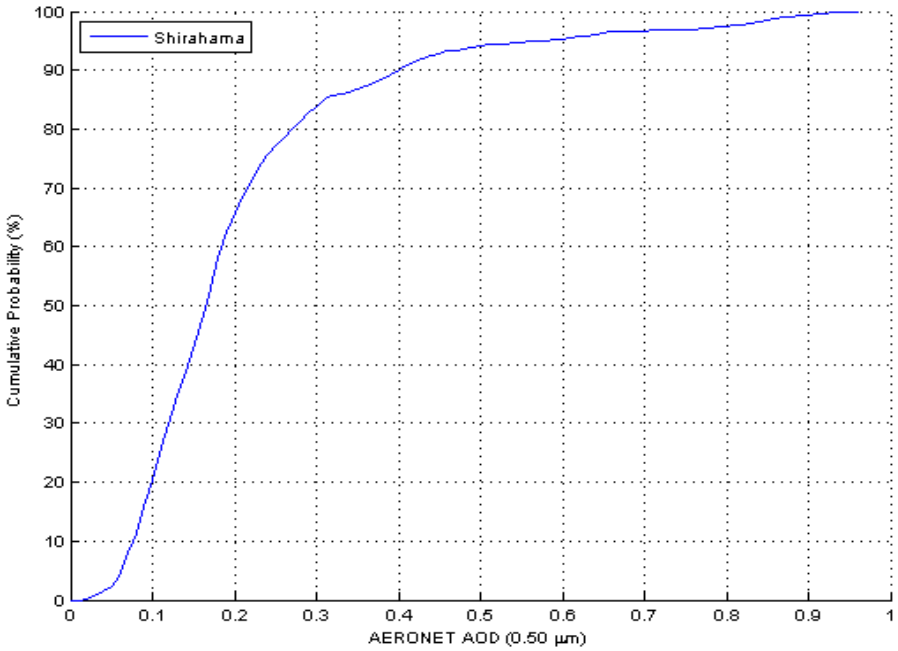

Figure 67. Two-year Winter cumulative frequency curves for the Japan Basin for 2006-2007. The cumulative frequency curve for each individual station is compared with the cumulative frequency curve computed from the histogram distribution for the combined dataset of the two stations (red curve). Here, no data is available from Osaka, so only Shirahama is shown.

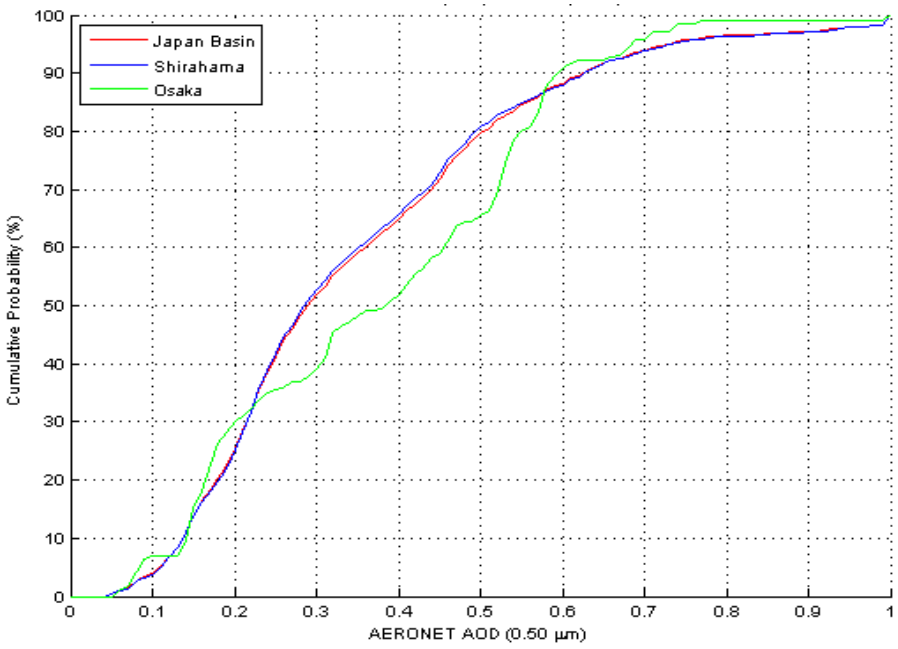

Figure 68. Same as Figure 67, but for Spring.

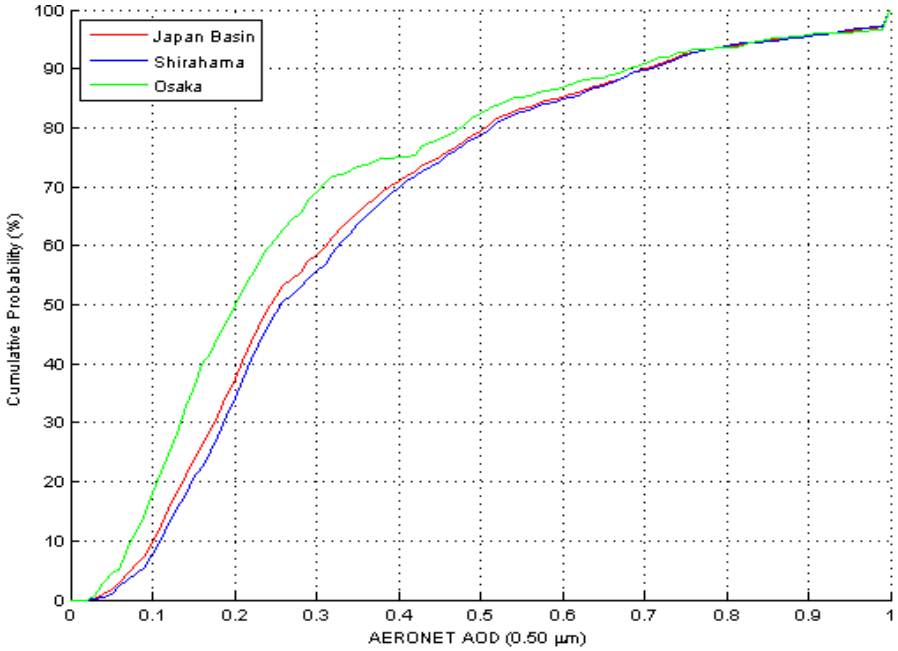

Figure 69. Same as Figure 67, but for Summer.

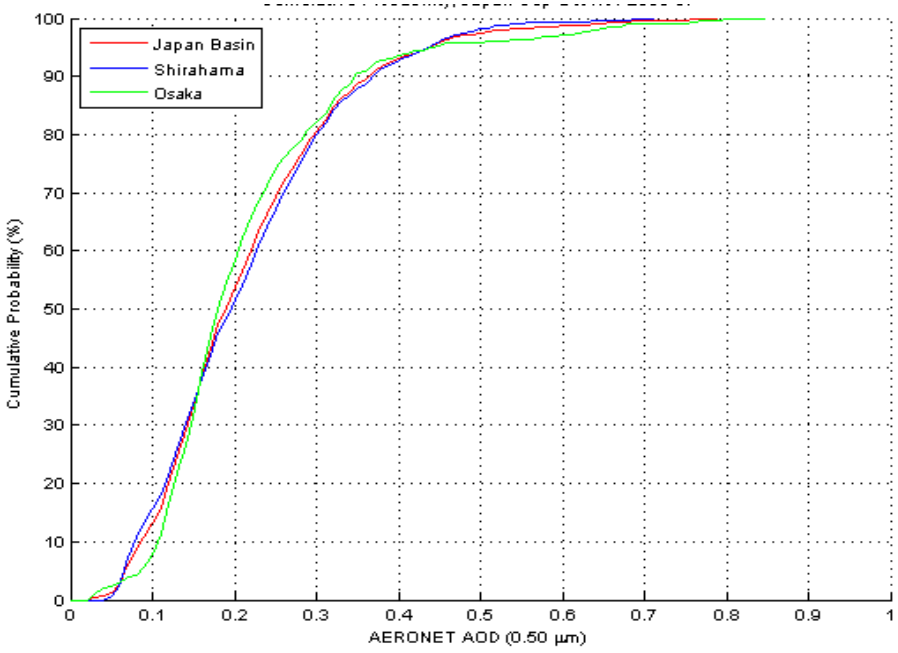

Figure 70. Same as Figure 67, but for Fall.

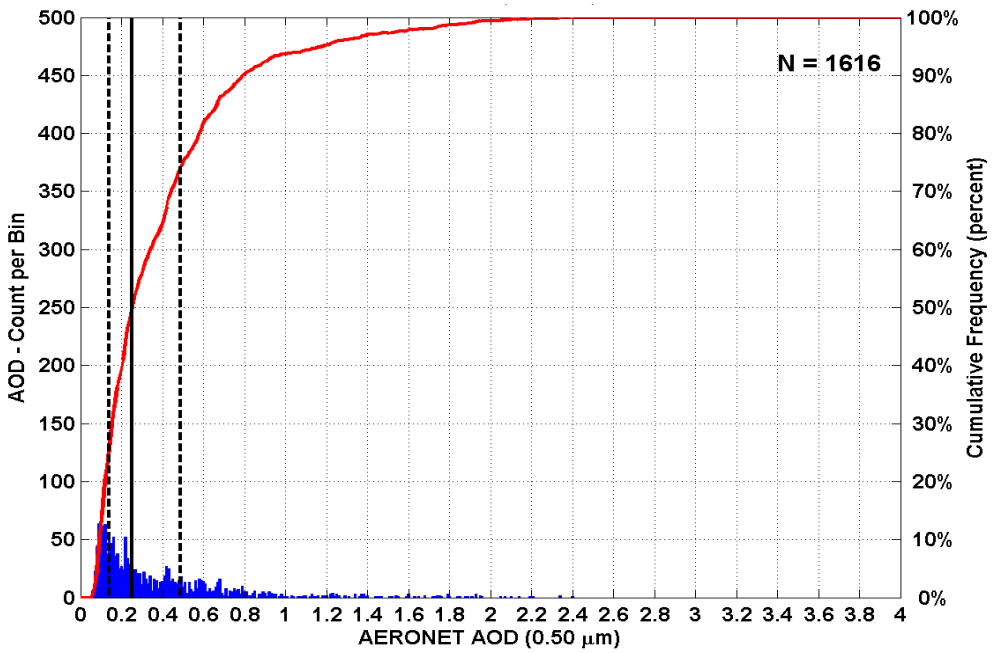

Figure 71. One-year distribution of 0.50 μm AERONET AOD values for the Korea basin for 2006. The histogram of AOD values (blue bars) and cumulative frequency distribution (red curve) corresponding to the histogram are denoted. The sample size is listed in the upper right corner. The vertical lines (black), from left to right, denote the quartiles of the distribution, 25% (dashed), 50% (solid), 75% (dashed).

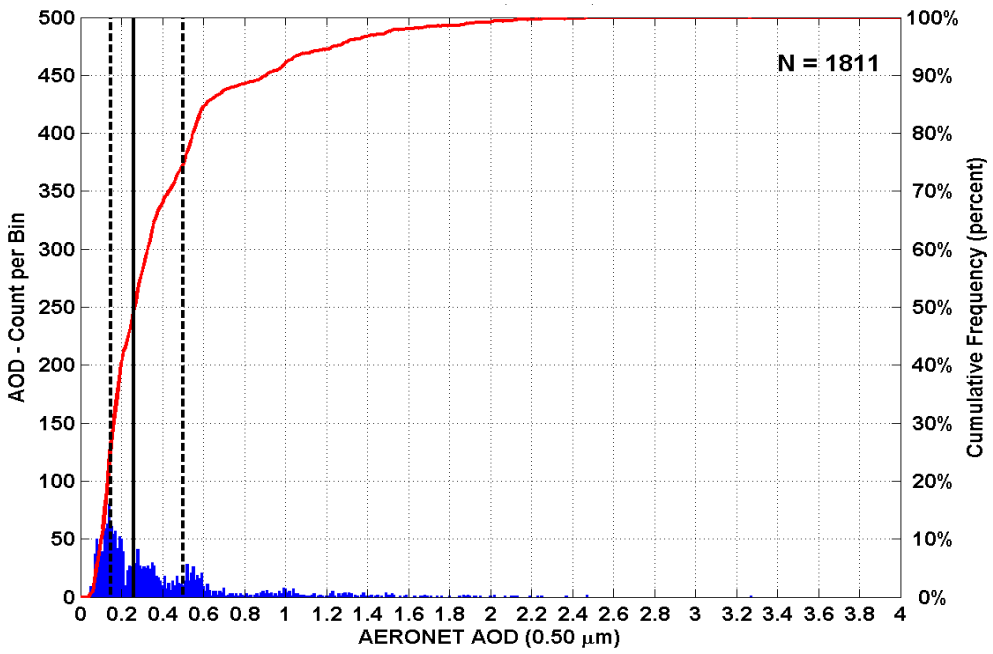

Figure 72. Same as Figure 71, but for 2007.

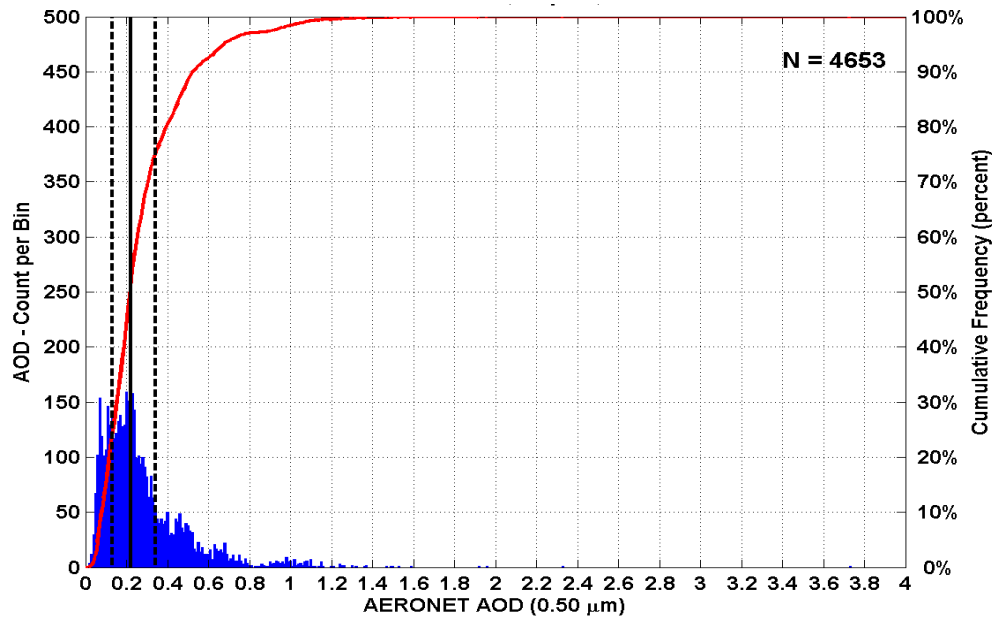

Figure 73. One-year distribution of 0.50 μm AERONET AOD values for the Japan basin for 2006. The histogram of AOD values (blue bars) and cumulative frequency distribution (red curve) corresponding to the histogram are denoted. The sample size is listed in the upper right corner. The vertical lines (black), from left to right, denote the quartiles of the distribution, 25% (dashed), 50% (solid), 75% (dashed).

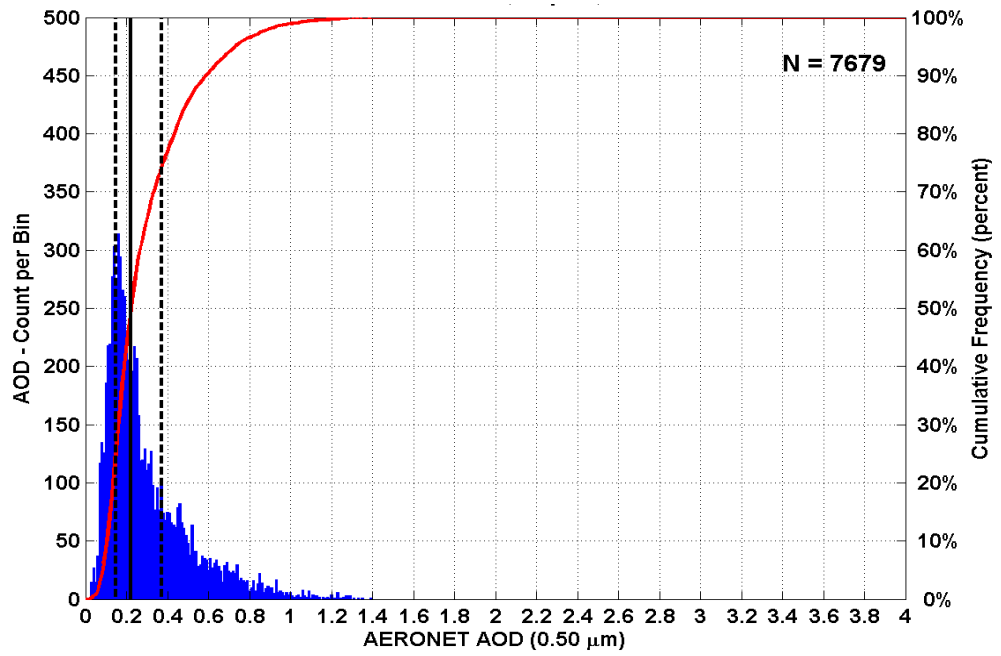

Figure 74. Same as Figure 73, but for 2007.

C. WEST AFRICA

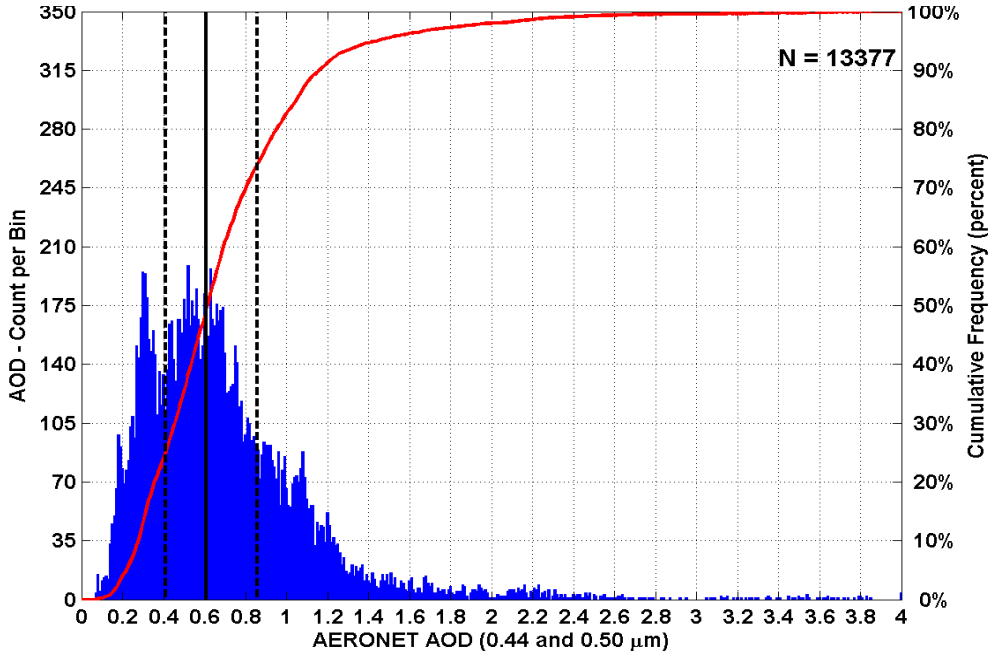

Figure 75. One-year distribution of 0.44μm and 0.50μm AERONET AOD values for the West Africa basin for 2006. The histogram of AOD values (blue bars) and cumulative frequency distribution (red curve) corresponding to the histogram are denoted. The sample size is listed in the upper right corner. The vertical lines (black), from left to right, denote the quartiles of the distribution, 25% (dashed), 50% (solid), 75% (dashed).

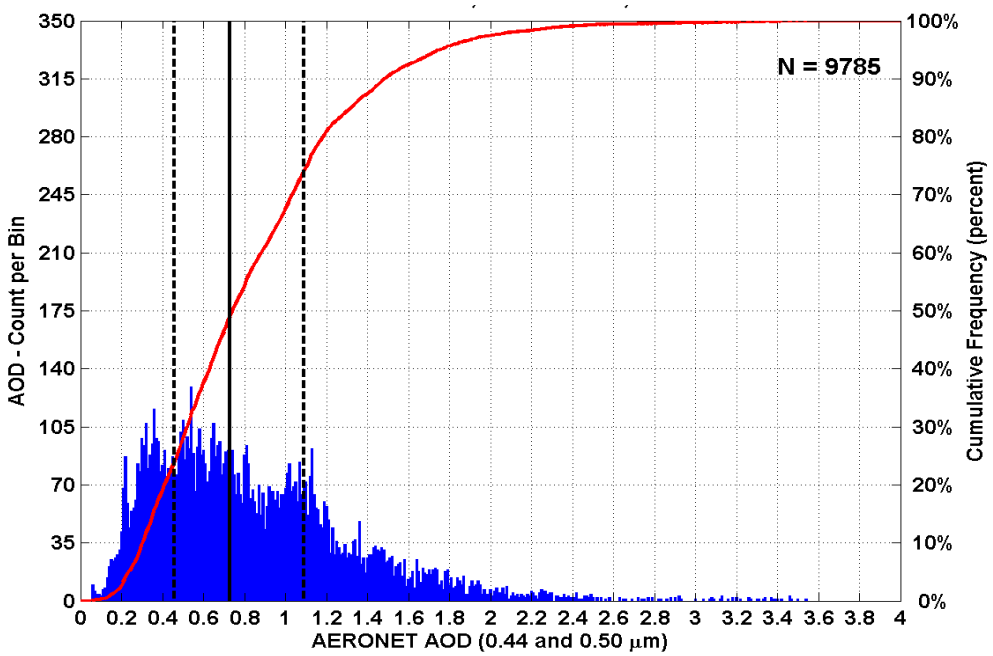

Figure 76. Same as Figure 75, but for 2007.

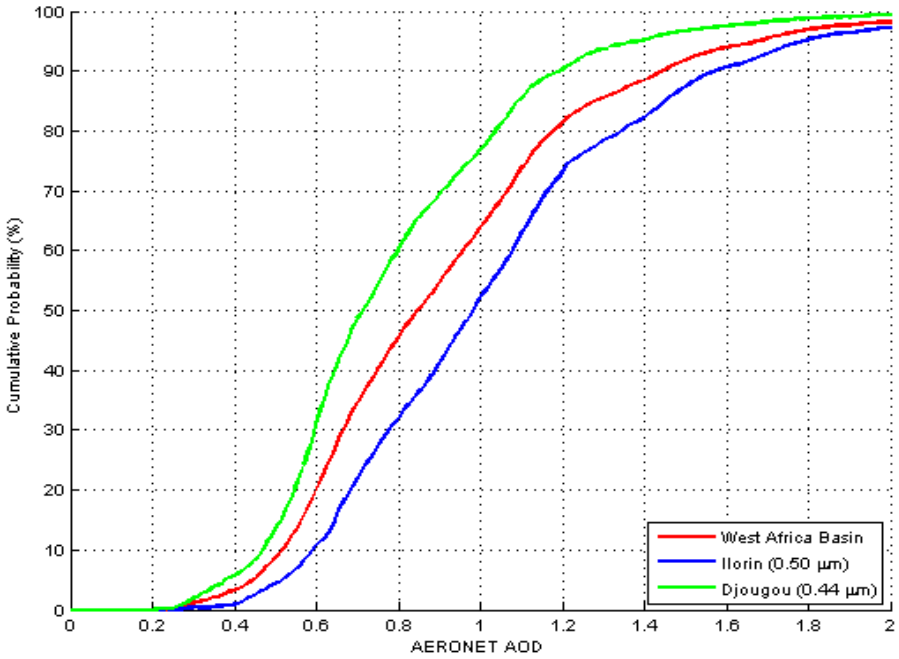

Figure 77. Two-year Winter cumulative frequency curves for the West Africa Basin for 2006-2007. The cumulative frequency curve for each individual station is compared with the cumulative frequency curve computed from the histogram distribution for the combined dataset of the two stations (red curve).

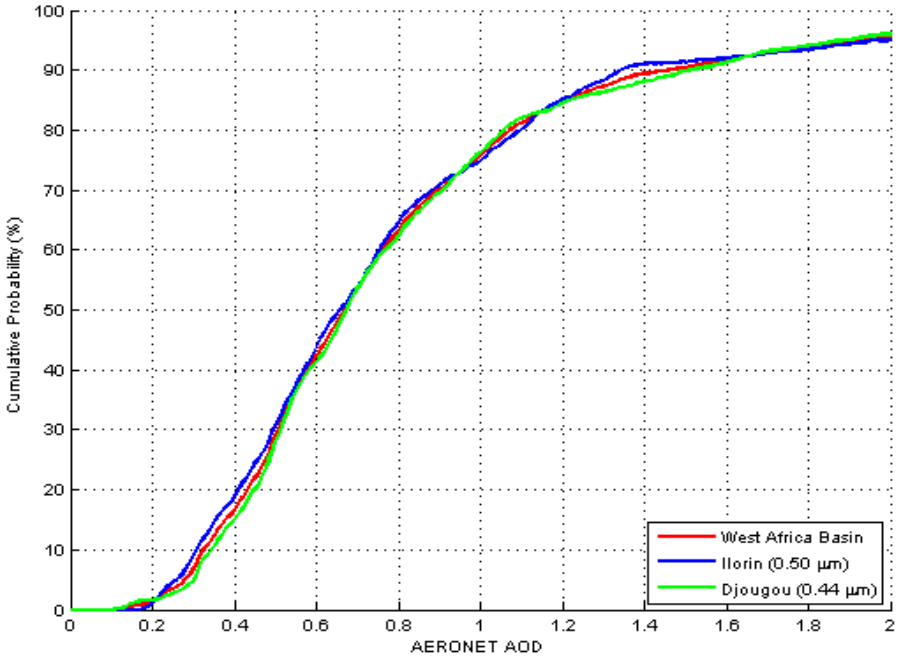

Figure 78. Same as Figure 77, but for Spring.

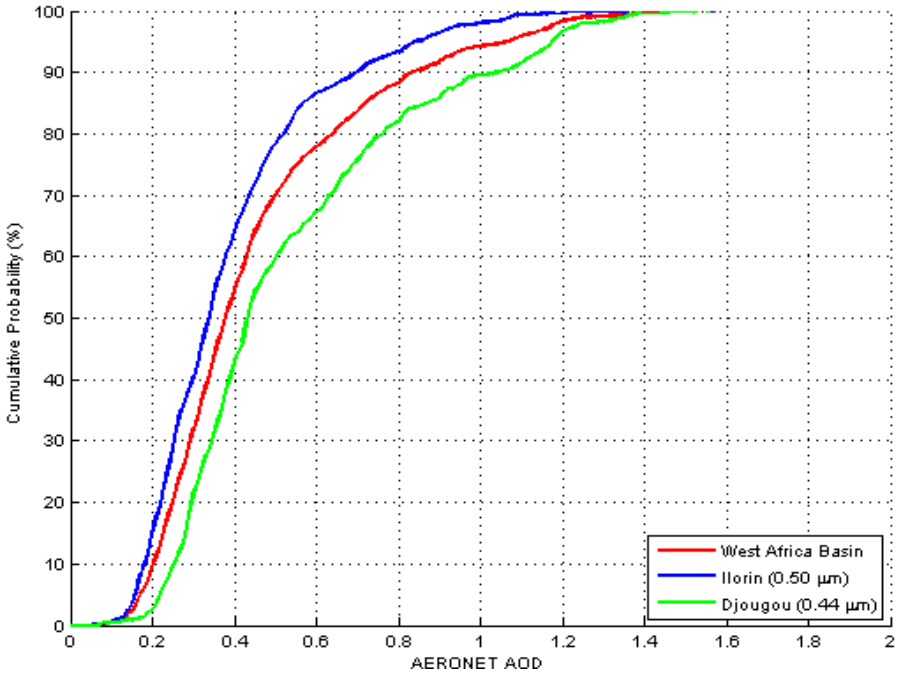

Figure 79. Same as Figure 77, but for Summer.

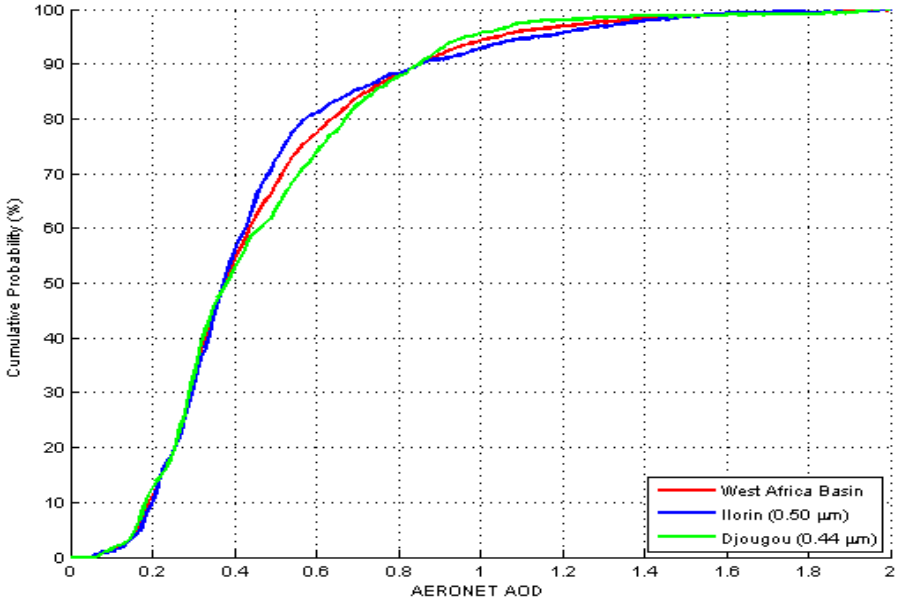

Figure 80. Same as Figure 77, but for Fall.

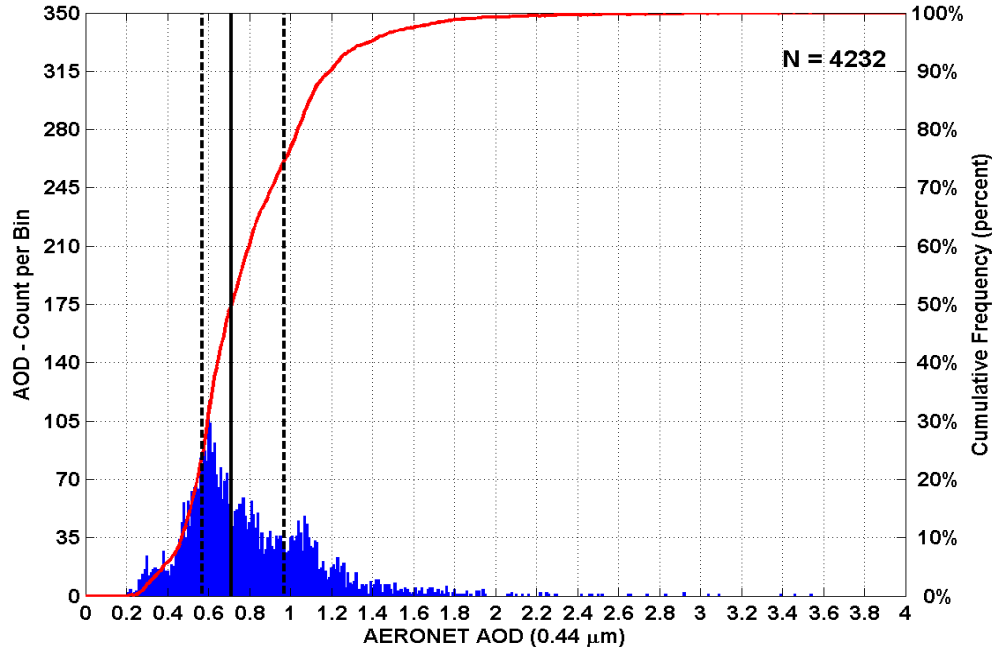

Figure 81. Winter distribution of AERONET AOD (0.44µm) values for station Djougou in the West Africa basin, for 2006-2007. The histogram of AOD values (blue bars) and cumulative frequency distribution (red curve) corresponding to the histogram are denoted, with AOD values ranging from 0 to 4. The vertical lines (black), from left to right, denote the quartiles of the distribution, 25% (dashed), 50% (solid), 75% (dashed).

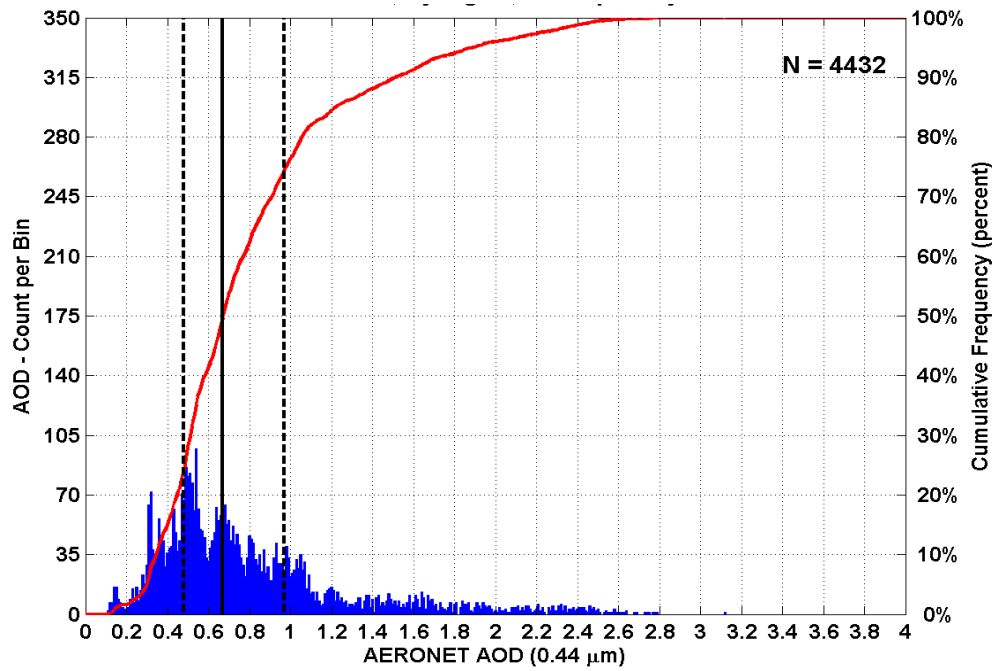

Figure 82. Same as Figure 81, but for Spring.

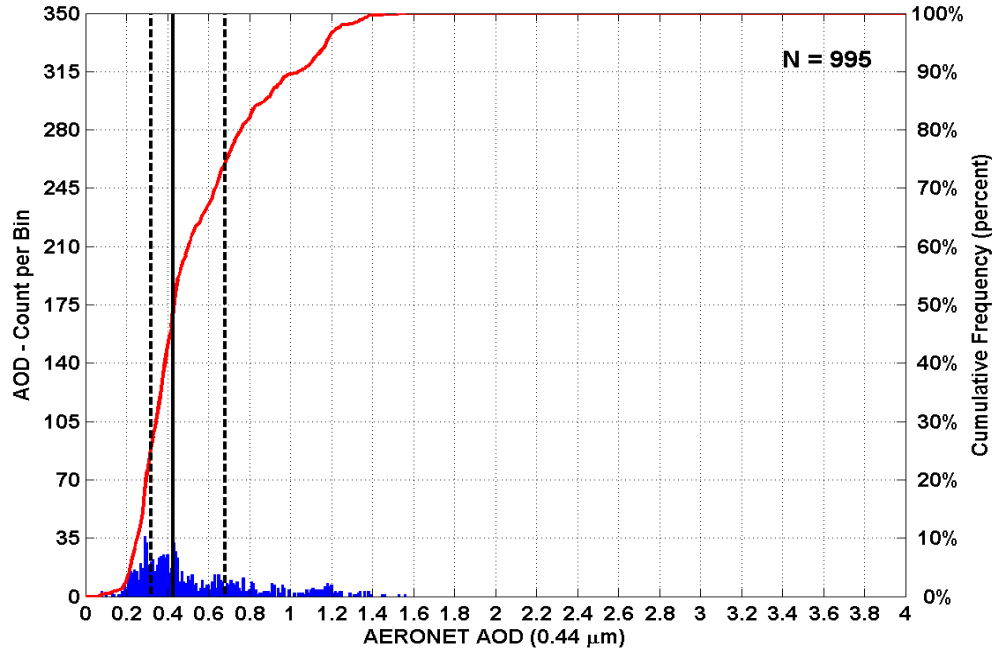

Figure 83. Same as Figure 81, but for Summer.

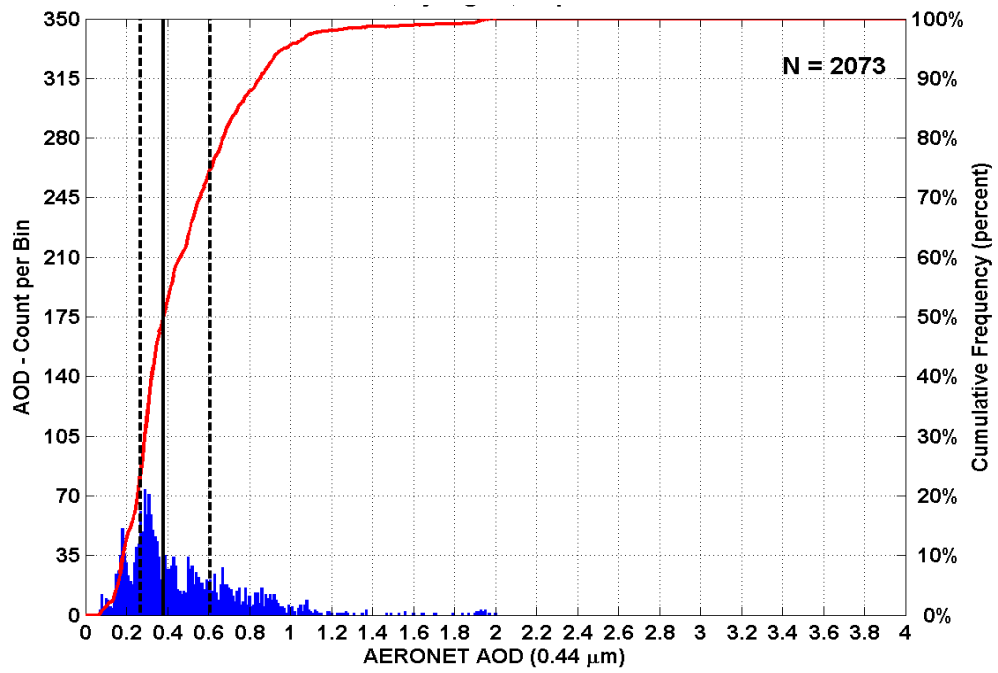

Figure 84. Same as Figure 81, but for Fall.

APPENDIX C: MODIS/AERONET COMPARISON

A. PERSIAN GULF

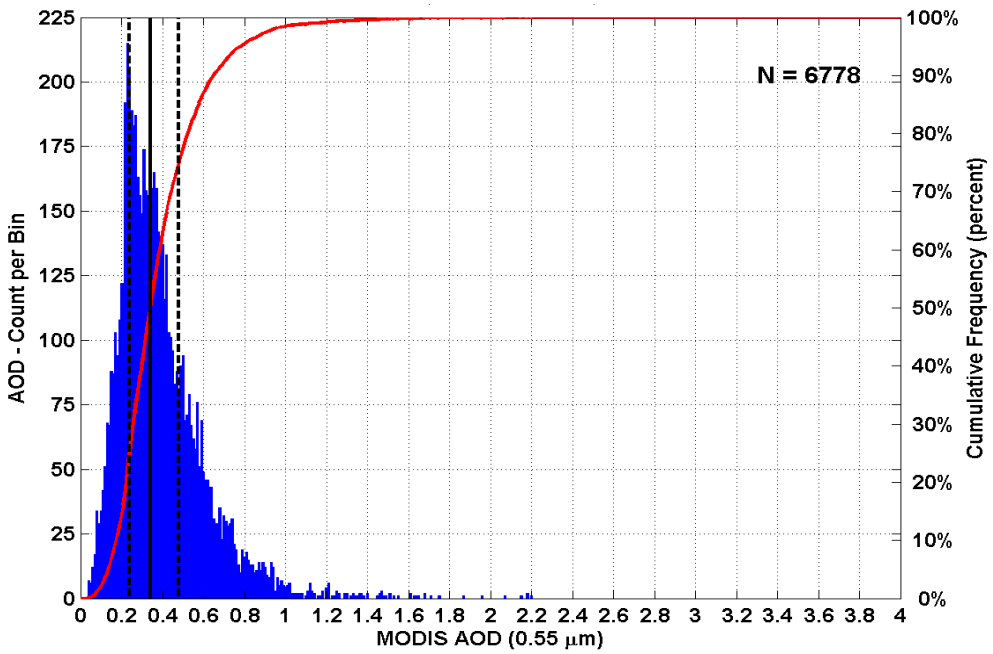

Figure 85. Two-year distribution of 0.55 μm MODIS AOD values for stations Solar Dhabi and Dhadnah in the Persian Gulf basin, for 2006-2007. The histogram of AOD values (blue bars) and cumulative frequency distribution (red curve) corresponding to the histogram are denoted. The sample size is listed in the upper right corner. The vertical lines (black), from left to right, denote the quartiles of the distribution, 25% (dashed), 50% (solid), 75% (dashed).

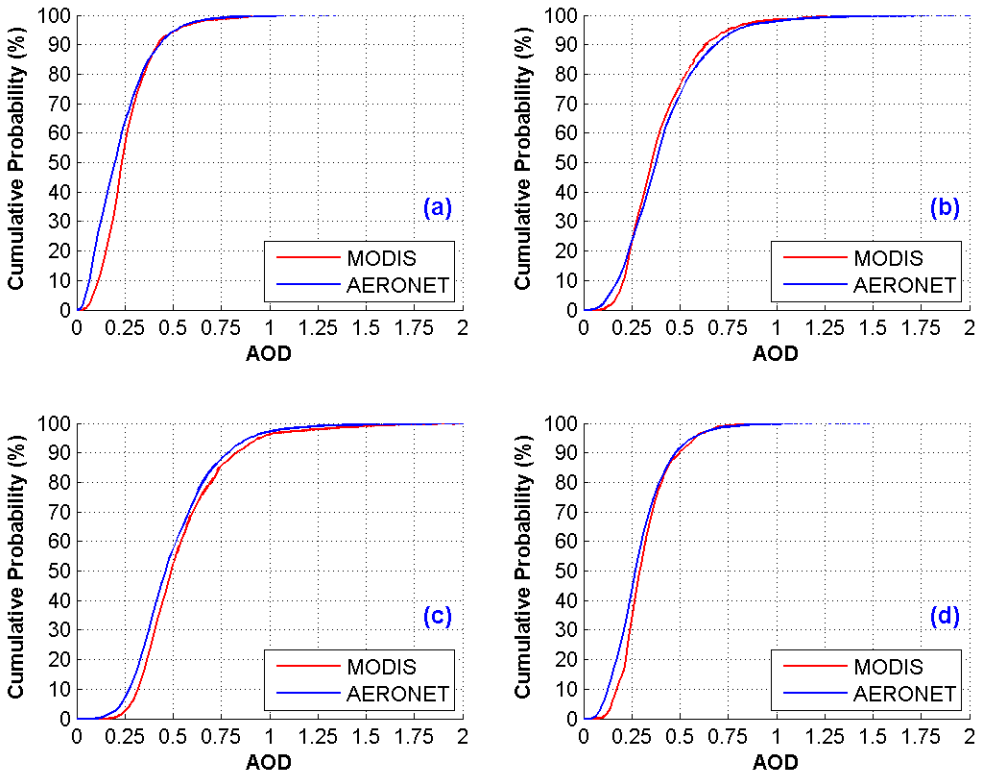

Figure 86. Seasonal cumulative frequency curves for the Persian Gulf basin MODIS (red) and AERONET (blue) AOD distributions for the 2006-2007 seasons: (a) Winter, (b) Spring, (c) Summer, (d) Fall. The y-axis indicates the cumulative probability of occurrence of an AOD. The x-axis indicates the AOD values.

B. EAST ASIA

1. Korea

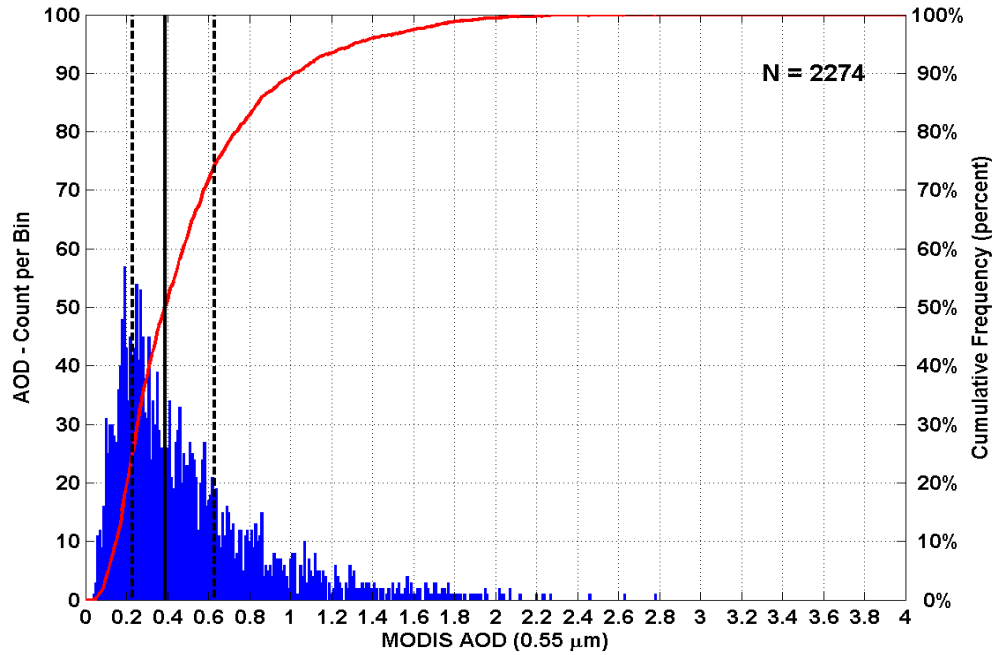

Figure 87. Two-year distribution of 0.55 μm MODIS AOD values for Anmyon in the Korea basin, for 2006-2007. The histogram of AOD values (blue bars) and cumulative frequency distribution (red curve) corresponding to the histogram are denoted. The sample size is listed in the upper right corner. The vertical lines (black), from left to right, denote the quartiles of the distribution, 25% (dashed), 50% (solid), 75% (dashed).

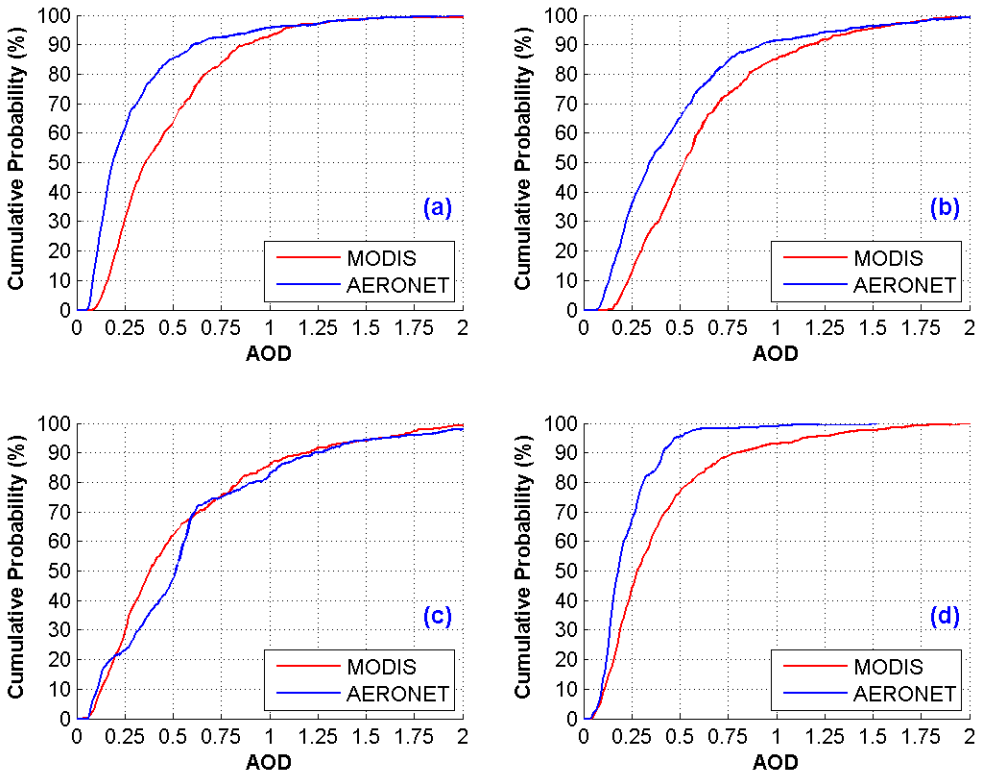

Figure 88. Seasonal cumulative frequency curves for the Korea basin MODIS (red) and AERONET (blue) AOD distributions for the 2006-2007 seasons: (a) Winter, (b) Spring, (c) Summer, (d) Fall. The y-axis indicates the cumulative probability of occurrence of an AOD. The x-axis indicates the AOD values.

2. Japan

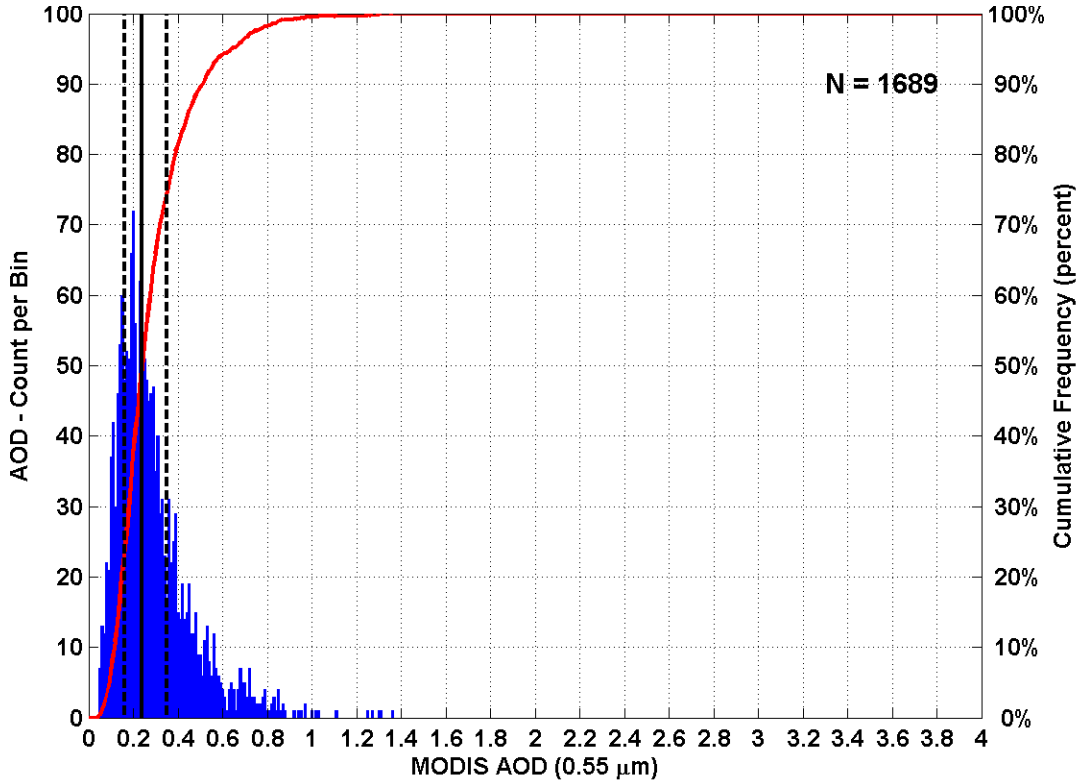

Figure 89. Two-year distribution of 0.55 μm MODIS AOD values for Shirahama in the Japan basin, for 2006-2007. The histogram of AOD values (blue bars) and cumulative frequency distribution (red curve) corresponding to the histogram are denoted. The sample size is listed in the upper right corner. The vertical lines (black), from left to right, denote the quartiles of the distribution, 25% (dashed), 50% (solid), 75% (dashed).

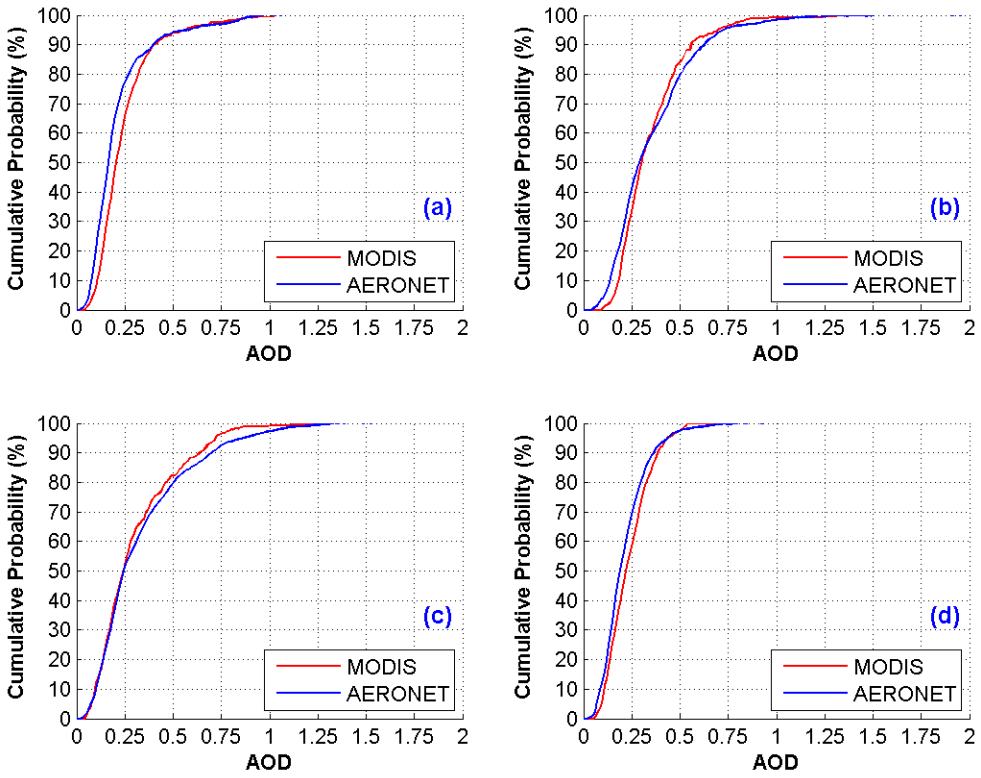

Figure 90. Seasonal cumulative frequency curves for the Japan basin MODIS (red) and AERONET (blue) AOD distributions for the 2006-2007 seasons: (a) Winter, (b) Spring, (c) Summer, (d) Fall. The y-axis indicates the cumulative probability of occurrence of an AOD. The x-axis indicates the AOD values.

C. WEST AFRICA

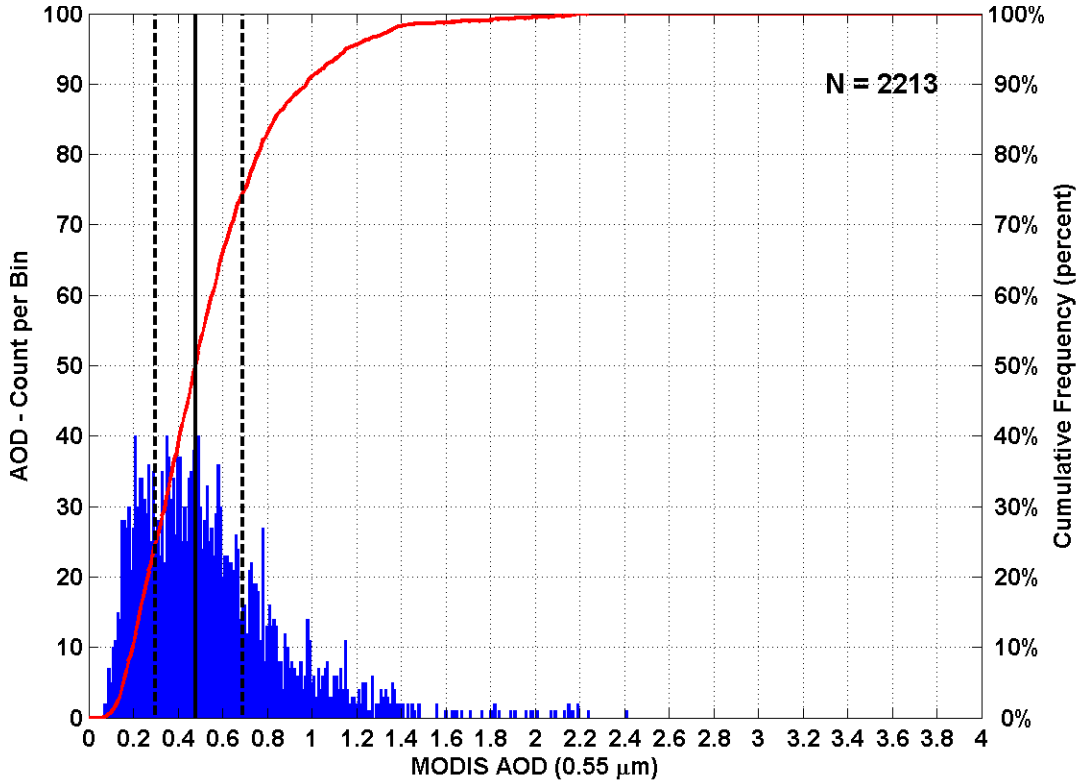

Figure 91. Two-year distribution of 0.55 μm MODIS AOD values for Ilorin in the West Africa basin, for 2006-2007. The histogram of AOD values (blue bars) and cumulative frequency distribution (red curve) corresponding to the histogram are denoted. The sample size is listed in the upper right corner. The vertical lines (black), from left to right, denote the quartiles of the distribution, 25% (dashed), 50% (solid), 75% (dashed).

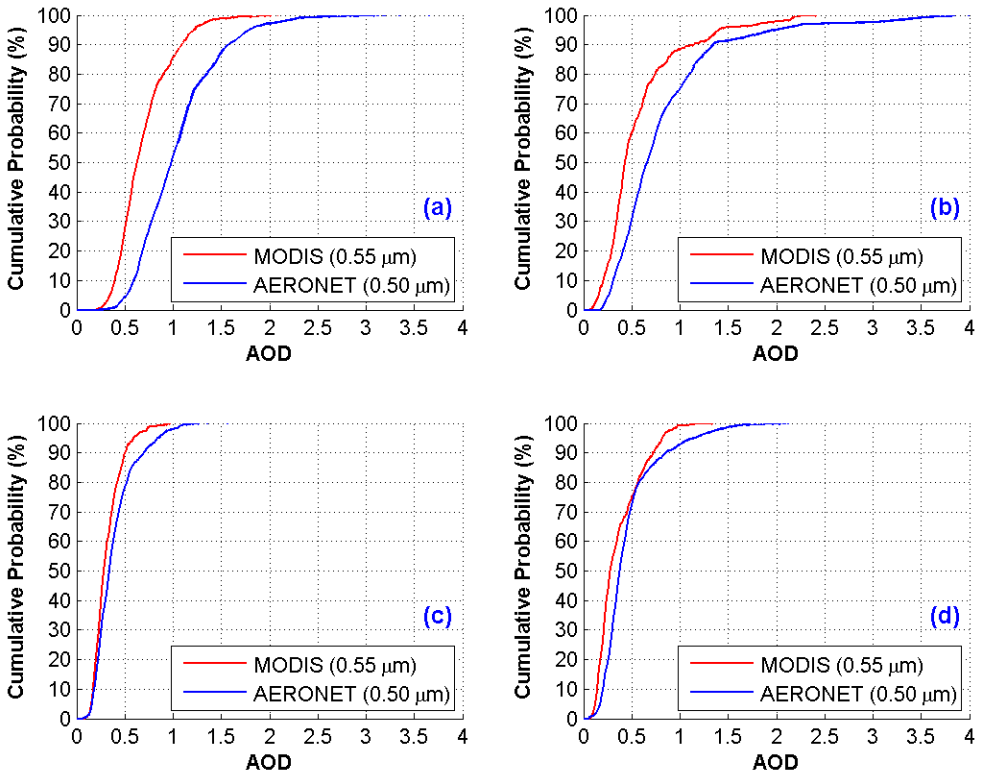

Figure 92. Seasonal cumulative frequency curves for the West Africa basin MODIS (red) and AERONET (blue) AOD distributions for the 2006-2007 seasons: (a) Winter, (b) Spring, (c) Summer, (d) Fall. The y-axis indicates the cumulative probability of occurrence of an AOD. The x-axis indicates the AOD values.

APPENDIX D: NAAPS/AERONET COMPARISON

A. PERSIAN GULF

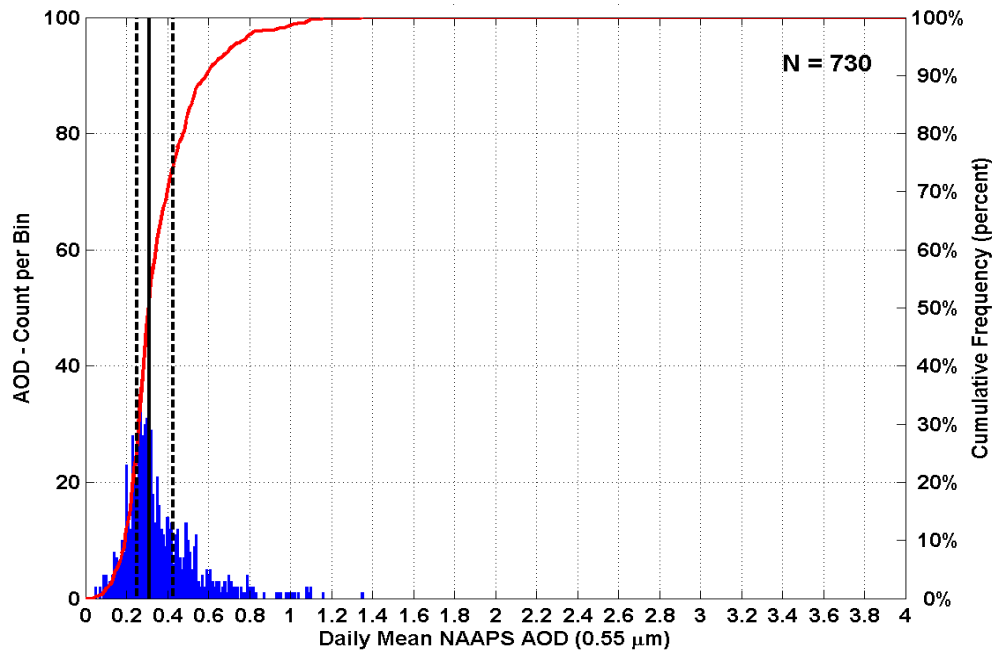

Figure 93. One-year distribution of 0.55μm NAAPS AOD values for stations Solar Village, Dhabi and Dhadnah in the Persian Gulf basin, for 2006. The histogram of AOD values (blue bars) and cumulative frequency distribution (red curve) corresponding to the histogram are denoted. The sample size is listed in the upper right corner. The vertical lines (black), from left to right, denote the quartiles of the distribution, 25% (dashed), 50% (solid), 75% (dashed).

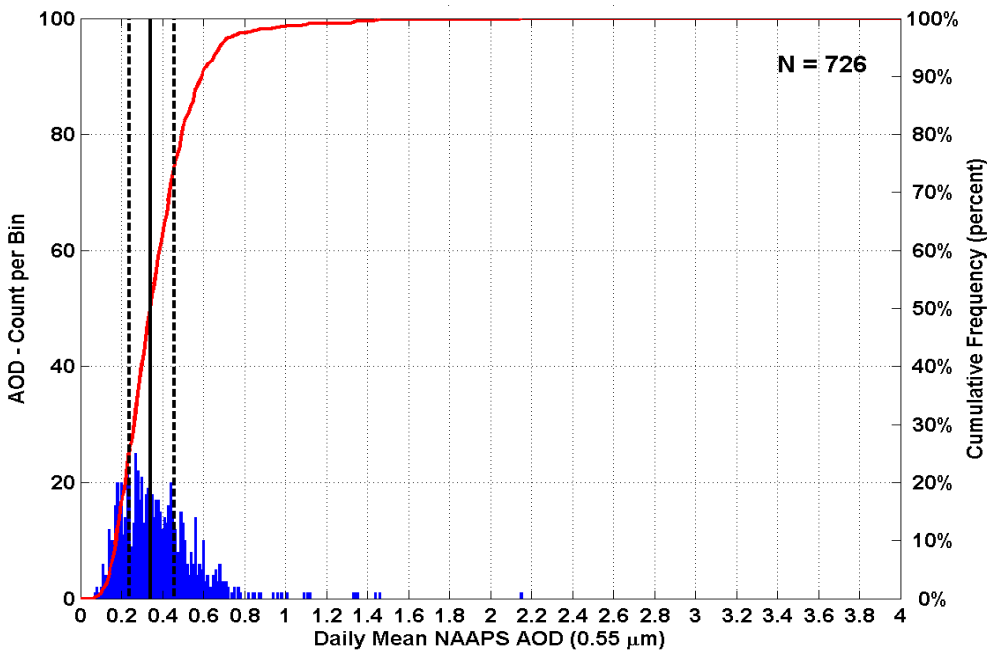

Figure 94. Same as Figure 93, but for 2007.

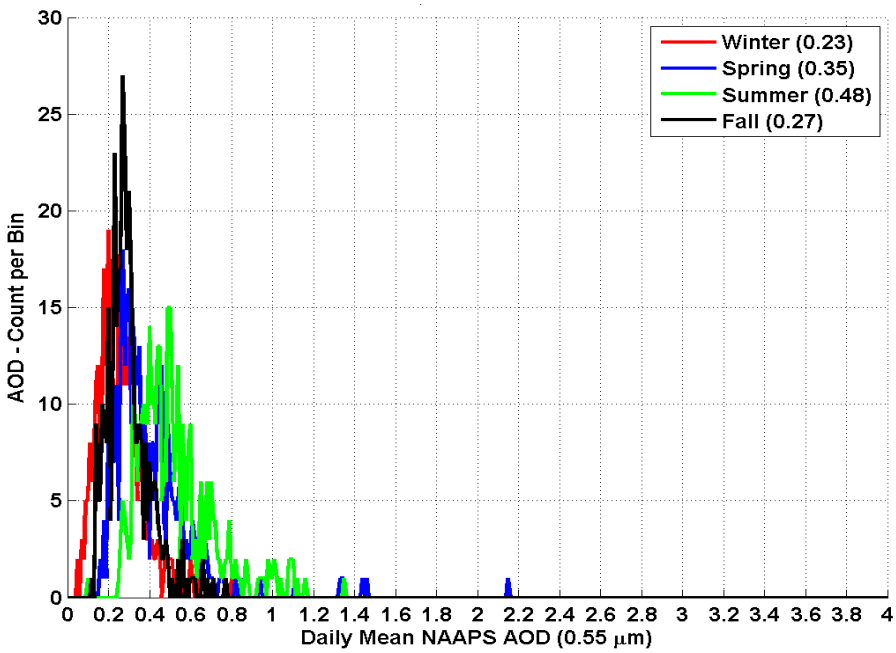

Figure 95. Seasonal distribution of 0.55μm NAAPS AOD values for the Persian Gulf basin, for 2006-2007. The seasons and their respective median values of the distribution are located in the upper right corner. The y-axis indicates the number of AOD samples per bin from 0 to 30, with the x-axis denoting AOD values at 0.55μm.

B. EAST ASIA

1. Korea

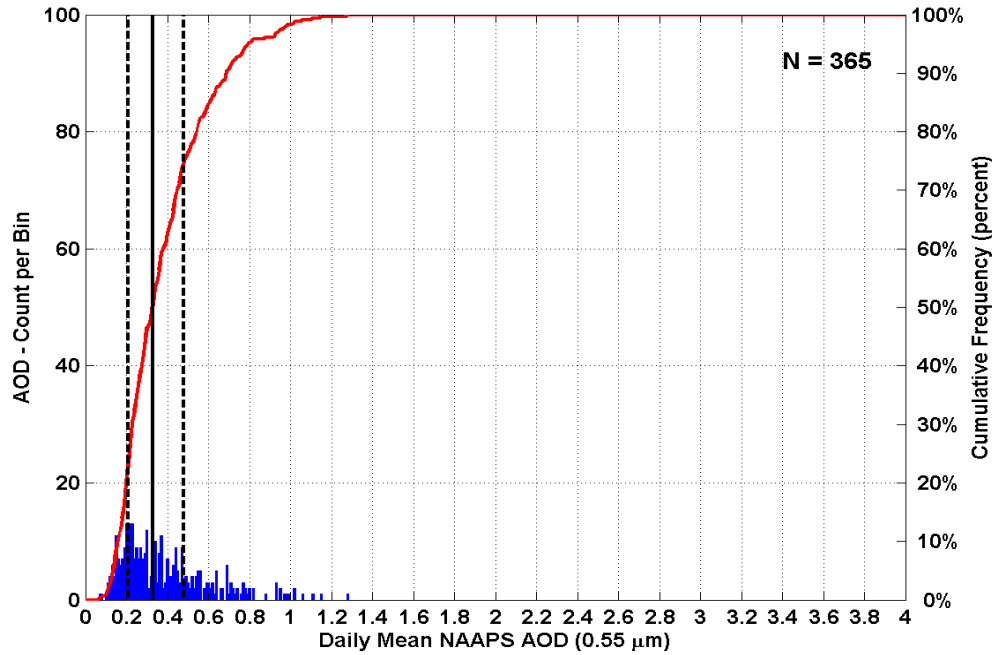

Figure 96. One-year distribution of 0.55μm NAAPS AOD values for Anmyon in the Korea basin, for 2006. The histogram of AOD values (blue bars) and cumulative frequency distribution (red curve) corresponding to the histogram are denoted. The sample size is listed in the upper right corner. The vertical lines (black), from left to right, denote the quartiles of the distribution, 25% (dashed), 50% (solid), 75% (dashed).

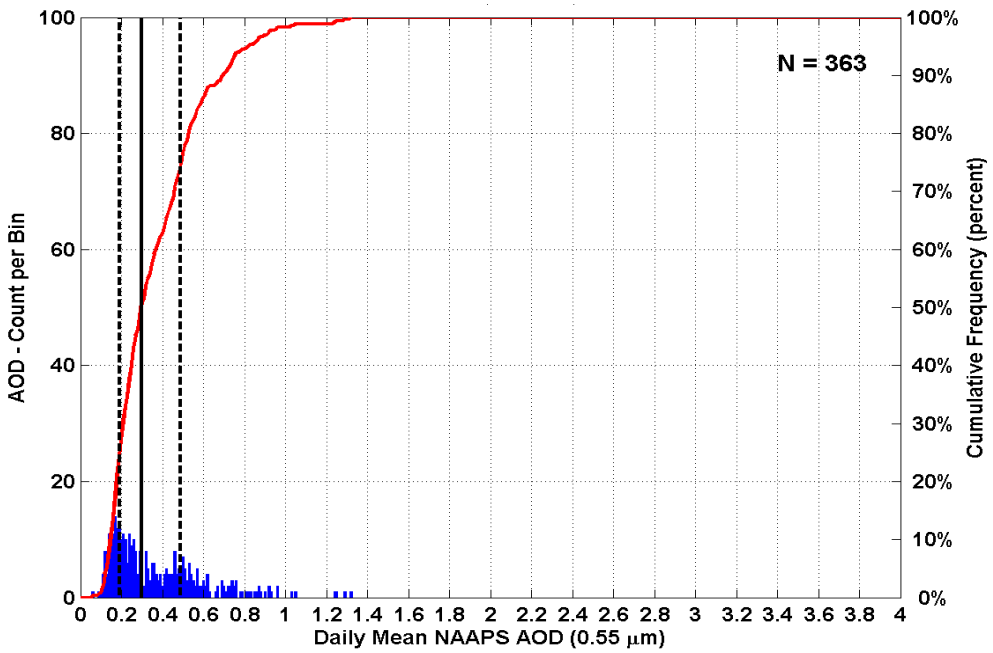

Figure 97. Same as Figure 96, but for 2007.

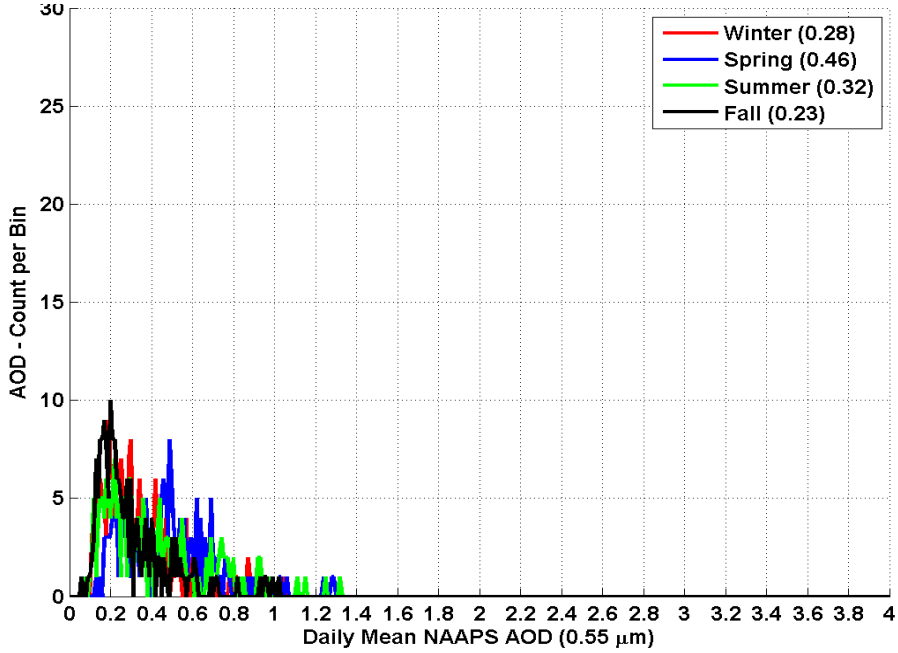

Figure 98. Seasonal distribution of 0.55μm NAAPS AOD values for the Korea basin, for 2006-2007. The seasons and their respective median values of the distribution are located in the upper right corner. The y-axis indicates the number of AOD samples per bin from 0 to 30, with the x-axis denoting AOD values at 0.55μm.

2. Japan

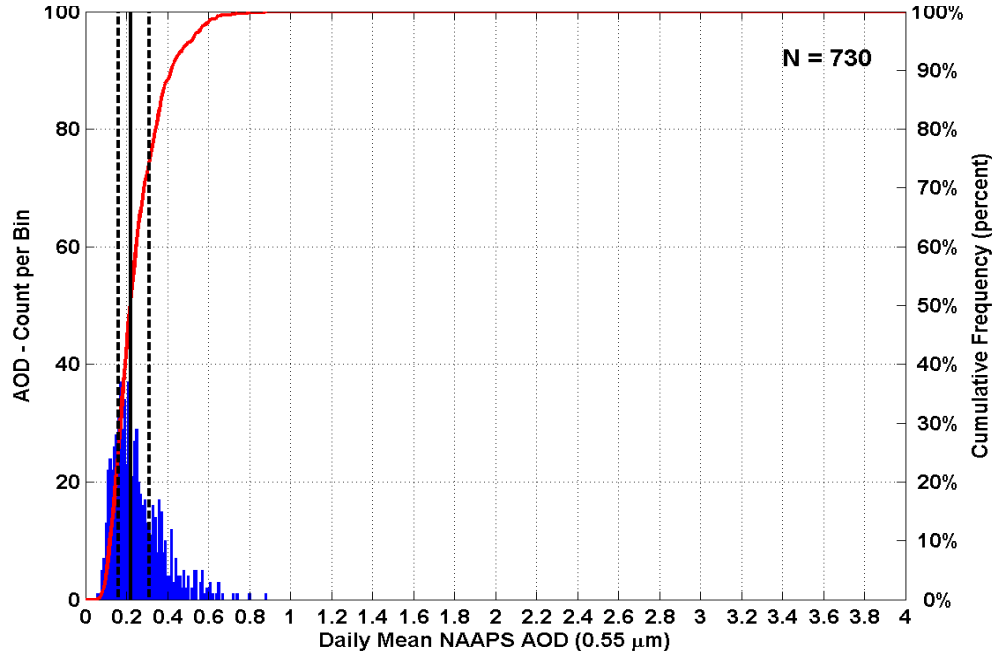

Figure 99. One-year distribution of 0.55μm NAAPS AOD values for Osaka and Shirahama in the Japan basin, for 2006. The histogram of AOD values (blue bars) and cumulative frequency distribution (red curve) corresponding to the histogram are denoted. The sample size is listed in the upper right corner. The vertical lines (black), from left to right, denote the quartiles of the distribution, 25% (dashed), 50% (solid), 75% (dashed).

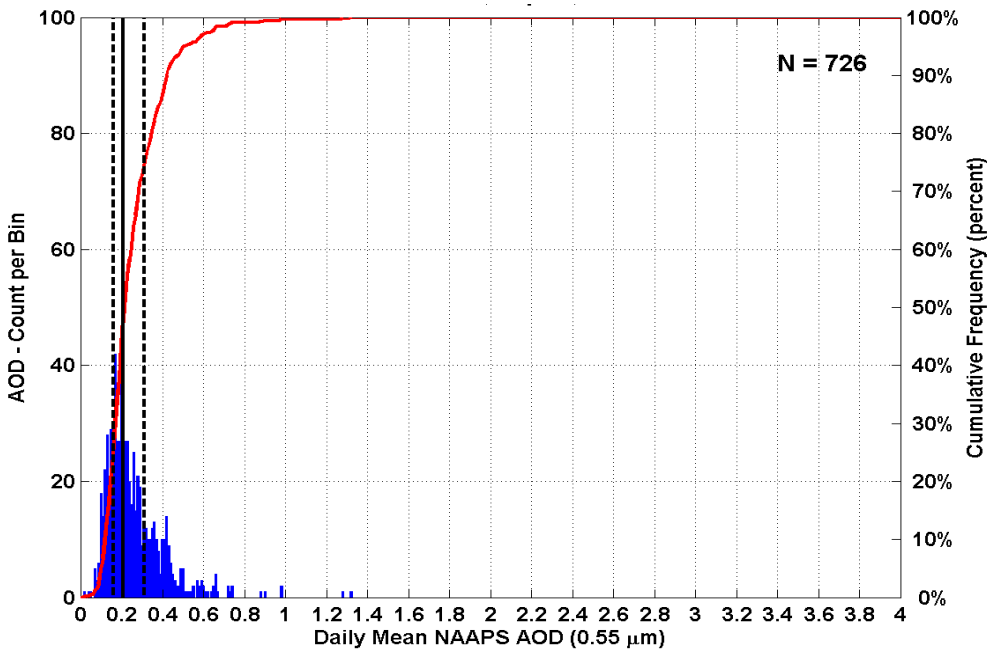

Figure 100. Same as Figure 99, but for 2007.

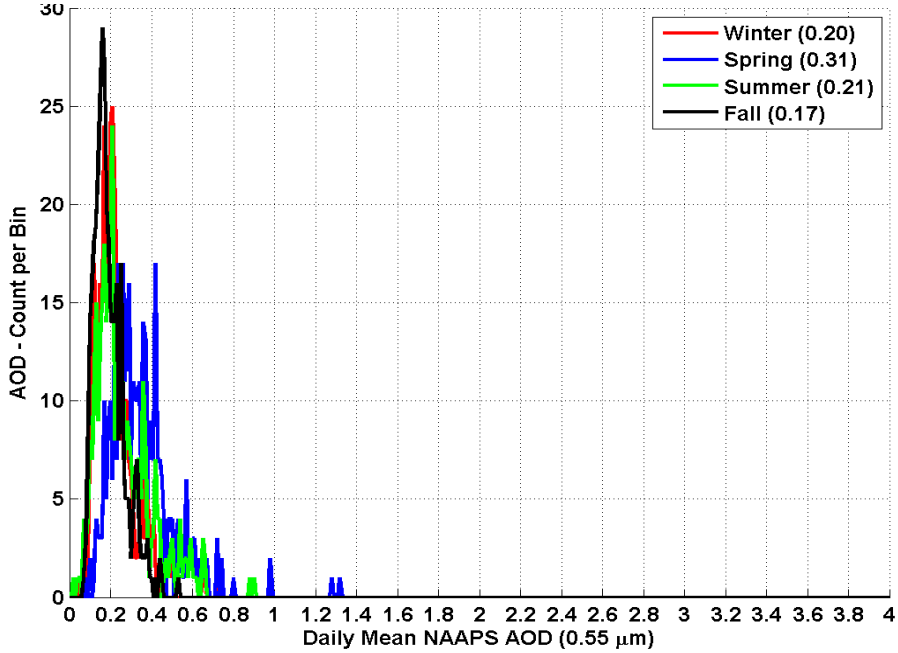

Figure 101. Seasonal distribution of 0.55μm NAAPS AOD values for the Japan basin, for 2006-2007. The seasons and their respective median AOD values of the distribution are located in the upper right corner. The y-axis indicates the number of AOD samples per bin from 0 to 30, with the x-axis denoting AOD values at 0.55μm.

C. WEST AFRICA

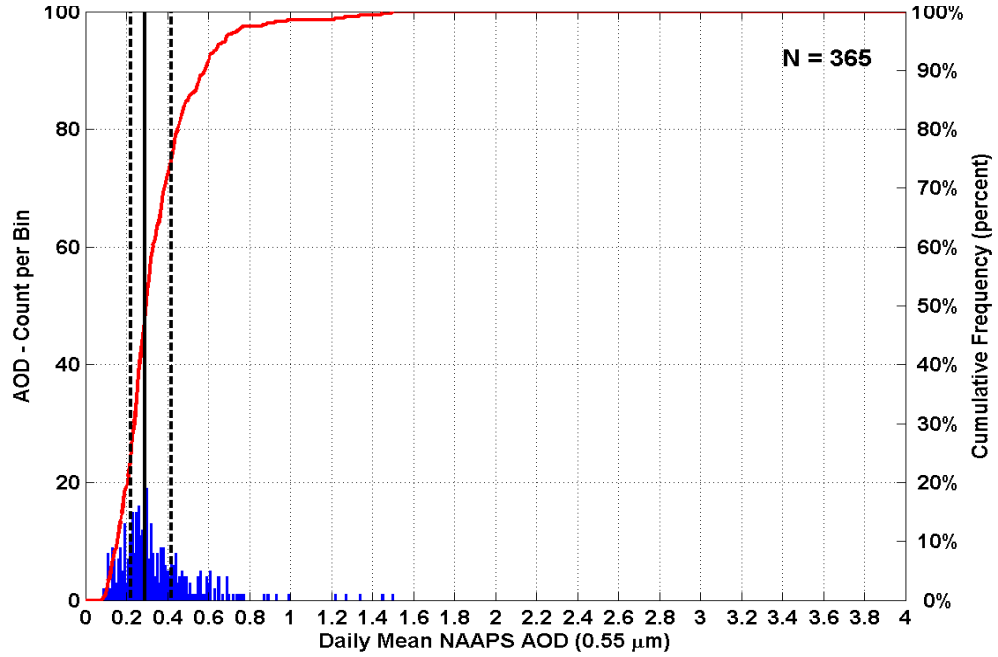

Figure 102. One-year distribution of 0.55μm NAAPS AOD values for Ilorin in the West Africa basin, for 2006. The histogram of AOD values (blue bars) and cumulative frequency distribution (red curve) corresponding to the histogram are denoted. The sample size is listed in the upper right corner. The vertical lines (black), from left to right, denote the quartiles of the distribution, 25% (dashed), 50% (solid), 75% (dashed).

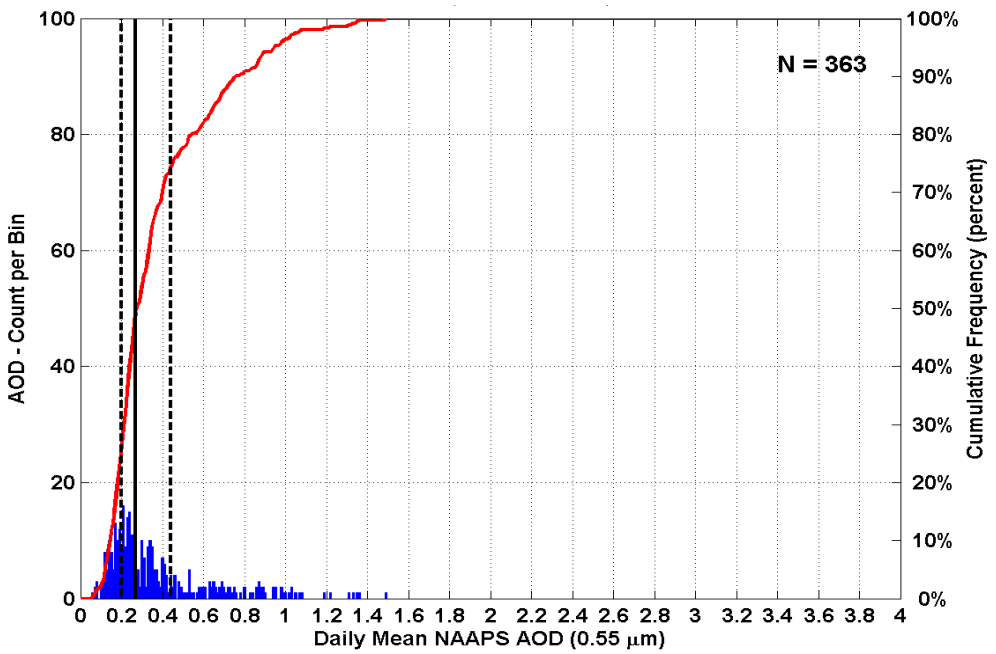

Figure 103. Same as Figure 102, but for 2007.

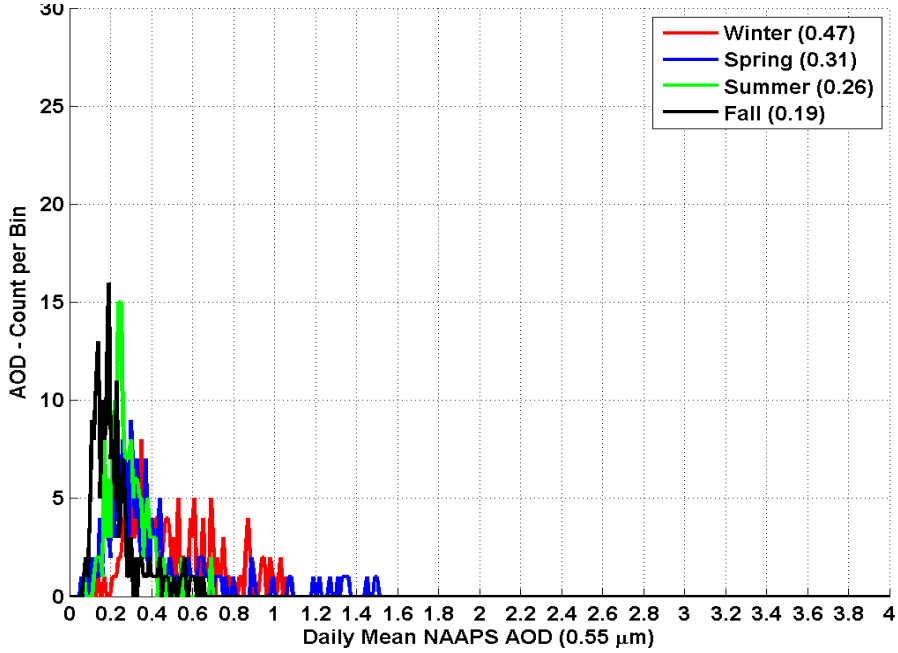

Figure 104. Seasonal distribution of 0.55μm NAAPS AOD values for the West Africa, for 2006-2007. The seasons and their respective median values of the distribution are located in the upper right corner. The y-axis indicates the number of AOD samples per bin from 0 to 30, with the x-axis denoting AOD values at 0.55μm.

LIST OF REFERENCES

ASTER Spectral Library, cited February 2009: Spectral Library. [Available online at http://speclib.jpl.nasa.gov/].

Chin, M., P. Ginoux, S. Kinne, O. Torres, B. N. Holben, B. N. Duncan, R. V. Martin, J. A. Logan, A. Higurashi, and T. Nakajima, 2002: Tropospheric aerosol optical thickness from the GOCART model and comparisons with satellite and sun photometer measurements. *J. Atmos. Sci.*, **59**, 461-483.

Chu, D. A., Y. J. Kaufman, C. Ichoku, L. A. Remer, D. Tanre, and B. N. Holben, 2002: Validation of MODIS aerosol optical depth retrieval over land. *Geophys. Res. Lett.*, **29**, 12, doi:10.1029/2001GL013205.

Durkee, P. A., F. Pfeil, E. M. Frost, and R. A. Shema, 1991: Global scale aerosol particle characteristics from satellite-detected radiance. Atmos. Environ., **25A**, 2457-2465.

Fourteenth Weather Squadron, cited February 2009: Standard Products-Narratives for Abu Dhabi Bateen Airport, Arabian Peninsula, Japan, Korean Peninsula, and Nigeria. [Available online at https://notus2.afccc.af.mil/SCIS/prodloc.asp].

Goddard Space Flight Center, cited February 2009: AERONET Data-Access and Dissemination Tools. [Available online at http://aeronet.gsfc.nasa.gov/new_web/data.html].

——, AERONET System Description. [Available online at http://aeronet.gsfc.nasa.gov/new_web/system_descriptions.html].

——, MODIS Specifications. [Available online at http://modis.gsfc.nasa.gov/about/specifications.php].

Google, Inc., cited February 2009: Google Maps. [Available online at http://maps.google.com/maps?hl=en&tab=wl]

Kidder, S. Q. and T. H. Vonder Haar, 1999: *Satellite Meteorology: An Introduction*. Academic Press, 466 pp.

Martins, J. V., D. Tanre, L. A. Remer, Y. J. Kaufman, S. Mattoo, R. Levy., 2002: MODIS Cloud screening for remote sensing of aerosols over oceans using spatial availability. *Geophys. Res. Lett.*, **29**, 12, doi:10.1029/2001GL013252.

Misra, A., A. Jayaraman, and D. Ganguly, 2008: Validation of MODIS derived optical depth over western India. *J. Geophys. Res.*, **113**, D04203, doi:10.1029/2007JD009075.

NASA, cited February 2009: S'Cool Definitions: [Available online at http://asd-www.larc.nasa.gov/SCOOL/definition.html].

Navy Research Laboratory Monterey, CA, cited February 2009: Description of NAAPS (Navy Aerosol Analysis and Prediction System) Global Aerosol Model. [Available online at http://www.nrlmry.navy.mil/aerosol_web/Docs/globaer_model.html].

Navy Research Laboratory Monterey, CA, cited February 2009: NexSat, NRL/NPOESS Next-Generation Weather Satellite Demonstration Project. [Available online at https://www.nrlmry.navy.mil/focus-bin/focus.cgi]

——, Overview of NAAPS: Navy Aerosol Analysis and Prediction System. [Available online at http://www.nrlmry.navy.mil/aerosol_web/Docs/nrlmryonrprop.html].

National Oceanic and Atmospheric Administration, cited February 2009: NOAA News Online (Story 1120). [Available online at http://www.noaanews.noaa.gov/stories/s1120.htm].

Remer, L. A., Y. J. Kaufman, D. Tanre, S. Mattoo, D. A. Chu, J. V. Martins, R. R. Li, C. Ichoku, R. C. Levy, R. G. Kleidman, T. F. Eck, E. Vermonte, and B. N. Holben, 2005: The MODIS aerosol algorithm, products, and validation. *J. Atmos. Sci.*, **62**, 947-973.

Westphal, D. L., O. B. Toon, and T. N. Carlson, 1988: A case study of mobilization and transport of Saharan dust. *J. Atmos. Sci.*, **45**, 2145-2175.

Zhang, J., J. S. Reid, 2006: MODIS aerosol product analysis for data assimilation: Assessment of over-ocean level 2 aerosol optical thickness retrievals. *J. Geophys. Res.*, **111**, D22207, doi:10.1029/2005JD006898.

——, Reid, D. L. Westphal, N. L. Baker, E. J. Hyer, 2008: A system for operational aerosol optical depth data assimilation over global oceans. *J. Geophys. Res.*, **113**, D10208, doi:10.1029/2007JD009065.

INITIAL DISTRIBUTION LIST

1. Defense Technical Information Center
   Ft. Belvoir, Virginia

2. Dudley Knox Library
   Naval Postgraduate School
   Monterey, California

3. Professor Philip A. Durkee (Code MR/DE)
   Department of Meteorology
   Naval Postgraduate School
   Monterey, California

4. Mary S. Jordan
   Department of Meteorology
   Naval Postgraduate School
   Monterey, California

5. Capt Kevin M. Quinn
   Department of Meteorology
   Naval Postgraduate School
   Monterey, California